Mechanistic binding of bioactive compounds with recombinant truncated domains and native mutants of human serum albumin

Thesis submitted for the degree of

DOCTOR OF PHILOSOPHY

By

Aparna Nerusu

Enrollment No. 13LPPH09

Department of Plant Sciences

School of Life Sciences

University of Hyderabad

Hyderabad – 500 046, INDIA.

January 2019

Department of Plant Sciences

School of Life Sciences

University of Hyderabad

Hyderabad – 500 046, Telangana, INDIA.

DECLARATION

I, **Aparna Nerusu,** hereby declare that this thesis entitled **"Mechanistic binding of bioactive compounds with recombinant truncated domains and native mutants of human serum albumin"** submitted by me under the guidance and supervision of **Prof. S. Rajagopal** is an original and independent research work. I also declare that it has not been submitted previously in part or in full to this University or any other University or Institution for the award of any degree or diploma.

Date:

Name:

Signature:

Regd. No.:

Prof. S. Rajagopal

(Research supervisor)

Department of Plant Sciences

School of Life Sciences

University of Hyderabad

Hyderabad – 500 046, Telangana, INDIA.

CERTIFICATE

This is to certify that this thesis entitled **"Mechanistic binding of bioactive compounds with recombinant truncated domains and native mutants of human serum albumin"** is a record of bonafide work done by **Ms. Aparna Nerusu**, registration number 13LPPH09, a research scholar for Ph.D. program in Plant Sciences, Department of Plant Sciences, School of Life Sciences, University of Hyderabad under my guidance and supervision. This thesis is free from plagiarism and has not been submitted previously in part or in full to this or any other University or Institution for the award of any degree or diploma.

Parts of the thesis have been:

A. Published in the following publication:

ACS Omega, 2017, 2 (10), pp 6514–6524, DOI: 10.1021/acsomega.7b00577.

B. Presented in the following conferences:

Poster presented in 82nd Annual Meeting of The Society of Biological Chemists (India) and International Conference on Genomes: Mechanism and Function. December 2-5, 2013.

Poster presented in International Conference and Workshop On Structure-based Drug Designing and Applications to Infectious Diseases. February 1-5, 2016.

Further, the student has passed the following courses towards fulfilment of course work requirement for the award of Ph.D.

SI.No	Course Code	Course Name	Credits	Pass/Fail
1	PL 801	Seminar 1	1	Pass
2	PL 802	Research Ethics & Management	2	Pass
3	PL 803	Biostatistics	2	Pass
4	PL 804	Analytical Techniques	3	Pass
5	PL 805	Lab Work	4	Pass

Prof. S. Rajagopal **Head of the Department** **Dean of the School**

Supervisor

Department of Plant Sciences

School of Life Sciences

University of Hyderabad

Hyderabad – 500 046, Telangana, INDIA.

Plagiarism Free Certificate

This is to certify that the similarity index of this as checked by the library of University of Hyderabad is 31% out of this 23% similarity has been found to be identified from the candidate's own publication which forms the major part of the thesis. The detail of student's publication is as follows:

Aparna Nerusu, P. Srinivasa Reddy, Dhevalapally B. Ramachary, Rajagopal Subramanyam, 2017. Unraveling the Stability of Plasma Proteins upon Interaction of Synthesized Androstenedione and Its Derivatives- A Biophysical and Computational Approach. *ACS Omega,* **2**, 6514-24.

About 8% similarity was identified from the external sources in the present thesis that is according to prescribed regulations of the University. The publication related to this thesis has been appended at the end of the thesis. Hence the present thesis may be considered to be plagiarism free.

Prof. S. Rajagopal

Supervisor

Acknowledgements

I would like to express my sincere gratitude to my supervisor, **Prof. Rajagopal Subramanyam** for his constant support, encouragement and guidance.

I would like to thank the present Dean **K. V. A. Ramaiah** and the former Deans, **Prof. R. P. Sharma, Prof. Aparna Dutta Gupta, Prof. A. S. Raghavendra, Prof. P. Reddanna, Prof. M. N. V. Prasad**, School of Life Sciences and the present Head, **Prof Ch. Venkata Ramana** and former Head, **Prof. A. R. Reddy**, Department of Plant Sciences for allowing me to use School and Department facilities.

I sincerely thank my doctoral committee members **Prof. Appa Rao Podile, Prof. Ch. Venkata Ramana and Prof. Naresh Babu V Sepuri** for their valuable suggestions.

I would like to express my special thanks to **Prof. Appa Rao Podile** and his lab members Dr. Ramakrishna, Dr. Shiva Ramakrishna, Dr. Papa rao, Bhuvan, Mohan, Rajesh, Dr. Sravani, Dr. Sandhya for making me to use their lab facilities and their help throughout my doctoral research.

I would like to thank Dr. A. Bindu Madhava Reddy and his lab members for allowing me to use their lab facilities.

I would also like to thank Dr. Cherish, for providing Pichia strains and pPIC9 vector and Prof. D. B. Ramachary, for providing the Androstenediones.

I am grateful to all the faculty members from School of Life Sciences.

Thanks to **Dr. Praveen Kumar** for his help in SPR work.

I thank my lab mates Dr. Ch. Dinesh Kumar, Dr. N. Veera babu, Dr. Monika, Dr. Mahesh, Dr. Sai Kiran, Dr. Daniel, Elsinraju, Srilatha, Shreya, Ranay, Nisha, Kunal, Jayendra pandey, Yusuf, Payal, Dheeraj, Latha and Ganesh for their cooperation and help.

I thank all my friends Nirosha, Divya, Niharika, Asif, Chaithanya, Rohini, Aswini, Bhuvan, Mohan, Rajesh, Madhavi, Jyothi, Saranya, Mahalakshmi, Mariya and all friends from School of Life sciences.

I thank Bioinformatics facility (SLS facility) for providing servers for molecular simulation studies.

I thank funding agencies DST-FIST, DBT CREBB, UGC, UGC-SAP, DST, DBT, CSIR and UPE-II for financial support to the department and lab.

I sincerely thank CSIR for the financial support in the form of JRF and SRF fellowship.

Thanks to the non-teaching and technical staff of School of Life Sciences.

I am immensely grateful to all my teachers from Department of Plant Sciences, University of Hyderabad and all teachers from my childhood.

Finally, I thank my parents (**Mr. N. Venkata Basava Nageswara Rao, Mrs. N.Venkata Lakshmi**), Husband (**Dr. K. Subba Rao**), sister (**N. Dhana Parvathi**), Uncle, aunt and all my family members for their love, affection and moral support throughout my doctoral research.

Aparna Nerusu

Dedicated

To

My Beloved Parents

Content

List of Figures

Figure 3.11 Interaction of IAA to HSA and its domains. For low concentration range, 12.5µM – 200 µM IAA was used and for high concentration 600-1600 µM of IAA, with linear concentration range is used. IAA used for high concentration analysis was purchased from SRL (88318)

Figure 3.12 Interaction of Melatonin to HSA and its domains. For low concentration range, 12.5µM – 200 µM melatonin was used and for high concentration 900-1600 µM of melatonin, with linear concentration range is used.

Figure 3.13 Interaction of CMPF to HSA and its domains. For low concentration range, 12.5µM – 200 µM CMPF was used and for high concentration 900-1600 µM of CMPF, with linear concentration range is used.

Figure 3.14 Interactions of HA to A) D2, B) D3, C) D2-3 and D) HSA were analyzed using molecular docking studies. The interactions involved in complex formation were visualized using PyMol software.

Figure 3.15 Interactions of IAA to A) D2, B) D3, C) D2-3 and D) HSA were analyzed using molecular docking studies. The interactions involved in complex formation were visualized using PyMol software.

Figure 3.16 Interactions of Melatonin to A) D2, B) D3, C) D2-3 and D) HSA were analyzed using molecular docking studies. The interactions involved in complex formation were visualized using PyMol software.

Figure 3.17 Interactions of CMPF to A) D2, B) D3, C) D2-3 and D) HSA were analyzed using molecular docking studies. The interactions involved in complex formation were visualized using PyMol software.

Figure 3.18 Pictorial representation of the final result of the study, showing that D3 has high affinity than D2 towards HA, IAA and Melatonin.

Figure 4.1 A) Q5 amplification of pPIC9K+HSA using primers having mutation. The band corresponds to 11 k.bp is the amplified product and Unamplified (Unampli) is the template plasmid. B) After *Dpn* I digestion the template was digested as there is no band in Unamplified and in case of mutants only PCR amplified product having mutation is there. C) Colony PCR conformation of the mutants.

Figure 4.2 SDS-PAGE gel showing migration of HSA and its variants.

Figure 4.3 Structural analysis of HSA and its variants using CD Spectroscopy. A) The CD spectra of 0.5μM rHSA, K240E, D375H and K240E/D375H. B) % of Secondary structures were obtained using CDNN software.

Figure 4.4 Fluorescence emission spectra of A) rHSA, B) K240E, C) D375H and D) K240E/D375H in presence of increasing concentration of phenylbutazone. Modified Stern-Volmer plots for the interaction of phenylbutazone to a) rHSA, b) K240E, c) D375H and d) K240E/D375H

Figure 4.5 CD spectroscopy studies to understand the effect of phenylbutazone binding on structure of A) K240E, B) D375H, C) K240E/D375H and D) rHSA.

Figure 4.6 Fluorescence emission spectra of A) rHSA, B) K240E, C) D375H and D) K240E/D375H in presence of increasing concentration of ibuprofen. Modified Stern-Volmer plots for the interaction of ibuprofen to a) rHSA, b) K240E, c) D375H and d) K240E/D375H.

Figure 4.7 CD spectroscopy studies to understand the effect of ibuprofen binding on structure of A) K240E, B) D375H, C) K240E/D375H and D) rHSA.

Figure 4.8 α-helical content of rHSA, K240E, D375H and K240E/D375H alone, in presence of 5μM phenylbutazone and in presence of 5μM ibuprofen.

Figure 5.1 Structures of 4A, 5A and 6M. The molecular weight of 4A, 5A and 6M is 286.41, 288.42 and 302.45 Da respectively.

Figure 5.2 A) Fluorescence emission spectra of PBS with pH 7.4, 10μM of 4A, 5A and 6M. B) Absorption spectra of DMSO, 10μM of 4A, 5A and 6M by taking PBS as baseline.

Figure 5.3 Stern–Volmer plot obtained by plotting concentration of A) 4A, B) 5A and C)6M on X axis and F_0 /F on Y axis. Slope of the graph gives Stern–Volmer quenching constant (K_{SV}), from that bimolecular quenching rate constant (K_q) was calculated. K_q is more than 2.0×10^{10} M^{-1} s^{-1} for all molecules showing the stable complex formation.

Figure 5.4 Fluorescence emission spectra of HSA in presence of increasing concentrations of A) 4A, B) 5A and C) 6M from 1μM to 9μM. Fluorescence quenching was shown with increasing concentrations of the molecules. There was no fluorescence emission for buffer and the ligands

in the given wavelength range from 300-500nm. Modified Stern–Volmer plots for a) 4A, b) 5A and c) 6M respectively, obtained by plotting Log [Q] values on X-axis and Log [dF/F] values on Y-axis.

Figure 5.5 Fluorescence emission spectra of AGP with increasing concentrations of A) 4A, B) 5A and C) 6M. Emission maximum for AGP is 340nm. Modified Stern–Volmer plots for a) 4A, b) 5A and c) 6M respectively, obtained by plotting Log [Q] values on X-axis and Log [dF/F] values on Y-axis.

Figure 5.6 Competitive binding analysis of A) 4A, B) 5A and C) 6M. 4A and 5A are competing with ibuprofen towards binding to HSA. 6M is competing with phenylbutazone. Modified Stern–Volmer plots for a) 4A, b) 5A and c) 6M respectively, obtained by plotting Log [Q] values on X-axis and Log [dF/F] values on Y-axis.

Figure 5.7 Circular Dichroism Spectra of HSA alone (red line) and with increasing concentrations of A) 4A, B) 5A and C) 6M. Characteristic spectrum of protein showing spectral minima at 208 and 222nm, indicating that the HSA is α-helical protein. Inset show the percentage of secondary structural elements of the HSA, obtained by deconvoluting CD spectra using CDNN software.

Figure 5.8 Docking of I) 4A, II) 5A and III) 6M with HSA. A), B) and C) from each panel is showing the HSA interaction, 3D view of ligand binding site and 2D view of ligand binding site with the interactions respectively. 4A and 5A are interacting with residues of IIIA domain. 6M is interacting with IIA domain of HSA.

Figure 5.9 A) Time dependent evolution of the radius of gyration and B) RMSD values for free HSA, HSA-4A, HSA-5A and HSA-6M complex during 100ns molecular dynamics (MD) simulation.

Figure 5.10 Root mean square fluctuations of atoms of HSA in free HSA compared to A) HSA-4A, B) HSA-5A and c) HSA-6M complex.

Figure 5.11 Interactions of 4A to HSA were shown after I) 3 ns, II) 6 ns and III) 10 ns from the 100ns molecular dynamics simulations. The 3D and 2D view of interactions were shown in panel A and B respectively. The 3D figure is showing the orientation of the molecule in the binding groove and the nature of the interactions were shown in 2D visualization.

Figure 5.12 Interactions of 5A to HSA were shown after I) 3 ns, II) 6 ns and III) 10 ns from the 100ns molecular dynamics simulations. The 3D and 2D view of interactions were shown in panel A and B respectively. The 3D figure is showing the orientation of the molecule in the binding groove and the nature of the interactions were shown in 2D visualization.

Figure 5.13 Interactions of 6M to HSA were shown after I) 3 ns, II) 6 ns and III) 10 ns from the 100ns molecular dynamics simulations. The 3D and 2D view of interactions were shown in panel A and B respectively. The 3D figure is showing the orientation of the molecule in the binding groove and the nature of the interactions were shown in 2D visualization.

List of Tables

Abbreviations

4A	4-Androstene-3-17-dione
5A	5β-androstane-3-17-dione
6M	(+)-6-methyl-5β androstane-3-17-dione
AGP	α 1-Acid Glycoprotein
AOX 1	Alcohol Oxidase 1
Aβ	Amyloid-β peptide
BCA	Bicinchoninic Acid
BMGY	Buffered Glycerol-complex Medium
BMMY	Buffered Methanol-complex Medium
CMPF	3-carboxy-4-methyl-5-propyl-2-furanpropanoic acid
D1	Domain 1
D1-2	Domain 1 and 2
D2	Domain 2
D2-3	Domain 2 and 3
D3	Domain 3
DMSO	Dimethyl sulfoxide
EDC	N-ethyl-N'-(dimethylaminopropyl) carbodiimide
FA	Fatty acid
FcRn	Neonatal Fc receptor
HA	Hippuric acid
HSA	Human Serum Albumin

HSQC	Heteronuclear single quantum coherence
IAA	Indole-3-acetic acid
MARS	Molecular Adsorbent Recirculating System
MDS	Molecular dynamics simulations
MV^{2+}	Methyl viologen
NHS	N-hydroxy-succinimide
NMR	Nuclear magnetic resonance
NO	Nitric Oxide
PAMAM	Polyamidoamine
PCR	Polymerase Chain Reaction
PDB	Protein Data Bank
RDB	Regeneration Dextrose Medium
Rg	Radius of gyration
RMSD	Root mean square deviations
RMSF	Root mean square fluctuations
RU	Response Units
SPAD	Single-pass albumin dialysis
SPR	Surface Plasmon Resonance
YNB	Yeast Nitrogen Base
YPD	Yeast Extract Peptone Dextrose Medium

Chapter 1

Introduction

Introduction

1.1 Human serum albumin (HSA)

Human serum albumin (HSA) is very attractive molecule for biochemists and chemists. It is the well-studied protein in the history of biochemistry. It is a member of a family of homologous proteins and this family includes afamin, α-fetoprotein (AFP) and vitamin D binding protein (DBP) (Peters Jr, 1995, Fanali et al., 2012). It is the most abundant, monomeric and multi-functional protein. Also well known for its extraordinary ligand binding nature and acts a major transport and depot protein for many exogenous and endogenous compounds. Most part of the literature exhibits that HSA is an important protein which have good binding properties with small molecules. Apart from its carrier property, this protein can regulate plasma oncotic pressure, displays (pseudo-) enzymatic properties and accounts for most of the anti-oxidant capacity of human plasma. Based on HSA properties numerous applications were emerged out in various fields of medicine and lot more strategies for drug design, drug delivery, and half-life extension of drugs.

1.2 Human serum albumin metabolism

HSA is the abundant plasma protein and comprises of 60-65% of the total plasma protein. It is also a component of body secretions including milk, sweat, tears and saliva. Liver is the major site of synthesis for HSA. Hepatocytes secrete 13-14 g of albumin every day. In the hepatocytes albumin gets produced as pre-pro-albumin with 609 amino acids. The cells secrets mature protein of 585 amino acids. Adults have 120 g of albumin in the circulation resulting in the plasma concentration of 0.6 mM and 240 g in extravascular pool at lower concentrations. 14 g of albumin, which is equivalent amount of HSA that produced every day, is catabolized every day. The circulatory half-life of the protein lies for 19 days (Peters Jr, 1995, Fanali et al., 2012).

1.3 HSA protein structure and biochemical properties

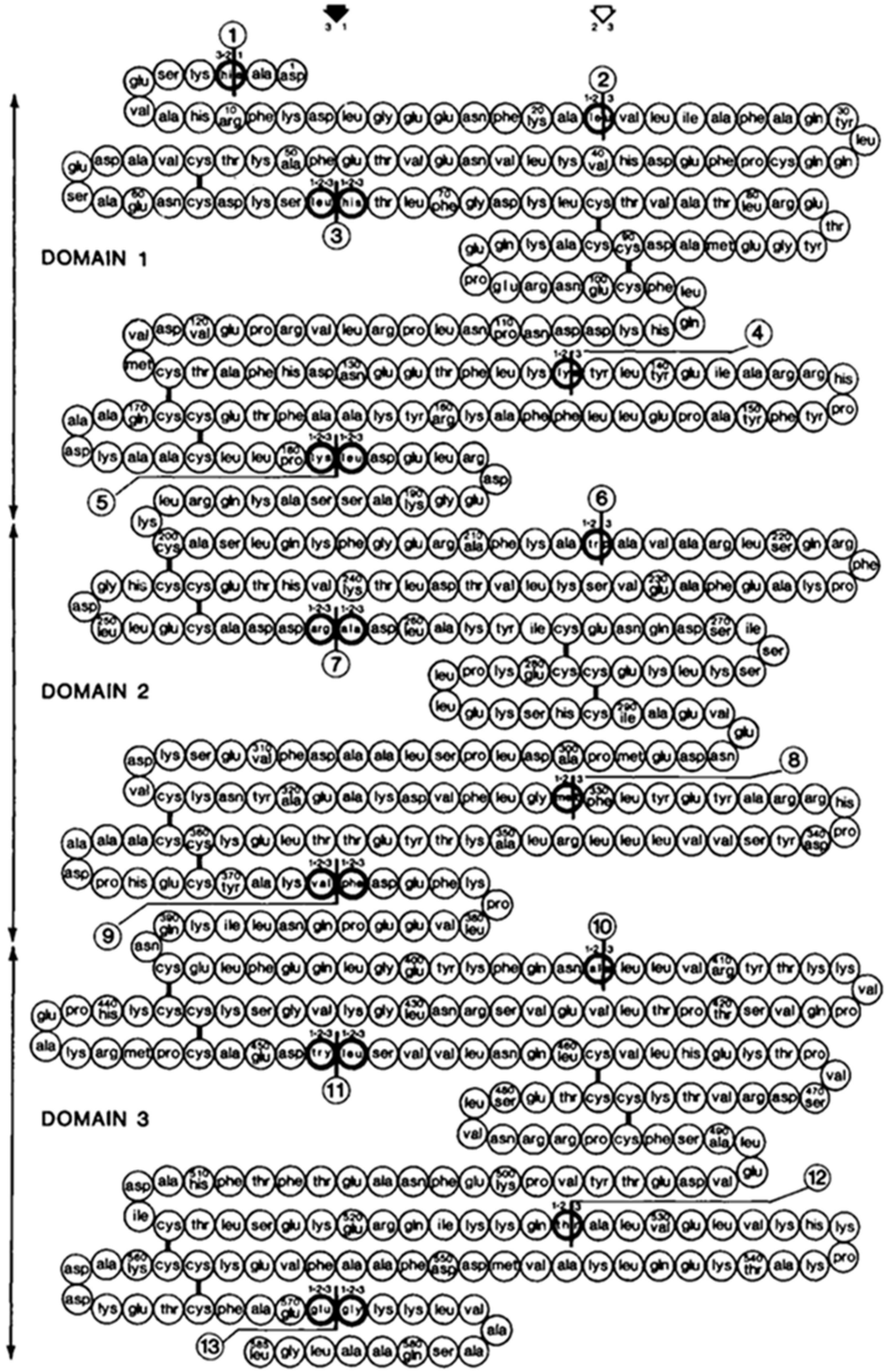

Figure 1.1 Primary structure of HSA (Adopted from Peters., 1995)

HSA is a single polypeptide chain comprises of 585 amino acids. The gene for HSA is located in chromosome 4 (ALB; GenBank reference sequence NC_000004.11). It is a non-glycosylated protein with the molecular mass of 66 kDa. Figure 1.1 shows the primary structure of HSA. There is only one single tryptophan residue is present at 214 position. Methionine and isoleucine are also low abundant in this protein. The protein is rich in hydrophobic amino acids such as alanine and leucine and also rich in charged ionic amino acids such as glutamic acid and lysine. There are 98 acidic amino acids (Glutamic acid 62 + Asparitic acid 36) and 83 basic amino acids (Lysine 59 and arginine 24) gives a net charge of -15 at physiological pH, which aids the solubility of the protein (Peters Jr, 1995). This highly charged and abundant protein creates Donnan effect in the capillaries and there by regulates the fluid distribution across the capillary wall (Kragh-Hansen et al., 2013). Due to the high number of acidic and basic amino acids, HSA structure undergoes conformational transitions at different pH values. This protein also shows significant buffering capacity. The significant feature of the protein is the presence of 35 cystine residues, out of which 34 are forming 17 disulfide bonds. One cystine residue (Cys34) exists as free thiol group and it has physiological significance as it is responsible for the redox property of the protein (Anraku et al., 2013, Bruschi et al., 2013). In adults, 80% of Cys34 is present as free thiol and the rest is in the form of disulfides with cysteine, homocysteine and glutathione.

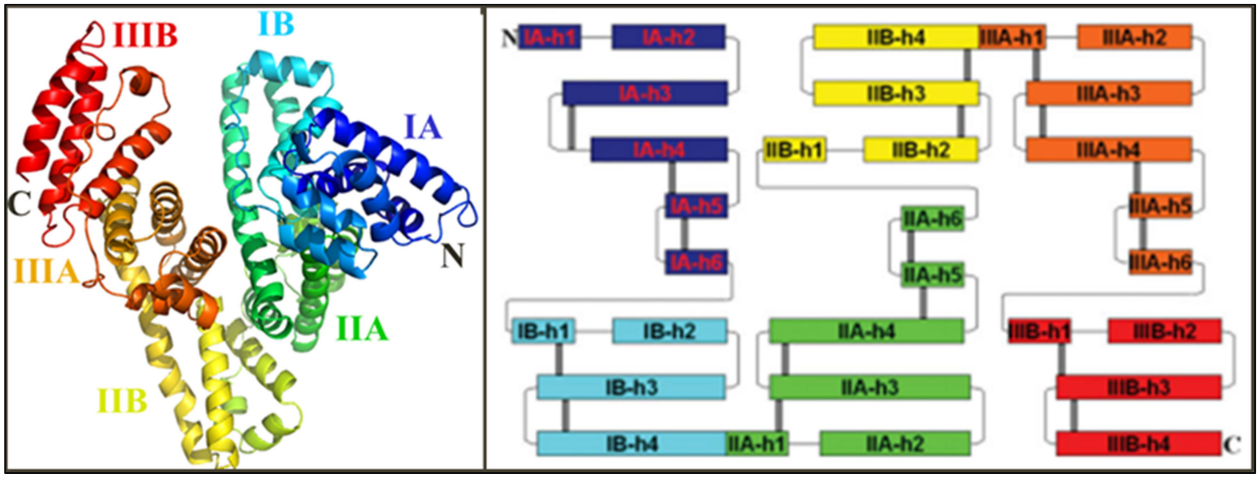

Figure 1.2 Three dimensional structure and domain organization of HSA. The distribution of disulfide bonds were shown in the picture (Adopted from Paris *et al.,* 2012).

In its tertiary structure the protein is a globular heart shaped molecule with an approximate dimension of 80 × 80 × 30 Å. He and Carter reported the first crystal structure of

HSA (He & Carter, 1992), after that around 70 crystal structures of HSA with bound ligands were deposited in PDB (Fanali et al., 2012). It has three homologous domains, namely, domain I, II and III and each domain can be further subdivided into two subdomains (A and B). The most unique structural feature of the protein is its α-helical content and its disulfide bond pattern. The protein is more abundant of α-helix with 67%. Each domain consists of ten helices out of which six are present in subdomain A and four are present in subdomain B. These two subdomains were connected by a long extended loop. There are eight Cys-Cys sequences, linked to the nearest residues in the chain before the pair and after the pair, to form paired loops. There exist a symmetry in the polypeptide folding and the distribution of disulfide bonds among the three homologous domains (Paris et al., 2012). Figure 1.2 shows the tertiary structure of HSA and the disulfide bond distribution. Despite their structural similarity, each domain interacts with the neighbor domain in different ways forming two dissimilar binding sites near the domain interface.

1.4 Functions of HSA

HSA contributes to the 80% of colloid osmotic blood pressure. Even though it is low molecular weight protein compared to other plasma proteins, due to its abundance and its net charge at physiological pH, the protein can regulate the colloid osmotic pressure of plasma. As the net charge is -14, it can create Donnan effect across capillary membranes, there by regulates the fluid distribution between intravascular and extra vascular compartments. Other important role of HSA in plasma is its transporter role. The protein acts as transport and depot for several endogenous as well as exogenous metabolites and drugs in the blood. Albumin is the major transporter for fatty acids.

HSA is not only a binding cargo for several ligands, but also can modify its bound ligands through its enzymatic activity, known as pseudo-enzymatic activity (Kragh-Hansen et al., 2002, Kragh-Hansen, 2013). Most pronounced enzyme activities of the protein are different kinds of hydrolysis reactions. The enzymatic activity of HSA includes esterase activity (Walker, 1976, Yvon & Wal, 1988, Sakurai et al., 2004). The esterase activity is performed by Tyr411 and Lys199, involves two different reaction mechanisms. The action mechanism involving Tyr411 include, nucleophile attack of Tyr411, results in the formation of acylated HSA. Further, in second step the acylated protein is deacylated by general acid or base catalysis by water and this

is the slow and rate limiting step (Sakurai et al., 2004). Lys199 performs nucleophilic substitution reaction. Along with esterase activity HSA can perform, thioesterase activities involving Cys34 (Pedersen & Jacobsen, 1980), RNA-hydrolyzing activity (Gerasimova et al., 2010), hydrolysis of acyl glucuronides (Georges et al., 2000), phosphatase activity (Kwon et al., 1987), detoxification reactions (Sogorb et al., 2008, Sogorb & Vilanova, 2010), activation of prodrugs by hydrolysis and enolase activity (Drmanovic et al., 1999). It can also performs condensation reactions such as, aldol condensation reaction (Benedetti et al., 2011) and biginelli reaction (Sharma et al., 2013). Due to its enzymatic property, it can modify some ligands and also can modify the toxins there by reducing their effect. Apart from enzymatic property, HSA has antioxidant property and Cys34 is responsible for the redox properties of HSA (Anraku et al., 2013). It can inactive reactive oxygen and nitrogen species due the presence of Cys34 and other six methionine residues (Iwao et al., 2012).

1.5 Ligand binding property of HSA

Albumin is an allosteric protein with more than one binding site and also can interact with wide spectrum of the molecules. The three dimensional structure of the protein enables it to accommodate more than one ligand at a time. Ligand binding property of HSA is very much useful to understand the drug distribution and which is major determinant of the pharmacokinetics and pharmacodynamic profile of the drugs and also enable drug designing. The binding affinity is the major parameter that determines the bound and free concentration of drugs and the unbound form of the drug that can perform its therapeutic effect. The drug binding to HSA can be affected by the presence of other endogenous ligands either by competition or by allosteric mechanism. For instance, the anti-coagulation activity of warfarin can be increased by co-administering phenyl butanone, which displaces the warfarin and thereby increasing free concentration of warfarin (Aggeler et al., 1967). The changes in albumin structure, albumin concentration and accumulation of endogenous ligands results in altered drug binding. For example, the reduced drug binding in uremic patients is due to the displacement of drugs from binding sites by increased level of uremic toxins (Takamura et al., 1997). Altered drug binding further alters the pharmacokinetic properties. Understanding the pharmacokinetics in diseased state or in case of modified albumin is very much useful to serve patient with proper medication. Thus, understanding drug–albumin interactions in various clinical situations is useful for optimal

therapy. In case of ligands, binding to HSA results in increased solubility of hydrophobic molecules, protects against oxidation and prolongs the half-life.

1.6 Nature of ligands that interact with HSA

Table 1.1 The association constant values obtained for the binding of phytochemicals to HSA.

Phytochemical	**Association constant value (M^{-1})**
3-trans-feruloyl maslinic acid	1.42 X 10^8 (Subramanyam et al., 2009b)
Asiatic acid	3.86 X 10^4 (Gokara et al., 2014)
Andrographolide	1.85 X 10^4 (Yeggoni et al., 2017)
Betulinic acid	1.685 X 10^6 (Subramanyam et al., 2009a)
Corilagin	4.2 X 10^5 (Yeggoni et al., 2016a)
Embelin	5.9 X 10^4 (Yeggoni et al., 2016b)
L-Dopa	1.8 X 10^4 (Yeggoni & Subramanyam, 2014)
Lupeol	1.84 X 10^4 (Kallubai et al., 2015)
Menthol	2.7 X 10^4 (Yeggoni et al., 2018)
Piperine	3 X 10^4 (Yeggoni et al., 2015)
β-Sitosterol	4.6 X 10^3 (Sudhamalla et al., 2010)
Trimethoxy flavone	1.0 X 10^3 (Gokara et al., 2010)

Enormous literature is available regarding HSA with binding of several ligand (or) drug molecules. Thus, HSA can interact with wide spectrum of molecules. The chemical nature of the molecules varies from inorganic metal ions, small organic hydrophobic molecules, peptides and proteins. The ligands that interact with HSA are both exogenous and endogenous in nature. Endogenous molecules include nutrients such as fatty acids and amino acids, hormones (tyroxines), metabolic wastes like (uremic toxins) etc. Exogenous ligands include drugs and other molecules.

The list of the ligands that interacts with HSA is very huge and some of them are given here. It can bind and transport nitric oxide (NO). Dendrimers such as PAMAM have tremendous applications in drug delivery and these molecules can interact with HSA (Giri et al., 2011). Further, HSA can interact with bacterial surface proteins (Lejon et al., 2004), carbon nano-

particles (Mandal et al., 2013), metal nanoparticles, various organic molecules such as antibiotics, organic dyes (Naveenraj & Anandan, 2013), C_{60} – fullerene (Qu et al., 2008). From our laboratory, we have reported the binding mechanism of various bioactive phytochemical to HSA and also reported the association constant values using fluorescence spectroscopy (Table 1.1) (Subramanyam et al., 2009a, Subramanyam et al., 2009b, Gokara et al., 2010, Sudhamalla et al., 2010, Gokara et al., 2014, Yeggoni & Subramanyam, 2014, Kallubai et al., 2015, Yeggoni et al., 2015, Yeggoni et al., 2016a, Yeggoni et al., 2016b, Yeggoni et al., 2017, Yeggoni et al., 2018).

1.7 Binding sites

1.7.1 Drug binding sites

For the first time in 1975 Sudlow showed the presence of two major drug binding sites in HSA, known as Site I and Site II (Sudlow et al., 1975, Sudlow et al., 1976). Later the albumin fragments generated by pepsin and trypsin were used to locate these two sites in HSA (Bos et al., 1988a, Bos et al., 1988b). The result of this study showed the location of Site I and Site II on domain II and III of HSA, respectively. Further, crystallographic studies enlighten the exact location and amino acid residues that are forming binding site (He & Carter, 1992). Site I is located in subdomain IIA and Site II is located in subdomain IIIA of HSA.

Site I is known as warfarin binding site and is located in IIA domain. This site is composed of two large apolar clusters and two polar clusters. One of the polar cluster comprises of basic amino acids, such as Lys195, Lys199, Arg218 and Arg222, is located at the entrance of the site and the second polar cluster is located at the bottom of the site. The second polar cluster includes side chains of Tyr150, His242 and Arg257. This site is larger and flexible site, which is larger than site II and it can be divided into sub sites (Yamasaki et al., 1996, Yamasaki et al., 2004). This site can accommodate more than one ligand at a time. This is having the extended binding regions, involving residues from IIB and IIIA. The entrance of the site faces towards IIIA and this site shows poor stereo selectivity. Ligands that binds to Site I are bulky heterocyclic molecules with negative charge. Warfarin, phenylbutazone, azapropazone, indomethacin, furosemide and bucolome are some of the drugs binding to site I.

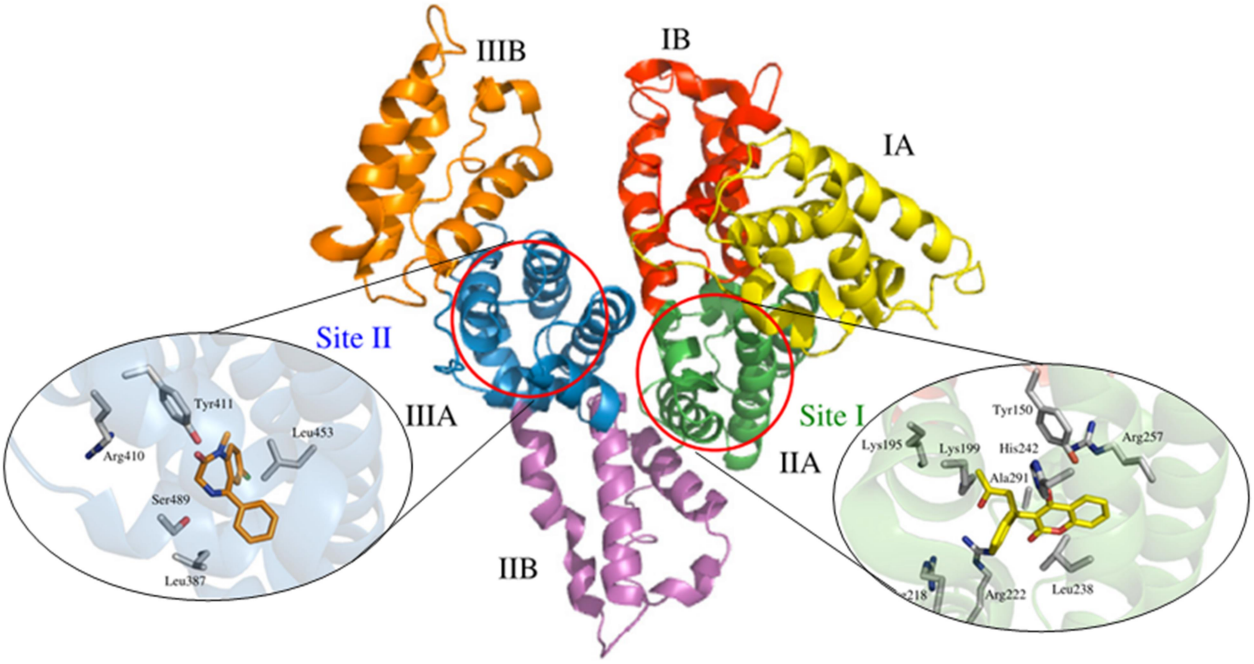

Figure 1.3 Location of drug site I and site II of HSA. The interaction of warfarin in site I (PDB ID: 2BXD) and the interaction of diazepam to site II (PDB ID: 2BXF) is shown in the picture (Adopted from Yamasaki *et al.,* 2013).

Site II is located in IIIA domain and is smaller, when compared to site I. The binding pocket entrance is exposed to the solvent. The binding pocket is apolar cavity with polar entrance with Tyr411 and Arg 410. The residues such as Glu450 and Arg485 in subdomain IIIA and Arg348 and Glu383 from subdomain IIB form salt bridges, which stabilizes the pocket entrance. The arrangement of the binding pocket residues favors the binding site II drugs, which are aromatic carboxylic acids. The narrow binding site shows steroselectivity. For e.g. the affinity of (R)-ibuprofen is higher than (S)-ibuprofen (Itoh et al., 1997). Diazepam, diflunisal, ibuprofen, diclofenac and etodolac are the drugs that can bind to site II. Figure 1.3 shows the location of the two drug binding sites in HSA.

Knowledge of drug binding site is a very important as it is useful to understand the binding mechanism such as competitive drug binding and allosteric interaction.

1.7.2 Fatty acid binding sites

HSA is the major transporter for fatty acids and interacts with both saturated and unsaturated fatty acids with different chain lengths. In physiological condition, the mole ratio of fatty acid to

HSA is around 0.5-4. Crystal structure (Petitpas et al., 2001, Curry, 2002, Curry, 2009, Fanali et al., 2012) and solution state structure using NMR studies (Krenzel et al., 2013, Barnett et al., 2013, Hamilton, 2013) provided the information regarding the fatty acid binding to HSA. Later MD simulation approaches using crystal structure data build upon the existing knowledge to better understand the binding nature of fatty acids and their effect on ligand binding (Fujiwara & Amisaki, 2013).

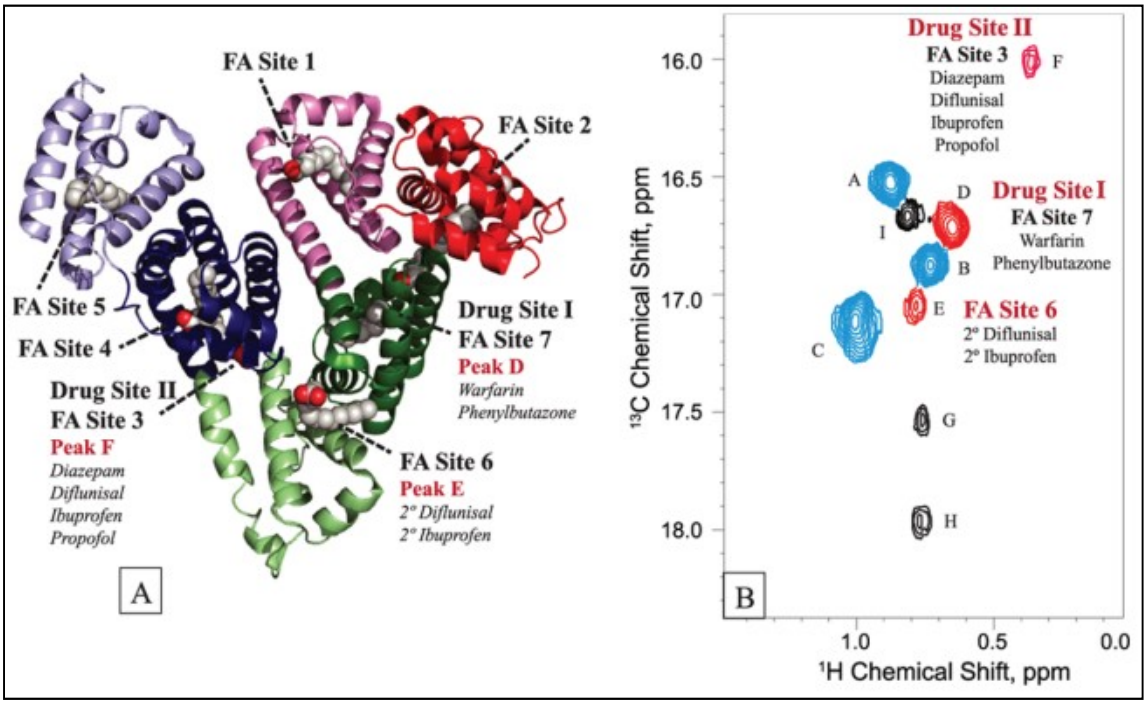

Figure 1.4 Correspondence of fatty acid and drug binding sites on HSA by 2D NMR study. A) Crystal structure of HSA bound to seven labeled myristic acid molecules along with that drugs and endogenous compound binding sites were also shown. B) $^{1}H - {}^{13}C$ HSQC spectrum of the oleic acid-HSA complex at 4:1 ratio (Adopted from Krenzel *et al.,* 2013).

Earlier it was found that there are seven fatty acid binding sites in HSA (Figure 1.4) and their affinities were studied (Simard et al., 2006). The sites are distributed across the three domains of HSA. FA site 1 is located in sub-domain IB, the heme binding site. Along with heme, other small molecules such as bilirubin and prostaglandins also bind to FA site 1. FA site 2 is located at the interface between IA and IIA. FA site 3 and FA site 4 are located within IIIB, which is the major drug binding site known as site II. FA site 5 is located at IIIB. FA site 6 is located between IIA and IIB and finally FA site 7 is at IIA, which is also a major drug binding

site known as site I. FA-binding sites 5, 4, and 2 are high-affinity sites, and 1, 3, 6, and 7 as low-affinity sites. Sites 5 and 6 have been identified as the sites with highest and low FA affinities, respectively. Later two other low affinity FA sites were also reported. FA binding can modulate ligand binding either by competitive or by allosteric mechanism (Barnett et al., 2013).

1.7.3 Heme binding site

HSA has a single heme binding site, located in subdomain IB region (Zunszain et al., 2003) as shown in Figure 1.5. It can bind and scavenge heme–Fe in plasma and plasma level of HSA–heme–Fe (III) is about $1X10^{-6}$ M. HSA–heme–Fe (II) can interact with O_2, CO, •NO and also possess (pseudo-)enzymatic property, where it can scavenge reactive nitrogen and oxygen species. As HSA–heme–Fe (II) can interact with O_2, tailor made heme pocket can be designed by HSA mutants as artificial O_2 carrier (Komatsu et al., 2004, Komatsu et al., 2005). Apart from heme-HSA complex, other porphyrin molecules also can bind with HSA at same site. The complex of HSA and copper–phthalocyanine can be used as catalyst in Diels–Alder reaction (Reetz & Jiao, 2006). HSA - (Zn(II)-protoporphyrin IX) complex can perform photosensitized reduction of water to hydrogen (H_2) using methyl viologen (MV^{2+}) as an electron relay (Komatsu et al., 2006).

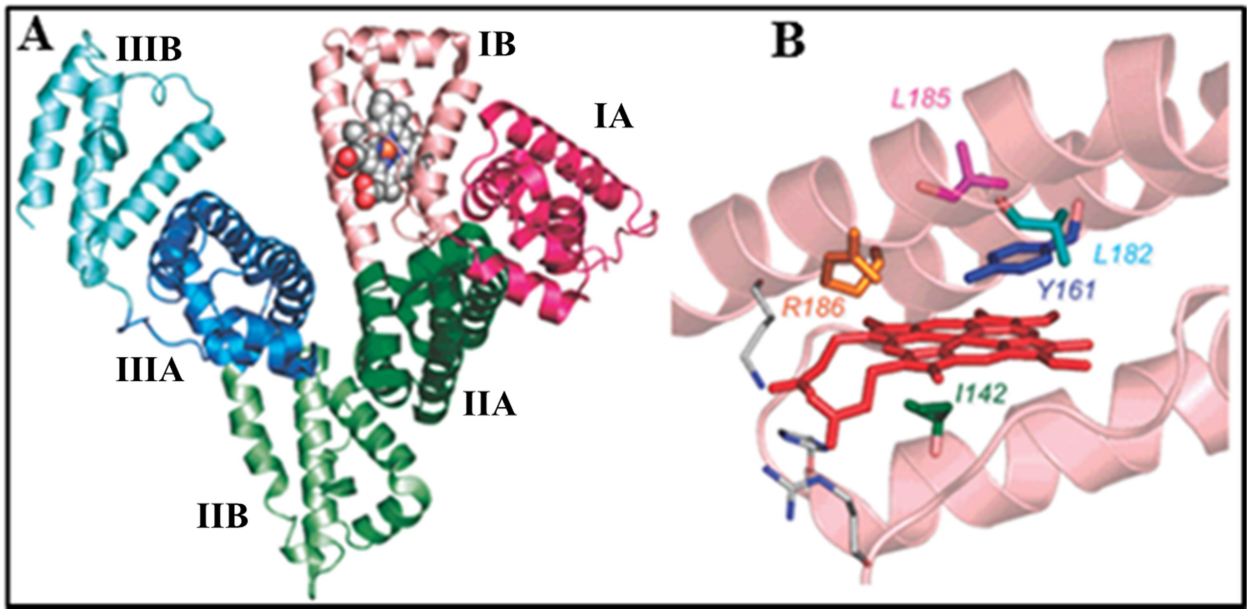

Figure 1.5 A) HSA-heme complex. Heme is shown in a space-filling representation. B) Heme pocket structure in subdomain IB and positions of amino acids (Adopted from Komatsu *et al.,* 2007).

1.7.4 Metal ion binding sites

In the blood specific proteins bind and transport metal ions, for e.g. transferrin and ceruloplasmin binds iron and copper respectively. Apart from these proteins some transition metal ions such as copper, zinc, cobalt, iron, mercury, nickel, cadmium, vanadium, gold and platinum can bind to HSA. HSA contains four metal binding sites, known as N-terminal site, Cys34 residue and its environment, site A (located at the interface of domains I and II) and site B. N-terminal site is composed of first three N terminal residues (Asp-Ala-His) and binds to metal ions such as Cu(II) and Ni(II) (Bal et al., 2013).

1.8 Applications of HSA

HSA is a valuable biomarker of many diseases such as cancer (Gupta & Lis, 2010), rheumatoid arthritis and ischemia (Sbarouni et al., 2011). HSA therapy was used in various clinical situations such as chronic liver disease, hypoalbuminemia, where HSA was given to the required patients externally (Mendez et al., 2005). Using plasma derived HSA has potential risk of transmitting pathogens such as viruses. There are several studies to replace plasma derived HSA with recombinant HSA (rHSA). rHSA produced using *P. pastoris* was intensively evaluated for this purpose (Kobayashi, 2006). Large scale production of rHSA was successfully achieved in yeast and rice expression systems (Kobayashi, 2006, Zhang et al., 2013). The presence of methanol inducible alcohol oxidase gene promoter (*AOX1*) enables high level expression of rHSA using methylotropic yeast *P. pastoris* and the expression levels achieved were above 3 g/L. Also from clinical trials the rHSA produced from *P. pastoris* showed similarly to plasma derived HSA in safety and pharmacodynamics tests (Chen et al., 2013).

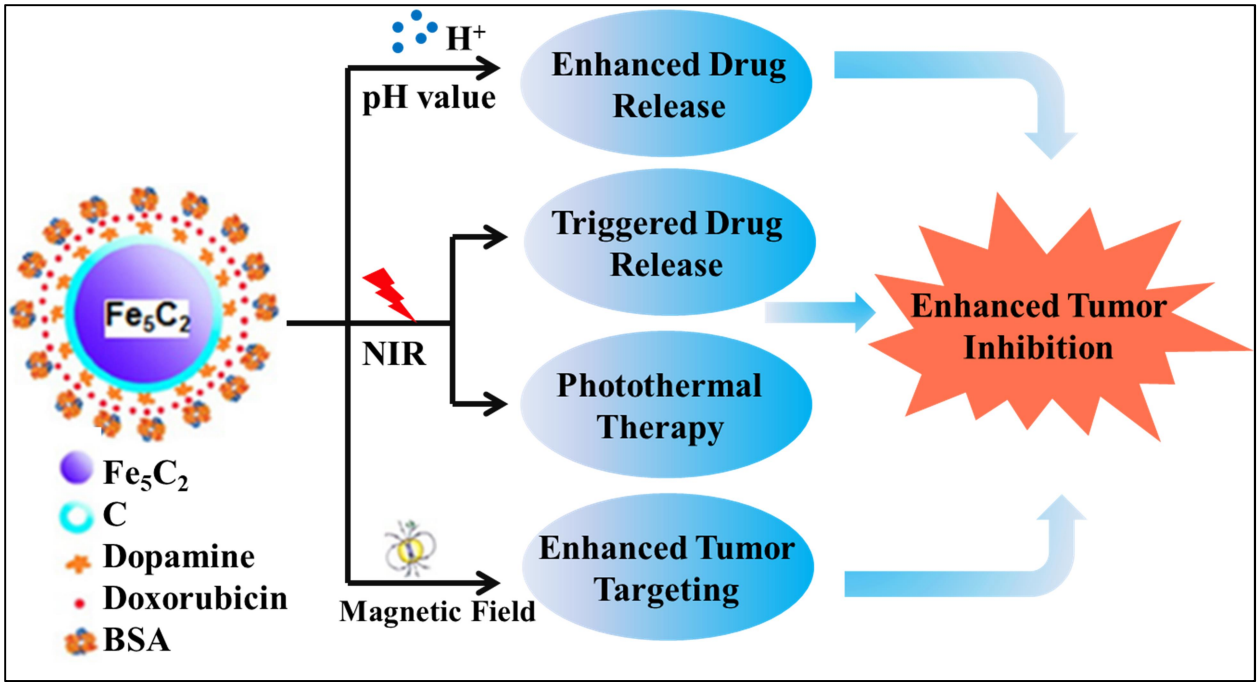

Figure 1.6 Multi-stimuli controlled drug carrier for cancer therapy (Adopted from Yu *et al.,* 2015).

The wide range of biochemical properties, binding nature and enzymatic properties of HSA enable the application of HSA in various fields of medicine, especially in case of drug design and drug delivery. The competitive binding or drug displacement phenomenon can be applied to increase the therapeutic outcome of drugs by administration of displacer drug. For e.g. the pain relief in rheumatoid arthritis patients using diclofenac suppository can be increased by administration of nabumetone (Setoguchi et al., 2013). The enzymatic properties of HSA make it useful for therapeutic purposes and for organic synthesis. HSA can be used as catalyst in chemical reactions such as Diels – Alder cycloaddition, Gewald condensation, Aldol and Knoevenagel condensation, Morita–Baylis–Hillman, Kemp elimination, Thio-Michael addition and Henry reaction (Albanese & Gaggero, 2015). Pharmacokinetic profile of the drugs can be improved based on albumin binding (Elsadek & Kratz, 2012). Prodrugs can be designed based on HSA binding and enzymatic property (Zheng et al., 2014).

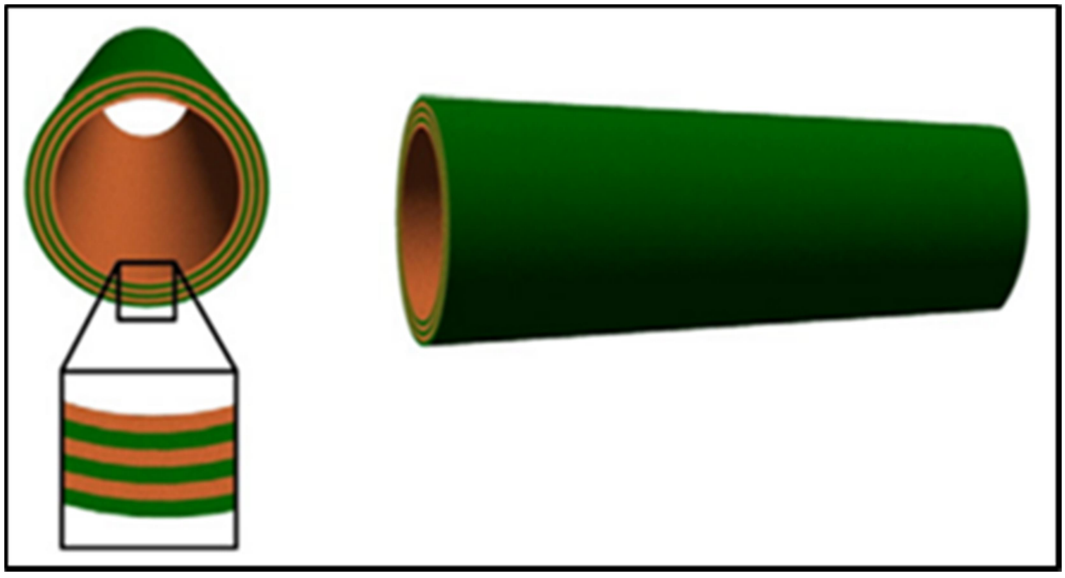

Figure 1.7 Schematic representation of a nanotube made of alternating layers of HSA (orange) and poly-L-arginine (green) (Adopted from Qu *et al.,* 2010).

Several kinds of nanomaterial were prepared using HSA for various applications. HSA nanoparticles were widely used for the drug delivery especially in case of cancer and also for imaging (Sheng et al., 2014, Lee et al., 2015, Lomis et al., 2016, An & Zhang, 2017). Figure 1.6 shows the scheme for stimuli controlled drug delivery using albumin nano formulation (Yu et al., 2015). HSA nanotubes (Figure 1.7) were prepared for several biomedical applications such as ligand capturing and virus trapping (Qu & Komatsu, 2009, Komatsu, 2012).

The binding of HSA to FcRn (Figure 1.8) is responsible for its extraordinary half-life of 19 days (Andersen et al., 2012, Sand et al., 2015). This property of albumin has been used to improve the half-life of several therapeutic molecules by direct genetic fusion (Santagostino et al., 2012) or by covalent (Kratz, 2008) or non-covalent association (Elsadek & Kratz, 2012) of the therapeutic molecules to albumin (Sleep et al., 2013). HSA can interact with amyloid-β peptide (Aβ) in blood plasma and inhibits Aβ fiber growth (Stanyon & Viles, 2012).

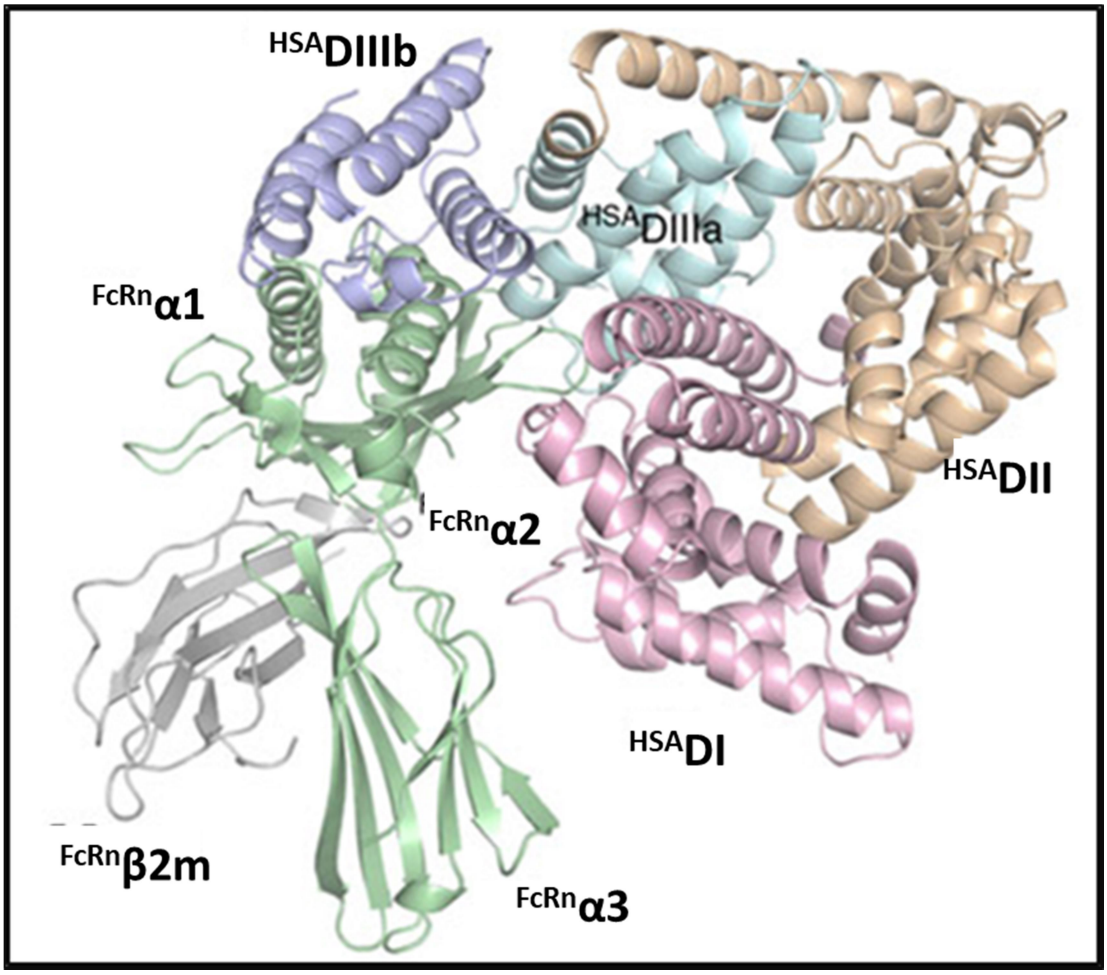

Figure 1.8 Interaction of FcRn to HSA (Adopted from Andersen *et al.,* 2012)

Albumin can be used as dialysate in extra corporeal dialysis. The liver support systems such as Molecular Adsorbent Recirculating System (MARS) (Figure 1.9) and the single-pass HSA dialysis (SPAD) were developed by using albumin as dialysate (Lee et al., 2015). In MARS, 20% HSA is used as dialysate and this dialysate can be further cleaned by passing through charcoal and an anion exchange resin (Figure 1.9). The HSA-heme-Fe (II) complex can be used to prepare artificial oxygen carriers (Komatsu et al., 2004, Komatsu et al., 2005, Mahammed & Gross, 2005, Komatsu et al., 2007,). Biomaterial such as surgical adhesives, and surgical sealants can be prepared using coagulating property of HSA (Spotnitz & Burks, 2008).

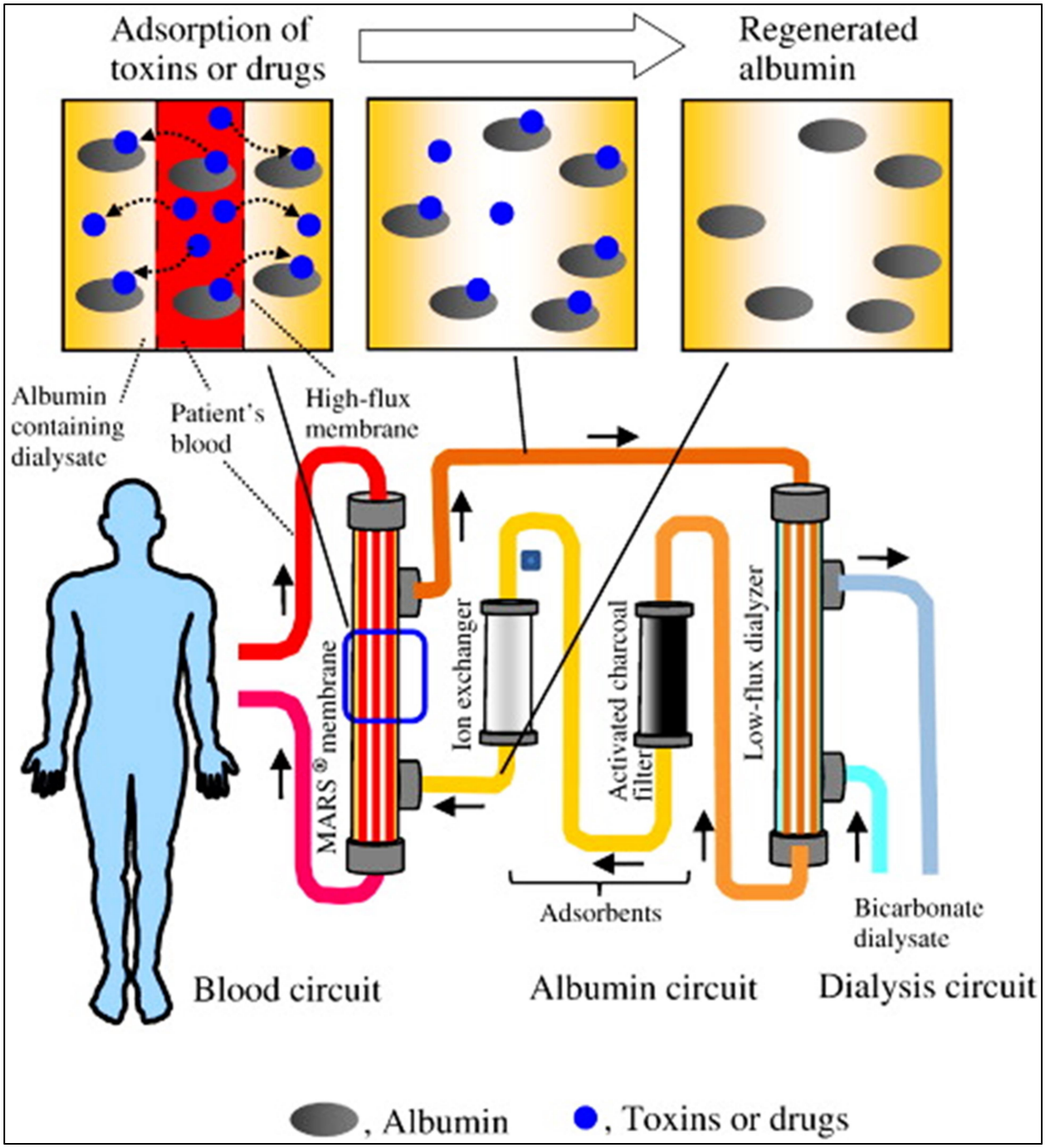

Figure 1.9 Schematic representation of MARS (Adopted from Yamasaki *et al.,* 2013)

As mentioned here HSA has an extraordinary ligand binding capacity and has several significant biochemical and physiological properties, due to which it has a lot of clinical applications. The ongoing research with this protein is mainly focused on application of this protein in the field of drug design and drug delivery, especially in case of cancer therapy. The ligand binding property of HSA was well exploited for this purpose and studying the binding mechanism of therapeutic molecules gives the basic knowledge for such trails. The binding mechanism of wide range of molecules, including cancer drugs, was reported in literature from several studies (Wang et al., 2013, Naveenraj & Anandan, 2013). Looking at the importance of HSA, here I have expressed the domains of HSA to understand the binding nature of different uremic toxins.

Here, I studied the interaction of HSA, its domains and mutants with some of the bioactive compounds. The interaction of protein bound uremic toxins with HSA and its domains was studies for my thesis. As I discussed in the applications part, HSA can be used as dialysate in the extracorporeal dialysis. Further understanding the binding mechanism of protein bound uremic toxins with HSA domains can help to improve the efficacy of dialysate. I have also studied the interaction of the drugs such as phenylbutazone and ibuprofen with the two natural variants of HSA, which gives the basic information to understand the effect of mutation on drug binding as well as to understand the pharmacokinetics of this drug in the populations having these natural variants. The two natural variants, Herborn (K240E) and Milano Slow (D375H) were reported for their reduced α-helical content. I want to know the effect of these mutations on the binding of phenylbutazone and ibuprofen. Further, I also studied the binding mechanism of HSA to androstenedione and its derivatives. With this we have framed the following three objectives for my present study.

Objectives

1. **Unravelling the binding efficiency of uremic toxins with the yeast expressed domains of human serum albumin.**

2. **Studying the effect of Herborn (K240E) and Milano Slow (D375H) human serum albumin variants towards binding of phenylbutazone and ibuprofen.**

3. **Unraveling the stability of plasma proteins upon interaction of synthesized androstenedione and its derivatives - biophysical and computational approach.**

Chapter 2

Methodology

Methodology

2.1 Cloning of HSA, its domains and its variants

2.1.1 Material used for cloning

Pichia pastoris strains and *Pichia* EasyComp transformation Kit were purchased from Invitrogen. Plasmid DNA isolation Miniprep kit and Gel extraction kit were obtained from MN technologies (MACHEREY-NAGEL GmbH & Co. KG), Germany. The primers used in this study were obtained from Integrated DNA Technologies, Inc. (IDT), USA. Restriction enzymes, T4 DNA ligase, and *Taq* polymerase were obtained from MBI Fermentas, Canada. High fidelity Q5 DNA polymerase was procured from NEB (New England Biolabs), USA. All the enzymes and kits were used as per the instructions given by respective manufacturers. Agarose was purchased from Sigma-Aldrich (USA) and antibiotic ampicillin was from Calbiochem. All routine media components for bacterial culture and yeast culture were obtained from HiMedia laboratories (India).

2.1.2 Media composition

Yeast Extract Peptone Dextrose Medium (YPD) Agar plates (for 100 ml):

Yeast extract, 1 g; Peptone, 2 g and Agar 2 g weighed and these three components were dissolved in 90 ml H_2O and autoclaved for 20 minutes. The solution was cool down to ~60 °C. 2g of D-Glucose was dissolved in 10 ml of water and added to the media after filter sterilization. The components were mixed and poured onto the petri plates.

LB Agar (or) Broth (For 1000 ml)

Yeast extract, 5 g; Peptone, 10 g; NaCl, 10 g; Agar, 15 g weight and dissolved in 1000 ml of distilled H_2O and autoclaved.

Buffered Glycerol-complex Medium and Buffered Methanol-complex Medium (BMGY and BMMY)

1% yeast extract; 2 % peptone; 100 mM potassium phosphate buffer, pH 6.0; 1.34% YNB (Yeast Nitrogen Base); 4×10^{-5} % biotin; 1% glycerol. For BMMY 1% methanol was used instead of glycerol.

Minimal Medium

1.34% YNB; 1% glycerol; 4×10^{-5} % biotin.

RDB Agar (Regeneration Dextrose Medium)

1 M Sorbitol; 1% Dextrose; 1.34% YNB; 4×10^{-5} % biotin; 0.005% of each amino acid (L-glutamic acid, L-methionine, L-lysine, L-leucine and L-iso-leucine).

2.1.3 Cloning of HSA and its domains

All the protocols for DNA isolation from *Pichia pastoris,* competent cells preparation, transformation and protein expression were adopted from Easy Select ^{TM} *Pichia* Expression Kit user manual (Invitrogen, 2010a, Invitrogen, 2010b). Genomic DNA was isolated from GS115/His^{+} Mut^{S} Albumin strain of *P. pastoris,* obtained with *Pichia* Expression Kit from Invitrogen, harboring HSA gene and used as template. Primers were specifically designed to amplify the required length of HSA coding sequence.

Table 2.1: Primer used for the amplification of domains of HSA

	Forward primer	Reverse primer
D1	5'CCGGAATTCGATGCACACAAGAGTGAGG 3'	5'TTGCGGCCGCTTATCTCTGTTTGGCAGAC 3'
D2	5'CCGGAATTCGATGAAGGGAAGGCTTCG 3'	5' TTGCGGCCGCTTACTGAGGCT CTTCCAC 3'
D3	5'CCGGAATTCGTGGAAGAGCCTCAG 3'	5' TTGCGGCCGCTTATAAGCCTAAGGCAG 3'
D1-2	5'CCGGAATTCGATGCACACAAGAGTGAGG 3'	5' TTGCGGCCGCTTACTGAGGCT CTTCCAC 3'
D2-3	5'CCGGAATTCGATGAAGGGAAGGCTTCG 3'	5' TTGCGGCCGCTTATAAGCCTAAGGCAG 3'

While designing primers, the restriction sites *Eco*RI and *Not* I were incorporated in forward and reverse primers respectively for the subsequent cloning into pPIC9K vector (Figure 2.1). The DNA sequences coding for HSA domains such as D1(1-197), D2 (187-385), D3 (381-585), D1-2 (1-385) and D2-3 (187-585) were obtained by PCR amplification of HSA gene using Q5 DNA polymerase and the primers were given in the Table 2.1. The amplified products and pPIC9K vector were subjected for double digestion with *Eco*RI and *Not* I followed by ligation with T4 DNA ligase. Restriction digestion was done by incubating the reaction mixture at 37 °C, whereas ligation was performed at 22 °C. Recombinant plasmids were transformed to *E.coli* (DH5α) cells and selection was done using ampicillin containing media. All clones were confirmed by PCR and by DNA sequencing with *AOX* 1 primers. Plasmids were isolated from confirmed clones and linearized using *Sal I* prior to *P. pastoris* transformation. GS115 strain of

P. pastoris was used for transformation. Linearized plasmids were transformed to *P. pastoris* GS115 cells using *Pichia* EasyComp transformation Kit from Invitrogen. *Pichia* clones were again confirmed by PCR.

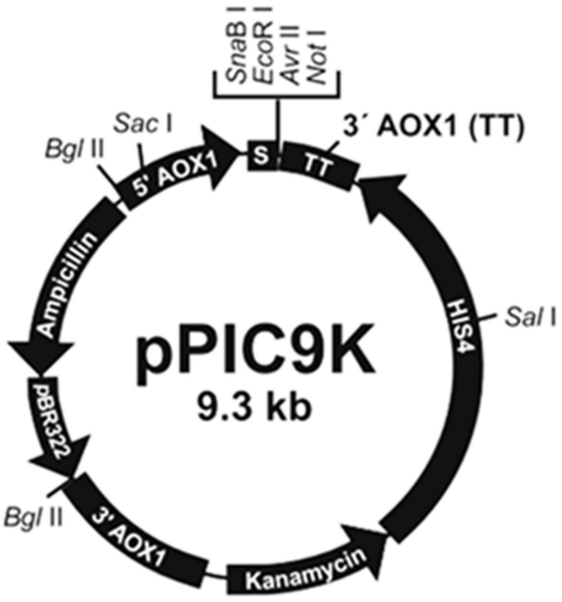

Figure 2.1 Map and features of pPIC9K vector (Adopted from Invitrogen manual, 2010).

2.1.4. Production of HSA variants by site directed mutagenesis

The gene for HSA coding sequence was cloned in pPIC9K vector and the complete recombinant vector having HSA gene (pPIC9K+HSA) was amplified using Q5 DNA polymerase. The primers harboring mutated codon were used for amplification (Table 2.2). The amplification was checked using agarose gel electrophoresis. After confirmation, the PCR product was subjected for *DpnI* digestion to eliminate the methylated parental DNA. After that the product was transformed to *E.coli* (DH5α) cells and selection was done using ampicillin containing media. All clones were confirmed by DNA sequencing with *AOX* 1 primers. Plasmids were isolated from confirmed clones and linearized using *Sal I* prior to *P. pastoris* (GS115 strain) transformation. Transformed *Pichia* clones were again confirmed by PCR.

Table 2.2: Primers used for the generation of HSA variants.

S.No.	Forward primer	Reverse primer
K240E	5'GAT CTT ACC **GAA** GTC CAC ACG GAA 3'	5' CGT GTG GAC **TTC** GGT AAG ATC TGT 3'
D375H	5'AAA GTG TTC **CAT** GAA TTT AAA CCT 3'	5' TTT AAA TTC **ATG** GAA CAC TTT GGC 3'

2.2 Expression of HSA, its domains and its variants

Expression was done by growing transformed *P. pastoris* cells initially in BMGY for 16 h, later to BMMY for 48 h. 1% (v/v) methanol was added every 24 h to induce expression and secretion of proteins into BMMY. Incubations for *P. pastoris* were performed at 30 ^{o}C on an orbital shaker at 180rpm. Protein expression was confirmed using 12% SDS-PAGE.

2.3 Purification using AlbuPure affinity matrix

Culture supernatants having proteins were harvested by centrifugation. Domains and variants of HSA were purified using AlbuPure affinity matrix (Prometic biosciences – 3151-00025). The culture supernatant was applied to Albupure matrix pre-equilibrated with 50 mM sodium acetate pH 5.3. Columns were washed with equilibration buffer, 50 mM sodium phosphate pH 7.0 and 50 mM ammonium acetate pH 8.0. Proteins were eluted with 50mM ammonium acetate pH 8.0 having 30 mM sodium octanoate. Elution fractions were checked using SDS-PAGE (Laemmli, 1970). The protein fractions were pooled and passed through Lipidex-1000 (Sigma–H6258) column for removal of fatty acids (Glatz & Veerkamp, 1983). The collected protein solutions were concentrated using Vivaspin turbo 10 kDa and Amicon ultra-15 30 kDa centrifugal filter devices. Protein estimation was done by BCA protein assay kit (GX-6410AR) and the absorbance was measured at 562 nm. The purified proteins were further confirmed by peptide mass finger printing analysis with MALDI-TOF/TOF instrument and results were searched with mascot database (Sengupta et al., 2011).

2.4 Fluorescence Spectroscopy studies

Fluorescence is one kind of luminescence, where the emission of light takes place at the rate of 10^{8} s^{-1}. The exited electrons go to the singlet states, where the electron is in opposite spin to the electron in the ground state. So that returning to the ground state is spin allowed there by occurs rapidly by emission of a photon. The processes that occur between the absorption and emission of light can be explained by Jablonski diagram (Figure 2.2).

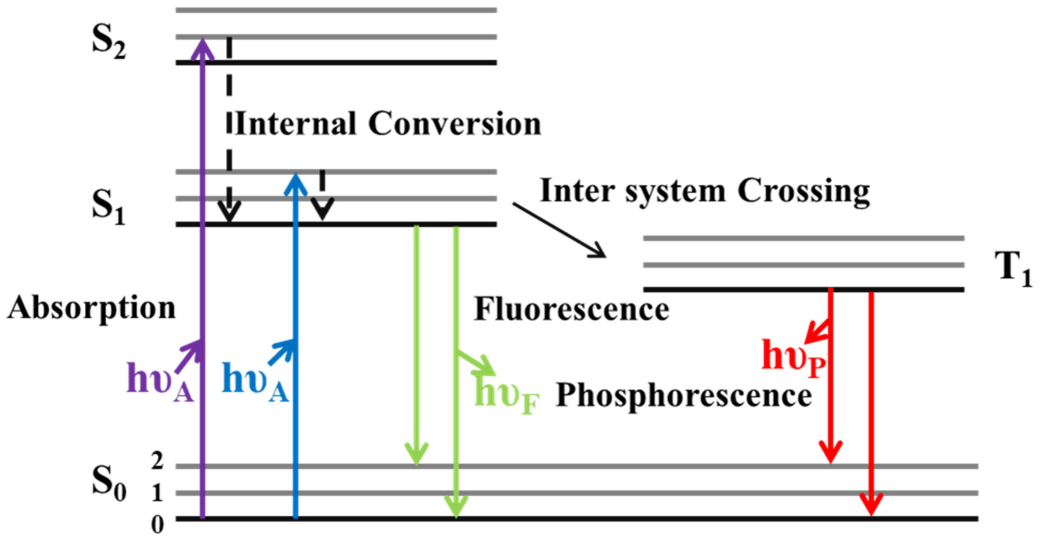

Figure 2.2 Jablonski diagram (Adopted from Lakowicz, 2009).

Fluorescence occurs typically from aromatic molecules. Usually in protein aromatic amino acids like tryptophan, tyrosine, and phenylalanine acts as intrinsic fluorophores. Among all the three aromatic amino acids, tryptophan has much stronger fluorescence intensity and has high quantum yield. Tyrosine also has a quantum yield similar to tryptophan but in native protein its fluorescence emission usually gets quenched by tryptophan or if it is ionized. Further, phenylalanine gives a very low quantum yield and hence the intrinsic fluorescence of a protein is solely contribution from tryptophan residue. Fluorescence emission spectrum of fluorophore depends upon the chemical structure of the fluorophore and the solvent in which it is dissolved.

Fluorescence quenching is a process by which fluorescence intensity of a sample gets decrease (Lakowicz, 2009b). The quenching can be due to excited-state reactions, energy transfer, molecular rearrangements, collisional quenching, and ground-state complex formation. As, quenching can also occur as a result of ground-state complex formation between the fluorophore and quencher, this phenomenon can be used to analyze bio-molecular interactions such as protein ligand interactions. Modified Stern–Volmer equation can be used to calculate association constant value from fluorescence quenching data for protein ligand interaction.

$$\frac{\log(F_0 - F)}{F} = \log K_a + n \log[Q]$$

Where F_o is fluorescence intensities in the absence of quencher, F is fluorescence intensities in the presence of quencher, n corresponds to the number of binding sites, K_a is the binding constant and [Q] is the quencher concentration.

2.4.1 Measurements of fluorescence emission

Fluorescence emission spectra were recorded at 25 ^oC from a wavelength range of 300–500 nm with an excitation wavelength of 285 nm, and slit width of 8.0 nm for both excitation and emission using PerkinElmer LS55 fluorescence spectrophotometer. Final concentration of protein (AGP, HSA and HSA variants) was fixed at 1×10^6 M^{-1} and titrated with increasing concentrations of compounds from 1 to 10×10^6 M^{-1}. The HSA and bioactive compounds were suspended in 0.1 M phosphate buffer with pH 7.4. Three independent experiments were performed and each time identical spectra were obtained. The obtained fluorescence quenching data was analyzed using Stern–Volmer equation. The binding constant value was calculated by using modified Stern–Volmer equation.

2.4.2. Molecular displacement experiment with site specific markers

For competitive binding studies the site specific probes were used. As we know the binding site of phenylbutazone and ibuprofen, we have selected these two molecules as site probes. The site markers phenylbutazone and ibuprofen specifically bind to IIA and IIIA subdomains of HSA. The solution having protein and site marker in the ratio of 1:1 was titrated with increasing concentrations of selected ligands in 1:1 to 1:10 to HSA. The fluorescence emission spectra were recorded as mentioned above. The binding constant values were evaluated using Stern–Volmer equation.

2.5 Surface Plasmon Resonance (SPR)

Surface plasmon resonance is another technique and widely used to study the protein ligand interaction (Biacore Manual, Brogioni & Berti, 2014). SPR is a phenomenon that occurs in thin conducting films (mostly gold) placed at the interface between two media of different refractive indices. In Biacore systems, thin gold film is sandwiched between the glass layer of a sensor chip and the sample solution flowing through the flow cell. Plane polarized light is focused on the back of the sensor chip under conditions of total internal reflection. At a certain angle of incident light, excitation of electrons in the gold film takes place resulting in the formation of surface

plasmons within the gold film with a drop in the intensity of the reflected light. When there is a change in the mass due to the binding event, the SPR angle shifts due to a change in refractive index near the sensor chip surface. This can be measured and used to analyze the binding (Figure 2.3).

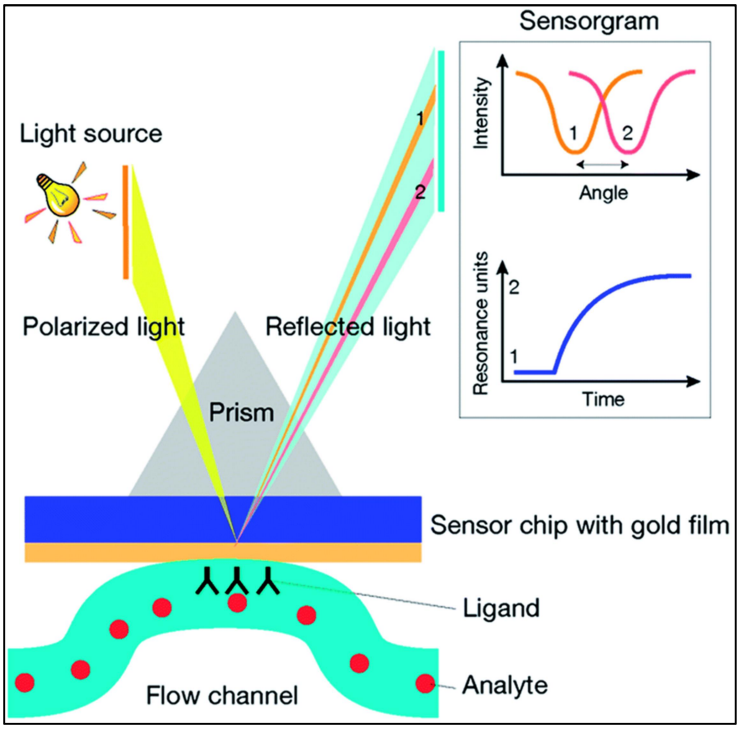

Figure 2.3 Surface plasmone resonance working principle (Adopted from Brogioni *et al.,* 2014)

To analyze the interaction between two bio molecules using SPR, one of the binding partner should be attach covalently to the sensor surface. This is known as immobilization. The gold film of sensor chip is attached to the immobilization matrix. The one that gets immobilized is known as ligand and other one is known as analyte. Different immobilization methods are available such as covalent immobilization (Amine coupling, Thiol coupling, Maleimide coupling, Aldehyde coupling) and ligand capturing (Figure 2.4). Amino coupling is generally used method where proteins by their free amine groups get immobilized on carboxy methyl-dextran matrix.

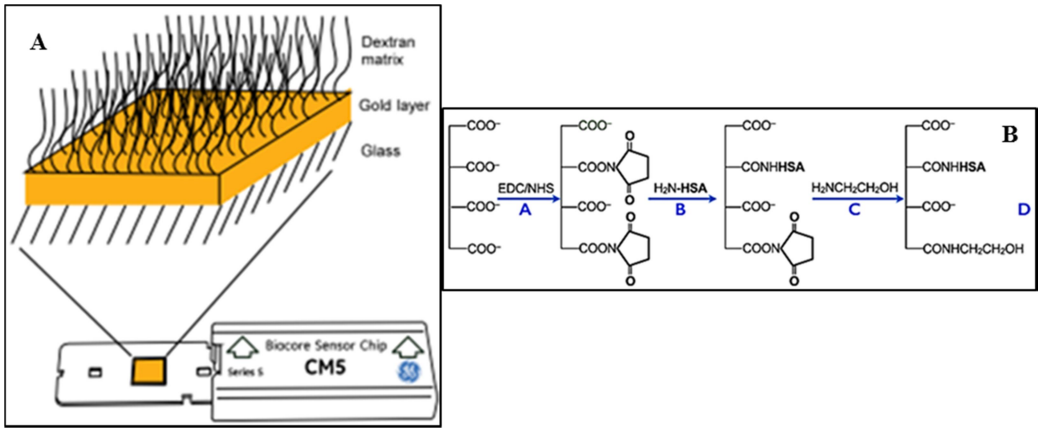

Figure 2.4 A) The surface of the CM5 sensor chip and B) immobilization by amine coupling (Adopted from Shim *et al.,* 2015).

A sensogram is a plot of the binding response in resonance units (RU) versus time in seconds (s) (Figure 2.5). Generally the sensogram provides two kinds of information. One is the rate of association and rate of dissociation, provides information of kinetic rate constants. The second one is response at different analyte concentrations, provides information on affinity constants. The affinity constant can be calculated using following equation.

$$R = \frac{R_{max} * C}{K_d + C}$$

Where R is the steady-state response value, R_{max} is maximum response, C is concentration of the analyte, K_d is the equilibrium dissociation constant (or) affinity constant

$$\text{Where } R_{max} = \left(\frac{MW_{analyte}}{MW_{ligand}}\right) X\ R_{ligand}\ X \text{ valency of ligand}$$

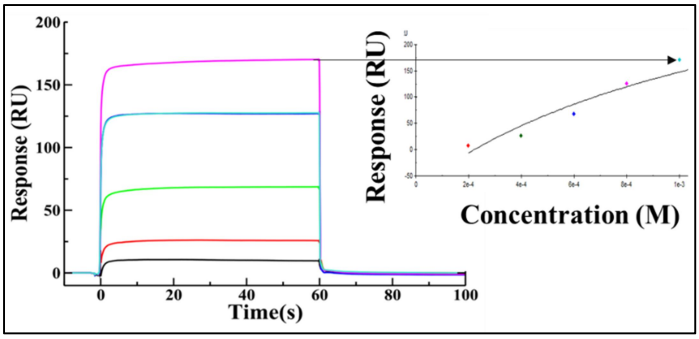

Figure 2.5 The sensogram and the affinity plot.

A Biacore T200 instrument (GE healthcare) was used to identify the affinity of PBUTs to HSA domains. The surface of CM5 sensor chips was coupled to HSA domains (800-2500 RU) and complete HSA (7000 RU) using amine coupling chemistry as described by the GE healthcare. pH scouting was done with 10 mM sodium acetate buffer with pH 4.0, 4.5, 5.0 and 5.5. Carboxymethyl dextran surface on the sensor chip was activated with 1:1 mix of 0.1 M NHS (N-hydroxy-succinimide) and 0.4M EDC (N-ethyl-N'-(dimethylaminopropyl) carbodiimide) to create N-hydroxy-succinamide esters with activation period of 7 min at a flow rate of 5 µL/min. Flow cell 1 and 3 of the chip were used for blank immobilization and the flow cell 2 and 4 were used for protein immobilization. Prior to immobilizing the domains, pre-concentration tests were done to determine the suitable injection times for immobilization. Protein (200 µg/mL) in 10 mM sodium acetate (pH 5.0) was introduced on to the activated sensor surface, with flow rate of 10 µL/min and the contact time was 7 min. Finally, the uncoupled esters were deactivated with 1M ethanolamine-HCl pH 8.5 with a flow rate of 10 µL/min and contact time of 7 min. The surface was washed with 50 mM NaOH.

The PBUTs viz., HA (112003-5G), IAA (I3750-5G-A) and Melatonin (M5250-1G) were procured from Sigma and CMPF was obtained from Cayman chemical (10007133-1). The PBUTs (40 mM) were prepared in 100% DMSO as stock solutions. From the stock solution, initial dilution to 800 µM was done with 10 mM PBS pH 7.4 with 0.05% P20, there by maintaining 2 % DMSO in the final dilution. Subsequent half dilutions (400 - 1.5 µM) were done with 10 mM PBS pH 7.4 with 0.05% P20 and 2% DMSO, which is also used as running buffer. For high concentration (800-1600 µM) analysis, the samples were prepared by maintaining 2% DMSO. The samples were injected both onto the reference and immobilized flow cell with the flow rate of 30 µL/min. The contact time and dissociation time were set at 60 and 600 seconds, respectively. 50% DMSO was used as regeneration buffer and was passed after each cycle. The buffer samples containing 1.5-2.8% DMSO were injected for solvent correction with the flow rate of 30 µL/min and 30 sec for each pulse. The solvent correction was repeated after every 10 cycles.

The analysis was performed at 25 ^{o}C and the data was collected at the rate of 10Hz. Each interaction study was performed 3-4 times and for each analysis, all the concentrations were passed along with buffer blank and by repeating one of the concentrations. For all the data solvent effect correction was done, blank adjustment and reference cell value subtraction was

also conducted. The binding affinities were calculated by fitting low concentration data in Langmuir adsorption isotherm model (equation1) (Sandblad et al., 2009) and high concentration data was calculated in hill equation (equation 2). The data fitting was done by using GraphPad Prism 5.

$$R = \frac{R_{max} * C}{K_d + C} \qquad \text{(equation 1)}$$

$$R = \frac{R_{max} * C^h}{{K_d}^h + C^h} \qquad \text{(equation 2)}$$

Where R is the steady-state response value; R_{max} is maximum response; C is concentration of the PBUTs, K_d is the equilibrium dissociation constant (or) affinity constant; h is hill coefficient.

2.6 Circular Dichroism (CD) Spectroscopy

Circular Dichroism (CD) Spectroscopy is one type of absorption spectroscopy, where it measures the difference in absorbance between left and right handed circularly polarized light (Kelly et al., 2005).

$$\mathbf{\Delta A = A_L - A_R = \Delta \varepsilon . d . c}$$

Where, A_L is left handed circularly polarized light, A_R right handed circularly polarized light. C is concentration (mg/mL), d is path length (cm).

If a chiral molecule has preferential absorption to left handed circularly polarized light ($A_L > A_R$) then the resulting CD will be positive. If $A_R > A_L$, the resulting CD will be negative.

In optically active substances, the right and left handed circularly polarized light travel at different speed and get absorbed to a different extent, resulting in the elliptically polarized light (Figure 2.6).

$$\mathbf{Ellipticity\ (\Theta) = \tan^{-1}\ (b/a)}$$

Where b and a, are the minor and major axes of the ellipse, respectively.

Generally the CD will be reported in terms of ellipticity (Θ) in degrees. The relation between ΔA and Θ can be given using following equation.

$$\Theta = 32.98\ \Delta A$$

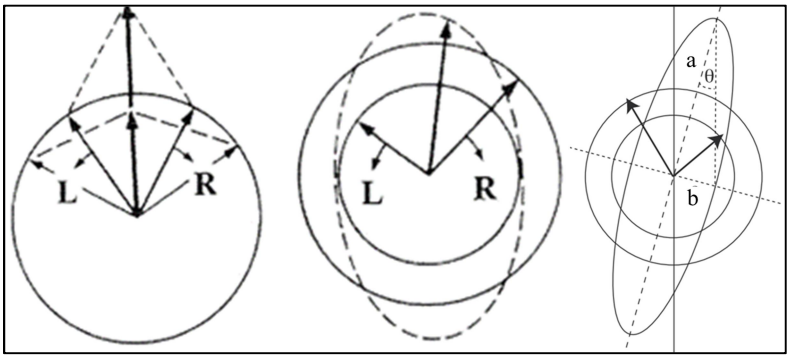

Figure 2.6 The left (L) and right (R) circularly polarized components of plane polarized light. When the two components have the same amplitude, gets combine to generate plane polarised radiation (Adopted from Kelly *et al.,* 2005).

In case of protein, peptide bond is the chromophore, which absorbs below 240 nm. The absorption of peptide bond at around 220 nm results in n → π* transition and at 190 nm results in π → π* transition. The intensity of these transitions depends on φ and ψ values. Then the CD spectra at far UV region give secondary structures information of the protein. The secondary structure composition (% α- helix, β-sheet and random coils) can be obtained by

$$\Theta(\lambda) = f_\alpha \Theta_\alpha(\lambda) + f_\beta \Theta_\beta(\lambda) + f_\gamma \Theta_\gamma(\lambda)$$

$\Theta(\lambda)$ is the total measured ellipticity at particular wave length. $\Theta_\alpha(\lambda)$ is the contribution from α-helix, $\Theta_\beta(\lambda)$ is from β-sheet and $\Theta_\gamma(\lambda)$ is from random coils. The corresponding f is the fraction of this contribution.

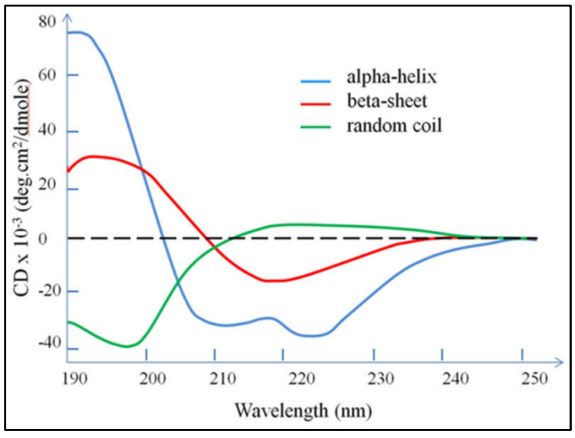

Figure 2.7 Far UV CD spectra with various types of secondary structures (Adopted from Wei *et al.,* 2014).

The secondary structure composition of unknown protein can be obtained from the known standards (Figure 2.7) (Wei et al., 2014). CD spectra at near UV region (260–320 nm), due to aromatic amino acids, gives the information regarding the tertiary structure of the protein.

2.6.1 CD Spectroscopy measurements

The CD measurements were carried out in the range of 190 – 260 nm using JASCO J-1500 CD spectropolorimeter. A quartz cell with a path length of 0.1 cm was used. The proteins were made into solution using 5 mM (for HSA variants) and 10 mM (for HSA and its domains) phosphate buffer with pH 7.4. Final protein concentration used was 2 μM in case of domains and 0.5 μM in case of variants. Three scans were accumulated at a scan speed of 100 nm min^{-1} and band width was kept at 2 nm. Two accumulations were taken for each scan and the baseline subtraction was done using phosphate buffer with pH 7.4. Finally, the CD spectral data was deconvoluted using CDNN 2.1 software to get percentage of secondary structural elements.

2.6.2 CD Spectroscopy measurements at different temperature

The JASCO J-1500 CD spectropolorimeter is attached to a peltier and facilitated to measure the temperature dependent stability of the domains. We measured the CD spectra from 25-95 ^{o}C by increasing 10 ^{o}C every time.

2.6.3 CD Spectroscopy measurements to check the effect of ligand binding

To check the effect of ligand binding on protein conformation, CD spectra of HSA and its variants were collected with increasing concentrations of phenylbutazone and ibuprofen. For this protein to ligand concentration was varied in a ratio of 1:1 to 1:10. In case of 4A, 5A and 6M, HSA to ligand concentration was in the ratio of 1:1 to 1:5.

2.7 Molecular docking using AutoDock 4.2.3

Autodock predicts the interactions between ligands and macromolecules such as proteins (Morris et al., 2009). This tool can predict bound conformations and binding free energies of the interacting molecules. AutoDock 4.2.3 uses Lamarckian genetic algorithm (Morris et al., 1998) for conformational searching and semi empirical free energy force field to predict binding free energies. The semiempirical free energy force field estimates the energetics of binding process in a water and uses pair-wise terms to evaluate the interaction of two molecules and an empirical

method to estimate the contribution from the surrounding water (Huey et al., 2007). It can be expressed as follow

$$\Delta G = (V_{bound}^{L-L} - V_{unbound}^{L-L}) + (V_{bound}^{P-P} - V_{unbound}^{P-P}) + \left(V_{bound}^{P-L} - V_{unbound}^{P-L} + \Delta S_{conf}\right)$$

Where V is pair-wise evaluations, ΔS_{conf} is conformational entropy lost upon binding, L refers to ligand and P refers to protein. The pair-wise terms evaluates dispersion/repulsion, hydrogen bonding, electrostatics and desolvation.

AutoDock 4.2.3 program was used for docking studies. The protocol used for docking was similar to our earlier reports from our laboratory (Gokara et al., 2014, Yeggoni et al., 2014, Nerusu et al., 2017). Briefly, the known crystal structure of HSA was taken from the protein data bank (PDB), and its PDB ID is 1AO6. The PDB files for domains were prepared from HSA PDB file by taking required sequence information. The proteins were edited in AutoDock by removing water molecules and ions. Hydrogen atoms were added to the functional groups and ionized as required at physiological pH. Further, Kollman united atom partial charges were assigned to the proteins. The ligand structures were designed using Discovery Studio 3.5 and the energy minimization was performed using Sybyl. Both protein and ligand files were saved in PDBQT format, a readable format for AutoDock. HSA was held rigid, all torsion bonds of the ligands were considered as free, and there was no consideration regarding the effect of solvent on the interactions. Blind docking was performed to locate the binding site of the ligands. For docking GA population size is set as 150 and maximum number of energy evolutions used is 250000. During docking, a maximum number of top 50 conformers were considered, and the rms cluster tolerance was set to 0.2 nm. A conformer with the least free energy was selected and visualized using PyMOL software (Pymol software 2015).

2.8 Molecular dynamics (MD) simulations

A Molecular dynamics simulation is a numerical technique to solve Newton's equation of motion for a group of atoms or molecules. This method can be used to study the interaction of protein and ligand system. This method predicts the state of the system such as positions and velocities at a given time by taking initial positions, velocities. For the present study, we have analyzed the radius of gyration (R_g), root mean square deviations (RMSD) and root mean square fluctuations (RMSF) and were calculated from 100 ns simulation of HSA-ligand complex.

The radius of gyration gives the information of size of the system and it can be calculated using following equation (Abraham et al., 2014).

$$R_g = \left(\frac{\sum_i \| r_i \|^2 m_i}{\sum_i m_i} \right)^{\frac{1}{2}}$$

Where m_i is the mass of atom i and r_i is the position of atom i with respect to the center of mass of the molecule.

We have calculated the root mean square deviation (RMSD) of atoms by taking the initial structure as reference. The following equation can be used to calculate RMSD (Abraham et al., 2014).

$$\text{RMSD}\ (t_1, t_2) = \left[\frac{1}{M} \sum_{i=1}^{N} m_i \ \| \ r_i\ (t_1) - r_i\ (t_2)\ \|^2 \right]^{\frac{1}{2}}$$

Where r_i (t) is the position of atom i at time t.

Similarly root mean square fluctuations (RMSF), which quantifies the flexibility of the molecule, can be calculated by using following equation.

$$\text{RMSF} = \frac{1}{N} \sum_{i=1}^{N} \sqrt{\frac{1}{T} \sum_{t=1}^{T} (r_i\ (t) - \langle r \rangle_i)^2}$$

Where N is number of atoms, r (t) is the position at time t and $\langle r \rangle$ is the time averaged position.

We have performed all this calculations using GROMACS 4.0 package and studied the HSA-ligand complexes. GROMACS 4.0 package uses GROMOS96 43a1 force field (Berendsen et al., 1995). The protein conformation with lowest binding energy, which is close to the experimentally obtained value, was taken as initial structure. The protein topology was prepared using pdb2gmx, which can read .PDB file and generates coordinate and topology in GROMACS format. The topology parameters of ligands were created using PRODRG2.5 server (Schüttelkopf & Van Aalten, 2004, Sudhamalla et al., 2010, Abraham et al., 2014). The box type used is dodecahedron, which defines the unit cell. The protein was placed at 1.0 nm from the box edge. The simulation was done in the aqueous system by taking SPC (simple point charge) water

model. HSA is a negatively charged protein and the neutralization was done by adding 15 Na^+ ions. Energy minimization was done for entire system having protein, ligand, ions and water molecules to release conflicting contacts. The minimization was performed, which optimizes geometry and solvent orientation, using steepest descent method of 1000 steps followed by another 1000 steps of conjugate-gradient energy minimization. Before proceeding to production MD step equilibration was done. Equilibration of the system brings it to proper temperature and pressure conditions. The equilibration was performed in two phases. In the first phase, NVT, position restrain of solute was done at 300 K for 100 ps followed by NPT at 1bar pressure. Berendsen thermostat and Parrinello-Rahman pressure coupling were used for temperature coupling and pressure coupling respectively (Sudhamalla et al., 2010). Then the system was subjected to 100ns MD at 300K temperature and 1 bar pressure. The motion equations were integrated using leaf-frog algorithm. The trajectories were recorded at every 10 ps interval.

Chapter 3

Unravelling the binding efficiency of uremic toxins with the yeast expressed domains of human serum albumin

3.1. Introduction

Uremic syndrome is the clinical manifestation of the renal failure, in which the deterioration of many biochemical and physiological functions take place due to the progressive retention of large number of compounds, called uremic toxins, which are generally excreted by the healthy kidneys. More than 100 different highly diverse group of uremic toxins were reported (Vanholder et al., 2003, Vanholder et al., 2008, Duranton et al., 2012) that can exert potential adverse effects on the functions of various cell types and organs (Satoh et al., 2003, Lisowska-Myjak, 2014). Removal of these toxins is essential for the survival of liver and kidney failure patients. There are three major categories of uremic toxins, known as small water-soluble compounds, the middle molecules and the protein-bound uremic toxins. Small water-soluble and middle molecules can be removed by conventional hemodialysis methods. But, the interaction of protein-bound uremic toxins (PBUTs) to serum albumin reduces the free fraction and limits their removal by hemodialysis. Apart from their adverse effects, the PBUTs enhance drug toxicity by competitively binding to the proteins (Takamura et al., 1997). The drug over dose could in turn exert its own toxicity. Efforts were made in the past to improve the efficacy of the dialysis methods to remove PBUTs, for the survival of renal failure patients (Dhondt et al., 2000, Tao et al., 2016). The extracorporeal dialysis methods, using albumin as dialysate include, Molecular Adsorbent Recirculating System (MARS), Single-Pass Albumin Dialysis (SPAD) and Prometheus (Mitzner et al., 2001, Mitzner, 2011, Yamasaki et al., 2013, Lee et al., 2015). The available knowledge of ligand binding properties of albumin led to the development of albumin based extracorporeal dialysis units. The extracorporeal dialysis proved to be effective tool for removing endogenous toxins or overdosed drugs from patients. The clearance efficiency for albumin bound substances, however, is relatively low in all these systems (Krisper et al., 2011). Studying the binding mechanism of HSA to PBUTs is therefore essential.

The binding of hippuric acid (HA) (Zaidi et al., 2013), indole-3-acetic acid (IAA) (Bertuzzi et al., 1997), melatonin (Li & Wang, 2015) and 3-carboxy-4-methyl-5-propyl-2-furanpropanoic acid (CMPF) (Ghuman et al., 2005) to HSA were studied. But, specific details of binding of PBUTs to HSA domains would be helpful to increase the efficacy of dialysate in extracorporeal dialysis. Here, we made an attempt to understand the binding affinity of some of

the PBUTs, such as HA, IAA, melatonin and CMPF (Figure 3.2) to HSA and its specific domains.

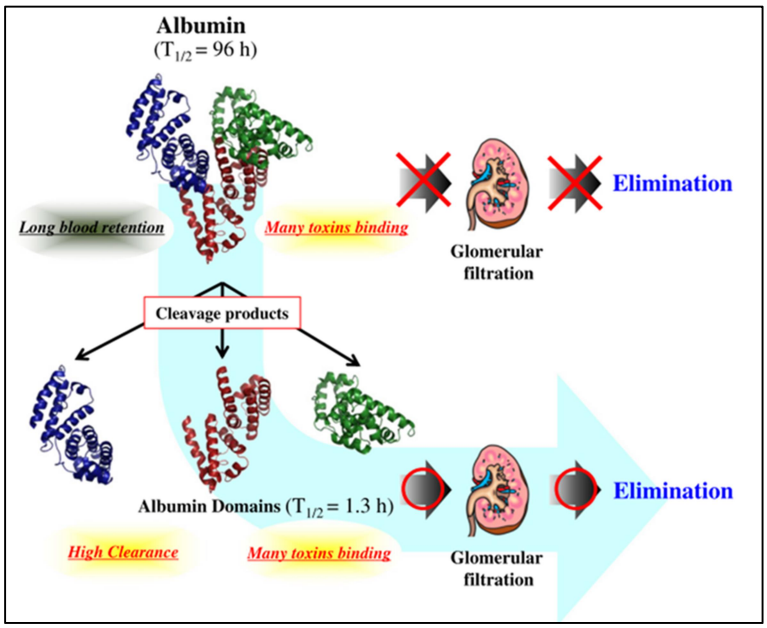

Figure 3.1 Toxins removal therapy by albumin domains (Adopted from Minomo *et al.,* 2013).

Three recombinant domains of HSA were purified and functionally characterized (Park et al., 1999, Dockal et al., 2000a, Dockal et al., 2000b, Mao et al., 2000, Shi et al., 2012). Compared to full length HSA, elimination of domains was possible through renal clearance (Figure 3.1). Domain II mutant, with high bilirubin binding affinity, binds and eliminates bilirubin through urine, useful in treating hyperbilirubinemia (Minomo et al., 2013). Domain I can be used as stand-alone protein for drug delivery as it possesses free cysteine residue (Matsushita et al., 2004). Domain III is known for its FcRn interaction that increases drug half-life (Kenanova et al., 2010, Andersen et al., 2012, Andersen et al., 2013). The individual domains have the ability to interact with drugs and other ligands. Thus, identification of the high affinity albumin domains towards PBUTs is highly useful, as they can be eliminated easily through renal clearance. These domains are also useful in extracorporeal dialysis, where the albumin can be replaced with HSA domains as dialysate.

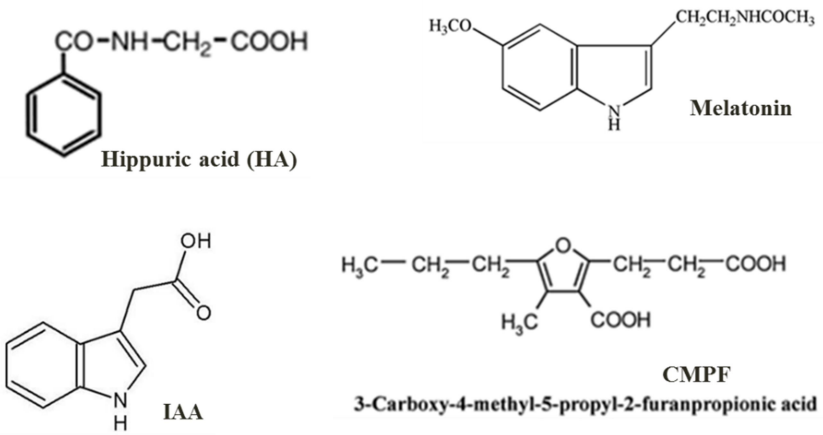

Figure 3.2 Selected protein-bound uremic toxins (PBUTs). Hippuric acid (MW 179.17 g/mol), Melatonin (MW 232.3g/mol), IAA (MW 175.19 g/mol) and CMPF (MW 240.3 g/mol).

With this background, in our present study we have aimed to understand the interaction of HSA and its domains to PBUTs like IAA, HA, melatonin and CMPF. The domains were cloned in pPIC9K vector and expressed heterologously in *Pichia pastoris* to characterize interaction between the domains and the selected PBUTs using biophysical techniques. Complete HSA protein was procured from sigma (A3782-1G). The full length HSA and heterologously expressed HSA domains were immobilized on CM5 sensor chip and subjected to surface plasmon resonance analysis to study the affinity of these proteins with PBUTs. Finally the molecular mechanism involved in complex formation was also studied using molecular docking studies.

3.2 Results and discussion

3.2.1 Cloning, expression and purification of recombinant domains of human serum albumin

P. pastoris, the methylotrophic yeast, is widely used for the production of recombinant HSA and HSA fusion proteins (Kobayashi et al., 2000, Tian et al., 2013). In the present study, we have cloned HSA and its domains in frame with the α-factor signal sequence of pPIC9K and expressed in *P. pastoris* GS115. All the domains (D1, D2, D3, D1-2 and D2-3) of HSA were successfully cloned in *P. pastoris* (Figure 3.3).

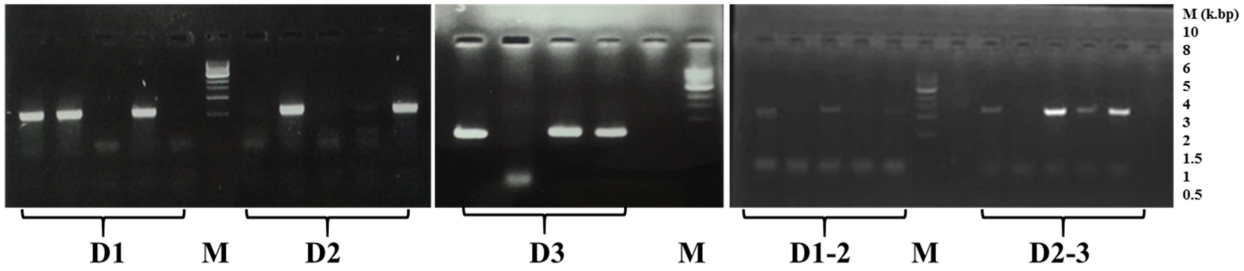

Figure 3.3 Colony PCR results confirming the successful transformation of HSA domains (D1, D2, D3, D1-2 and D2-3) to *P. pastoris* cells. D1, D2 and D3 are having 0.6 k. bp, whereas D1-2 and D2-3 are of 1.2 k. bp.

HSA and its domains were expressed into extracellular media and purified using affinity matrix. Figure 3.4 shows the migration of purified HSA and domains in 12% SDS-PAGE gel. We obtained D2, D3, D1-2, D2-3 and rHSA in pure form. But we could not able to get the required purity and yield in case of D1, after multiple trials also. As the major binding sites in HSA are located in D2 and D3, we further proceeded with the purified proteins by eliminating D1. Further, the mass and sequence of the purified domains were also confirmed from mass spectrometry (MALDI-TOF/TOF). Figure 3.5 shows the mass spectra of D2, D3, D1-2, D2-3 and rHSA, respectively. The sequence coverage of analyzed peptides confirms the purified domains. Thus, the expressed domains of D2, D3, D1-2 and D2-3 were pure and intact.

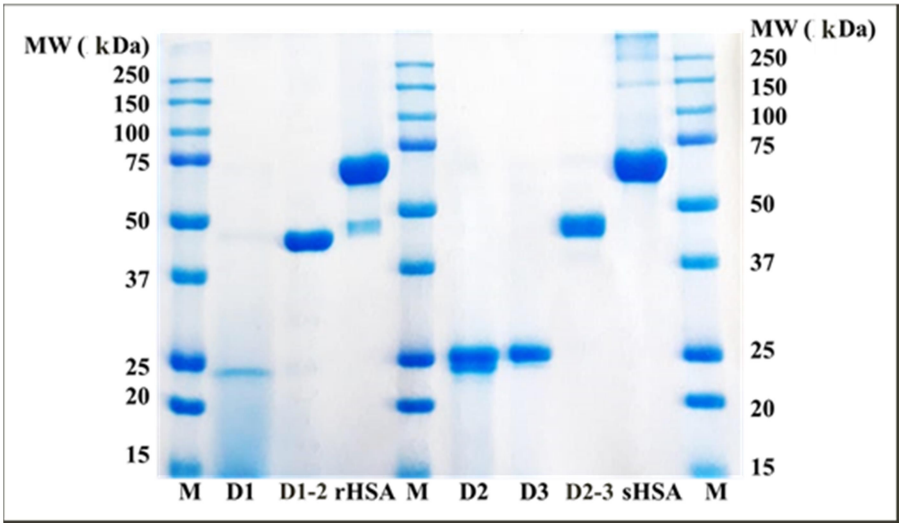

Figure 3.4 SDS- PAGE. The gel picture is showing the migration of domains. D1 (22 k.Da), D2 (22 k.Da.), D3 (22k.Da.), D1-2 (44 k. Da.), D2-3 (44 k.Da.) and HSA (66k.Da., rHSA-recombinant HSA, sHSA- HSA purchased from Sigma).

While designing the domains, we have taken care of the positions of cysteine disulfide bonds, as they should not be located at N (or) C terminal positions. There should not be changes

in the disulfide bond pattern to ensure that no changes in protein folding. Table 3.1 gives the information regarding the biochemical properties of purified HSA domains. We have produced 187-385 amino acids of HSA as D2, with 199 amino acids and the molecular weight of 22 kDa. This domain is also rich in negatively charged amino acids, with net charge of -9. Whereas, the D3 is positively charged protein with net charge of +1. We have obtained 381-585 amino acids of HSA as D3, with 205 amino acids and the molecular weight of 22.5 kDa. As there is a significant difference in the net charge, these proteins can also be separated using ion exchange chromatography. The sequence similarity between D2 and D3 was also analyzed. There exists 20 % of the sequence identity. For D1-2, we have considered 1-385 amino acids of HSA with 385 amino acids. The molecular weight and net charge of D1-2 is 42.4 kDa and -18 respectively. This is highly charged protein among all the purified domains. Finally, for the D2-3 domain, we have considered 187-585 amino acids, with 399 amino acids and the molecular weight of 44 kDa and the net charge of -6.

Table 3.1: Amino acid content, Molecular weight, pI and net charge at physiological pH of HSA and its domains.

S.No.	DOMAIN	AMINO ACIDS	Molecular weight (kDa)	Theoretical PI	Number of negatively charged Amino acids	Number of positively charged Amino acids	Net charge
1	D1	1-197 (197AA)	21.67	5.43	35	27	-8
2	D2	187-385 (199 AA)	21.89	5.16	37	28	-9
3	D3	381-585 (205 AA)	22.5	7.58	30	31	+1
4	D1-2	1-385 (385AA)	42.35	5.23	70	52	-18
5	D2-3	187-585 (399 AA)	43.8	5.97	65	59	-6
6	HSA	1-585 (585 AA)	66.5	5.73	98	84	-14

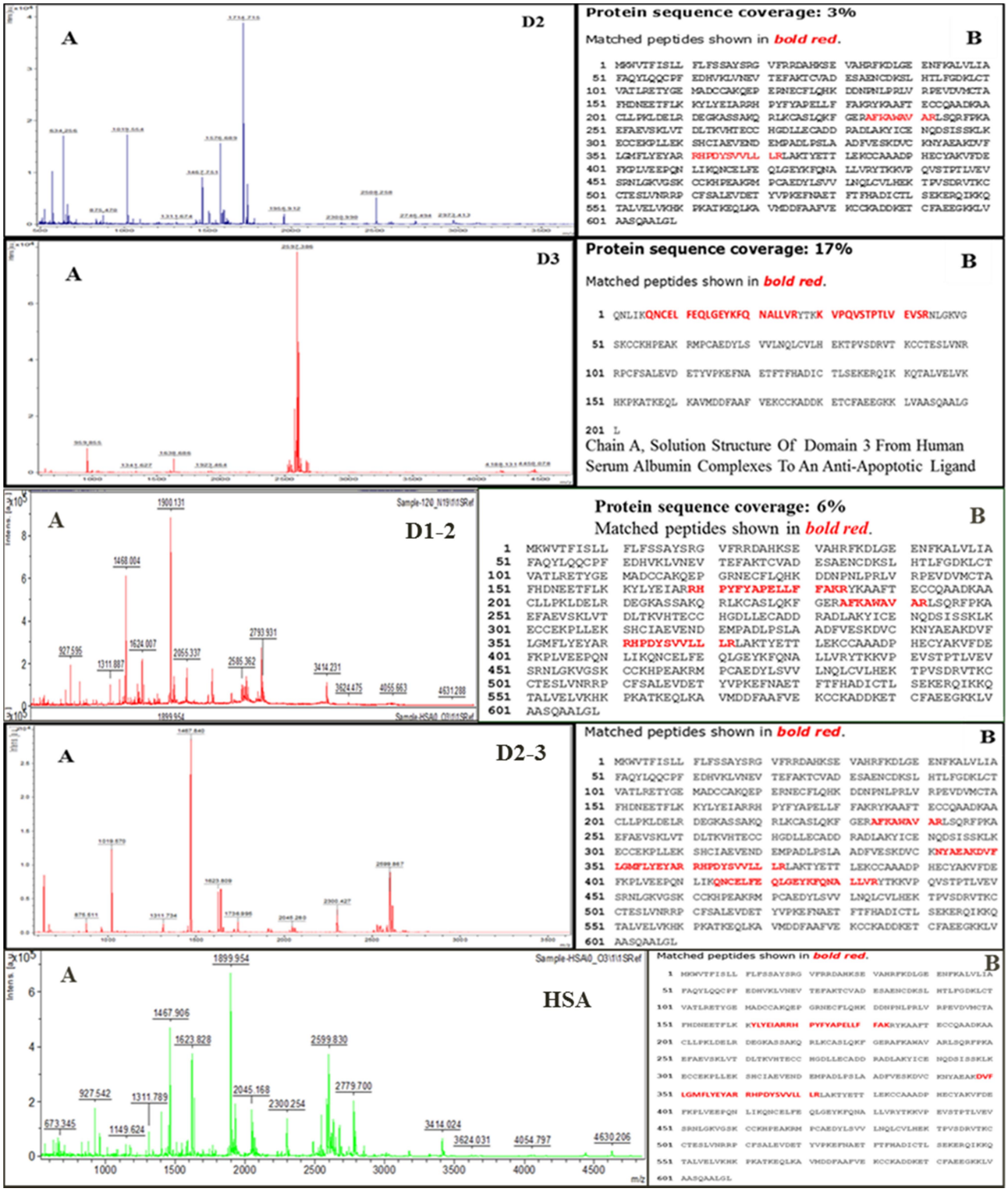

Figure 3.5 Peptide mass finger printing analysis of D2 (187-385), D3 (381-585), D1-2 (1-385), D2-3 (187-585) and rHSA (1-585). A) Mass spectrum and B) Sequence coverage of the obtained peptides, which confirms the purified domains.

3.2.2. Circular dichroism spectroscopy

CD spectroscopic studies were performed to understand the secondary structural elements composition and the conformational changes that occur with increasing temperature (Kelly et al., 2005). The CD spectra of D2 and D3 were similar to the earlier reports (Dockal et al., 1999, Dockal et al., 2000a) (Figure 3.7). The protein HSA is rich in α-helix (67%) and is stabilized by 17 disulfide bonds. There exists a symmetry in the distribution of disulfide bonds among the individual domains (Paris et al., 2012). Figure 3.6 shows the secondary structure element content of HSA and its domains and shows that all the proteins D2, D3, D1-2, D2-3 and HSA are rich in α-helix. In order to check the thermal stability of these domains, the temperature was raised from 25-95 ^{o}C, with 10 ^{o}C interval.

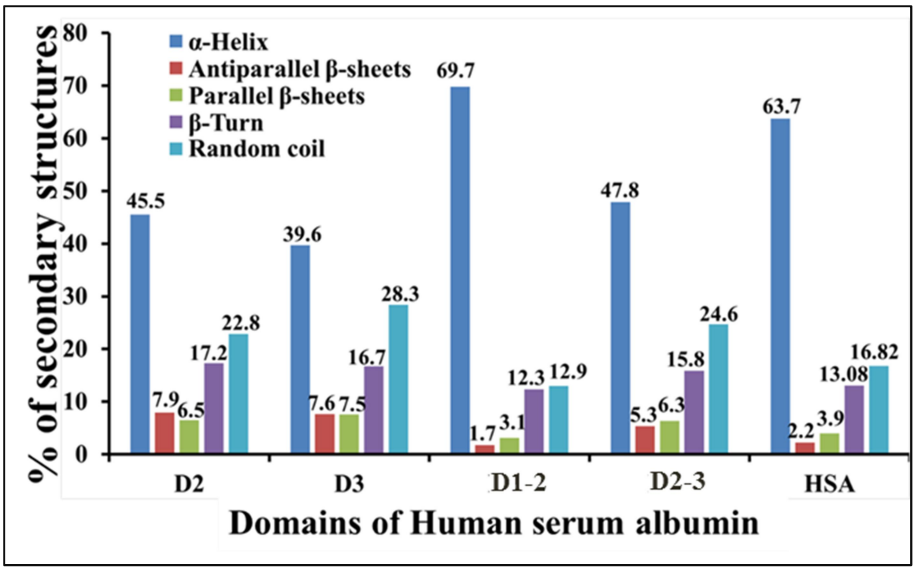

Figure 3.6 Percentage of secondary structure analysis of domains of HSA. CDNN software analysis of CD data shows that all the domains of HSA, along with HSA are rich in α- helix.

In case of D2 domain, the secondary structure of α-helix was obtained around 45.5% at 25 ^{o}C. With gradual increase in temperature, there is a slight decrease in α-helix, and increase in β-elements and random coils. The random coil percentage increased more with increasing temperature (Figure 3.7). The structural changes from α-helix to random coils show that there is a slow unwinding of the protein with temperature. Similarly, D3 was analyzed at different temperatures, and it have 39.6% of α-helix at 25 ^{o}C. Interestingly, there was no change in

random coils percentage with increasing temperature. But, there is a gradual decrease in α-helix with gradual increase in β-elements (Figure 3.7). It indicates that there is structural transition from one conformation to the other conformation.

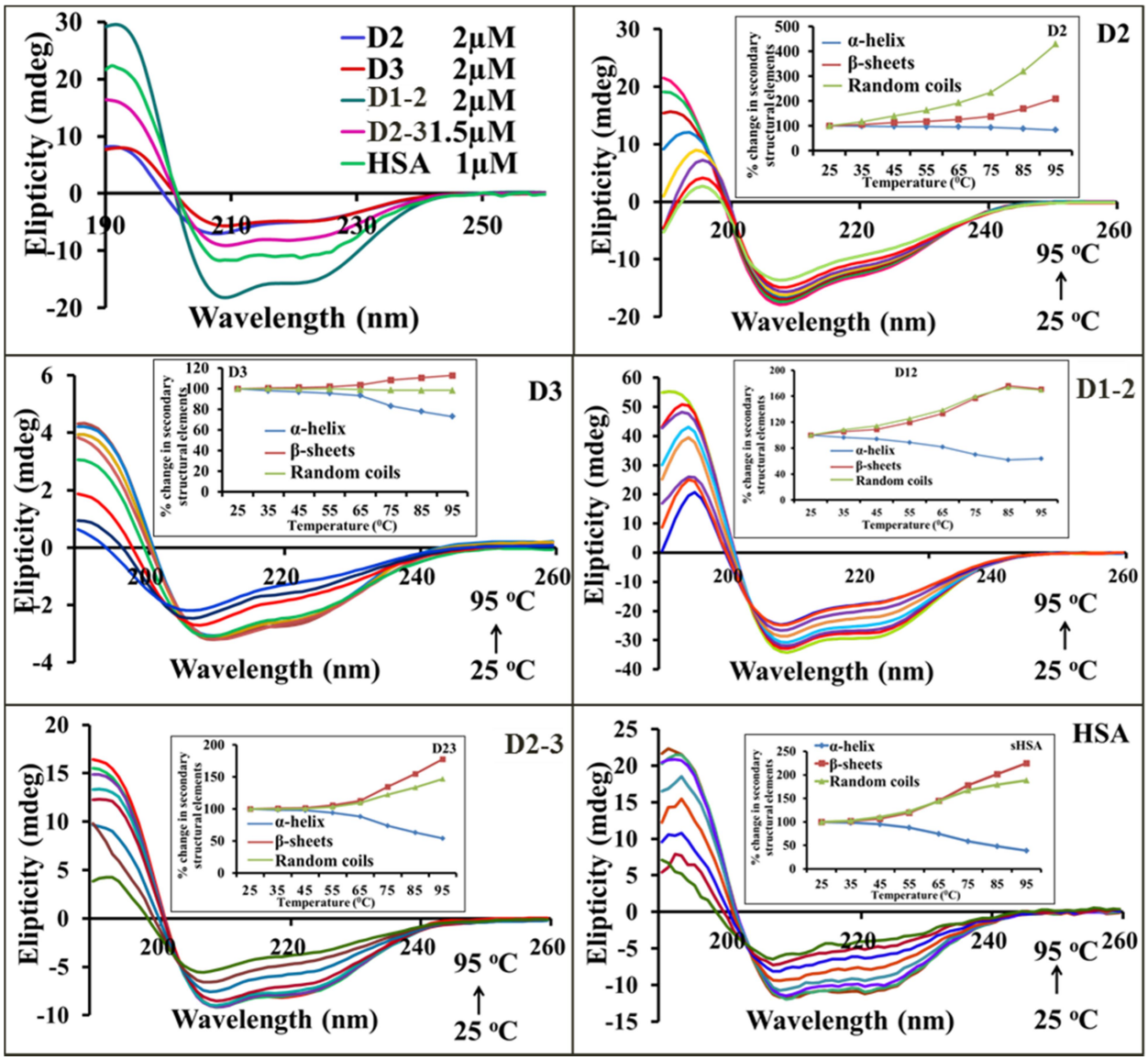

Figure 3.7 Conformational analysis and thermal stability of HSA and its domains. The CD spectra of D2, D3, D1-2, D2-3 and HSA and the same at increasing temperatures were shown. The increasing temperature from 25 – 95 °C was applied with 10 °C interval to analyze the structural changes. The insets were showing the changes in secondary structural elements with increasing temperature.

In D1-2, there is decrease in α-helix with increase in β-elements and random coils. The increment is same for β-elements and random coils. In D2-3, there is a slight increase in random

coils like in D2, but the increase is less compared to β-sheets; it shows cumulative behavior of D2 and D3 to increasing temperature. In case of HSA which has all the three domains, there is an intermediate behavior to D1-2 and D2-3. This shows that, the structure of purified domains is similar to the respective portion of complete HSA i.e. native structure was preserved. There are no changes in protein folding and disulfide bond distribution in the domains, hence, no changes in binding sites. Further, the data shows that, all the four proteins are stable up to 50 ^{o}C with D2 domain being more stable than other domains.

3.2.3. Surface Plasmon Resonance (SPR)

SPR is widely used technique for quantification of K_d values, due to its reliability. A number of reports are available about the interaction of HSA with ligands using SPR (Frostell-Karlsson et al., 2000, Rich et al., 2001, Banères-Roquet et al., 2009, Rempel et al., 2011, Shim & Reaney, 2015, Fabini et al., 2016). HSA is an allosteric protein which can interact with more than one ligand at a time. The major drug binding sites, site I and site II are located in D2 and D3 of HSA, respectively. Here, we have selected D2, D3, D2-3 domains and complete HSA protein and analyzed the interaction with PBUTs to find an alternate therapeutic approach to remove the PBUTs. We have immobilized the purified proteins on sensor surface of CM5 chip and the immobilization levels obtained is 2275.3, 778.6, 1976.6 and 6991.6 RU for D2, D3, D2-3 and HSA, respectively. The sensorgrams obtained for immobilization are given in Figure 3.8.

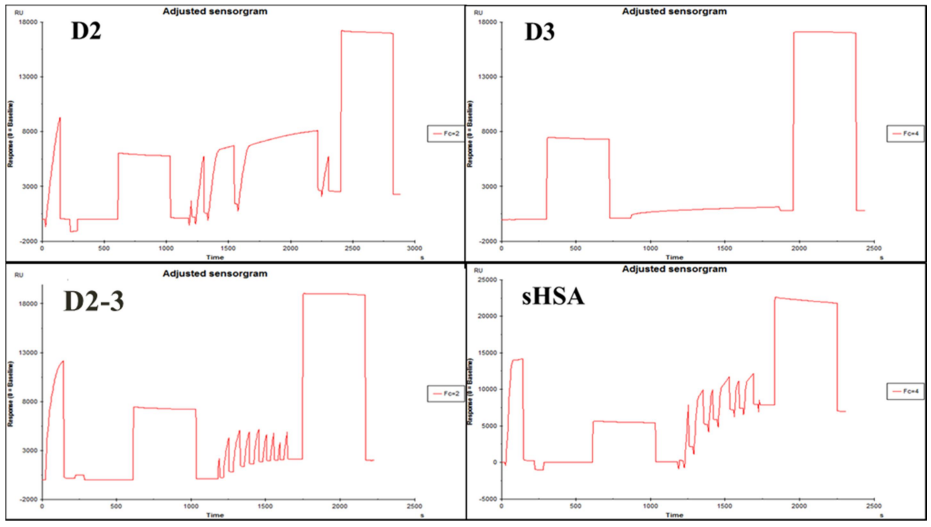

Figure 3.8 Immobilization of D2, D3, D2-3 and HSA on the surface of CM5 sensor chip using amino coupling chemistry. The final response for immobilization of D2, D3, D2-3 and HSA is 2275.3, 778.6, 1976.6 and 6991.6 RU respectively.

Other reports are available for the interaction of selected PBUTs to complete HSA protein. It was reported that site II, i.e. D3, is the major binding site for HA and IAA (Sakai et al., 1995, Tao et al., 2016). HA has two binding sites in HSA with the primary binding site located in D3 (site II). The binding constant obtained for the primary binding site of HSA and HA is $2.75 \pm 0.51 \times 10^4\ M^{-1}$ (Zaidi et al., 2013). Similar to HA, IAA also have more than one binding site in HSA and the binding constant values reported for high affinity primary binding site is $1.15 \times 10^4\ M^{-1}$ (Bertuzzi et al., 1997). But, it was reported that melatonin has single binding site for HSA and the binding constant value is $1.44 \pm 0.67 \times 10^5\ M^{-1}$ (Li & Wang, 2015). The interaction of CMPF to HSA also well characterized and crystal structure for HSA-CMPF complex is available (PDB ID: 2BXA). The primary binding site for CMPF is located in site I with the binding constant of $1.3 \times 10^7\ M^{-1}$ and forms five hydrogen-bond or salt-bridge inter-actions with binding pocket residues (Ghuman et al., 2005). In case of CMPF also more than one binding site were reported. For better understanding of the mechanism of interaction to HSA domains, we have made an attempt to study the affinity of three PBUTs to the three domains and full length HSA.

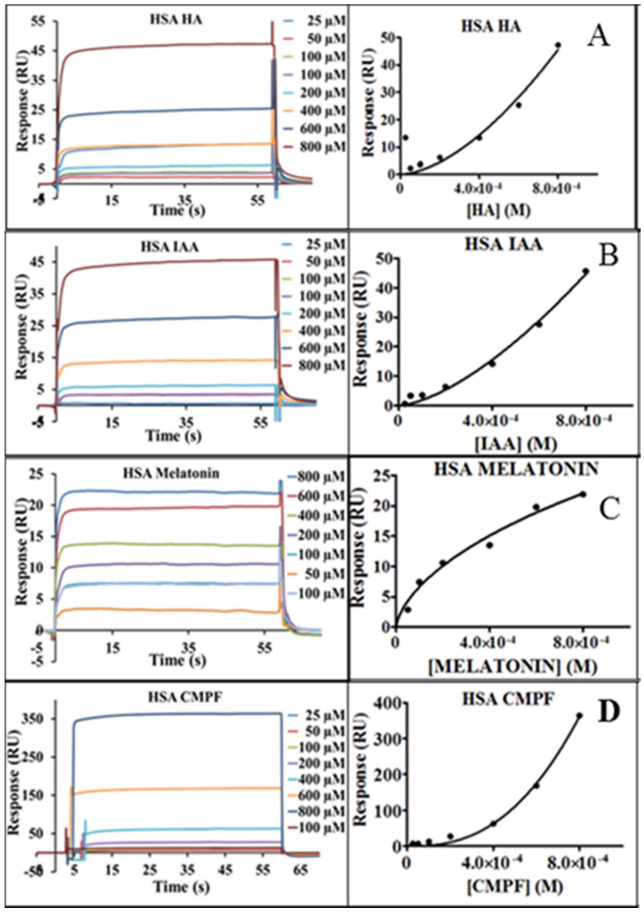

Figure 3.9 From 25-800µM was considered as medium concentration range and used for the analysis. The interaction of A) HA, B) IAA, C) Melatonin and D) CMPF to HSA in the medium concentration range.

Initially, we have used the concentration range from 200 - 1.56 µM of PBUTs. As we did not get the saturation, we increased the concentration up to 800 µM and further to 1600 µM. Finally, we considered 200 - 1.56 µM as low concentration range, 25 – 800 µM as medium concentration range and 800 - 1600 µM as high concentration range. However, to high concentration range, the linear concentrations were used. Further, the low concentration data was fitted using Langmuir adsorption isotherm model and high concentration data was fitted using hill equation. To make it clear for interaction of D2 to IAA and melatonin, the low concentration data was also fitting in hill equation.

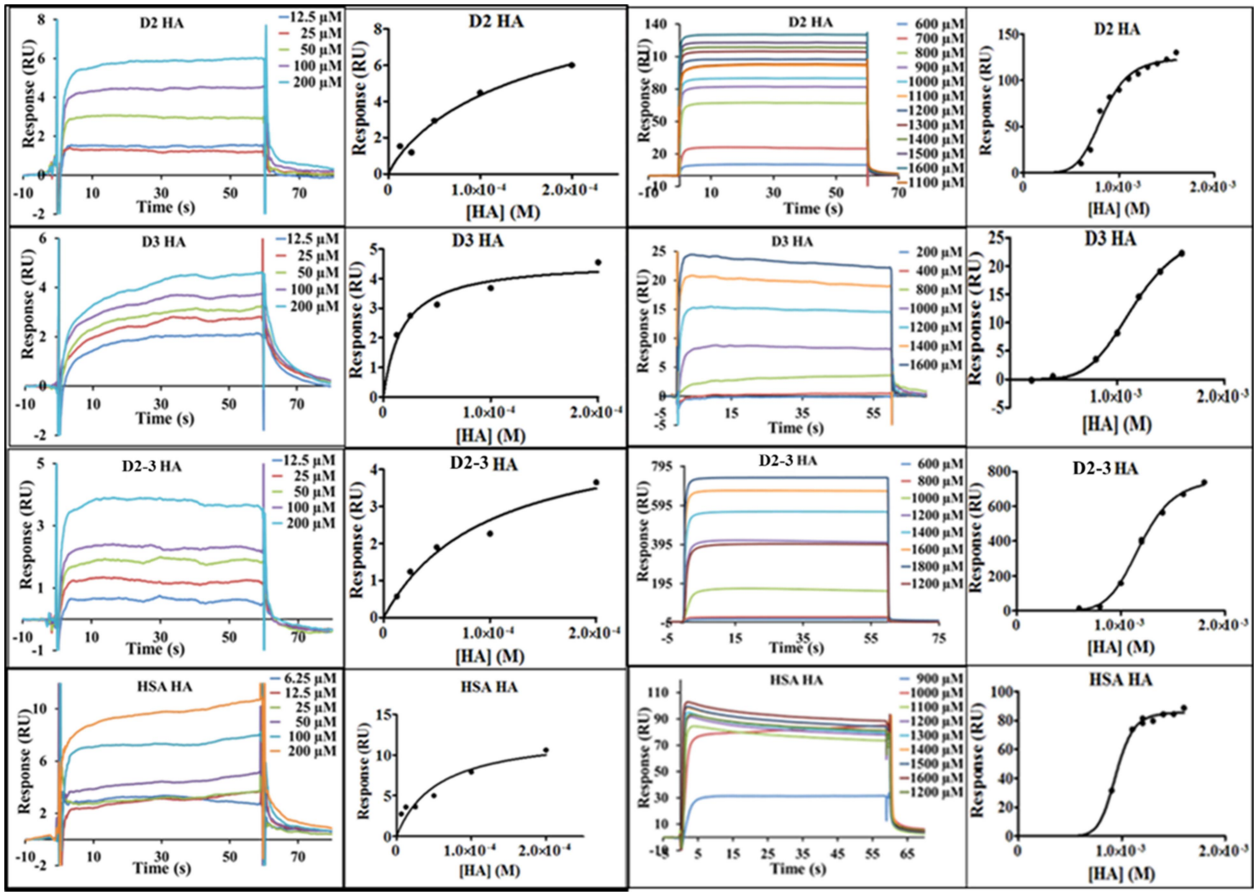

Figure 3.10 Interaction of Hippuric acid (HA) to HSA and its domains. For low concentration range, 12.5µM – 200 µM HA was used and for high concentration 600-1600 µM of HA, with linear concentration range is used. HA used for high concentration analysis was purchased from SRL (35696).

Figure 3.10 shows the interaction of HA with HSA and its domains. The K_d values obtained for the interaction of HA to D2, D3, D2-3 and HSA found to be $1.05\pm0.11\times10^{-4}$ M, $1.73\pm0.05\times10^{-5}$ M, $1.08\pm0.16\times10^{-4}$ M and $4.74\pm1.07\times10^{-5}$ M, respectively, which is considered to be strong binding. The h vales obtained from high concentration data for HA to D2, D3, D2-3 and HSA found to be 5.9, 4.7, 7.2 and 10.9, respectively. The interaction of HA to both the domains of HSA indicating the presence of more than one binding site in HSA and they were located in D2 and D3. Among all four proteins D3 is showing high affinity towards HA. Further, the positive h value from high concentration data is giving the possibility of more than one site in individual domains. Further, Figure 3.9 shows the interaction of HA, IAA, melatonin and CMPF to HSA at medium concentration range and the data is not fitting in any of the equations.

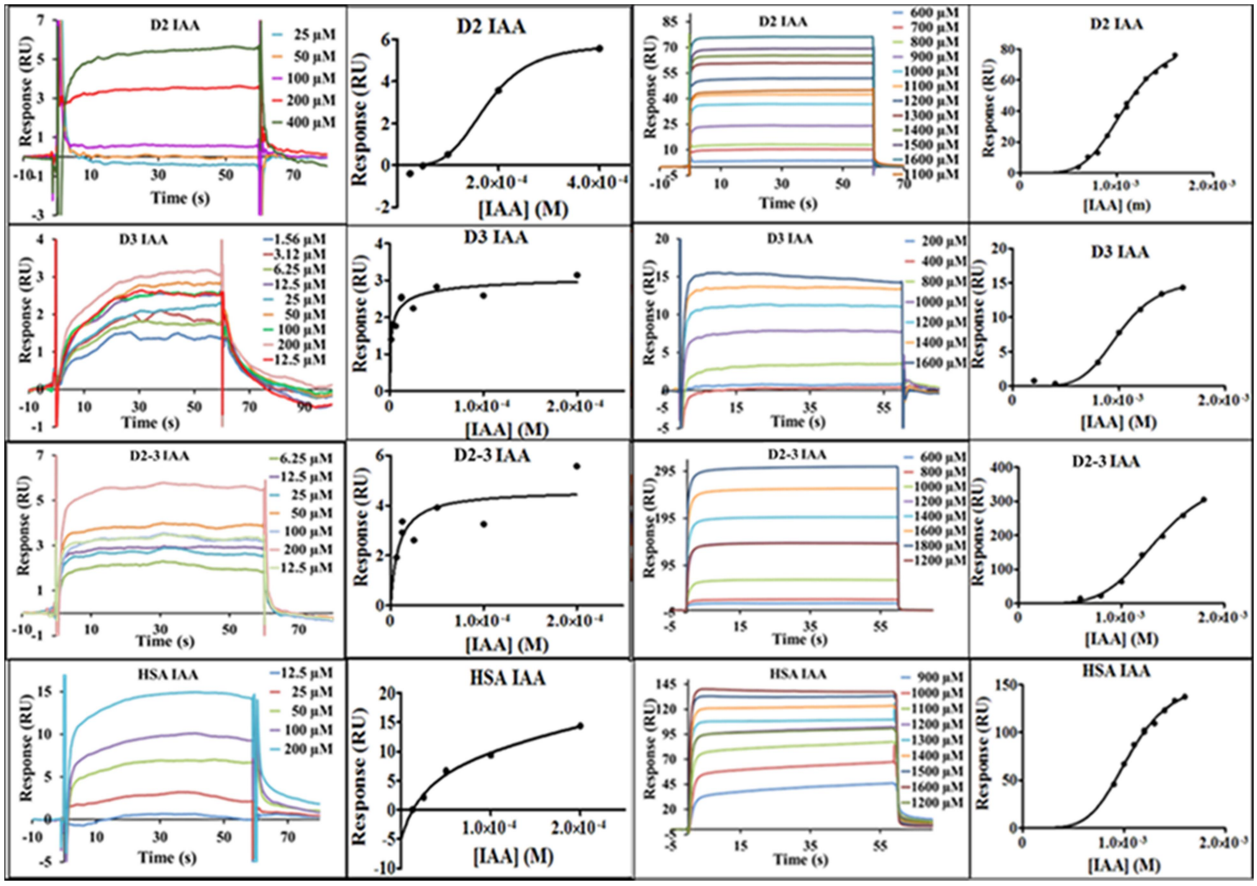

Figure 3.11 Interaction of IAA to HSA and its domains. For low concentration range, 12.5μM – 200 μM IAA was used and for high concentration 600-1600 μM of IAA, with linear concentration range is used. IAA used for high concentration analysis was purchased from SRL (88318)

Similar to HA, IAA also has multiple binding sites in HSA. The K_d values obtained for the interaction of IAA to D2, D3, D2-3 and HSA are 1.69± 0.17×10^{-4} M, 2.15± 0.22×10^{-6} M, 7.97± 0.89×10^{-6}M and 3.63 ± 0.53×10^{-5} M, respectively. The h vales obtained from high concentration data for IAA to D2, D3, D2-3 and HSA are 5, 5.3, 4.8 and 5.4 respectively. Figure 3.11 shows the interaction of IAA with HSA and its domains. In case of melatonin, The K_d values obtained for D2, D3, D2-3 and HSA are 2.24 ± 0.51×10^{-4} M, 3.88 ± 1.5×10^{-5} M, 1.20 ± 0.14×10^{-4}M and 5.19 ± 1.10×10^{-5} M, respectively, and the h values obtained for D2, D3, D2-3 and HSA are 2.6, no, 1.7 and 2.4, respectively. This indicates that D3 is the high affinity domain towards melatonin. There exists a single binding site for melatonin in D3. Figure 3.12 shows the interaction of melatonin with HSA and its domains.

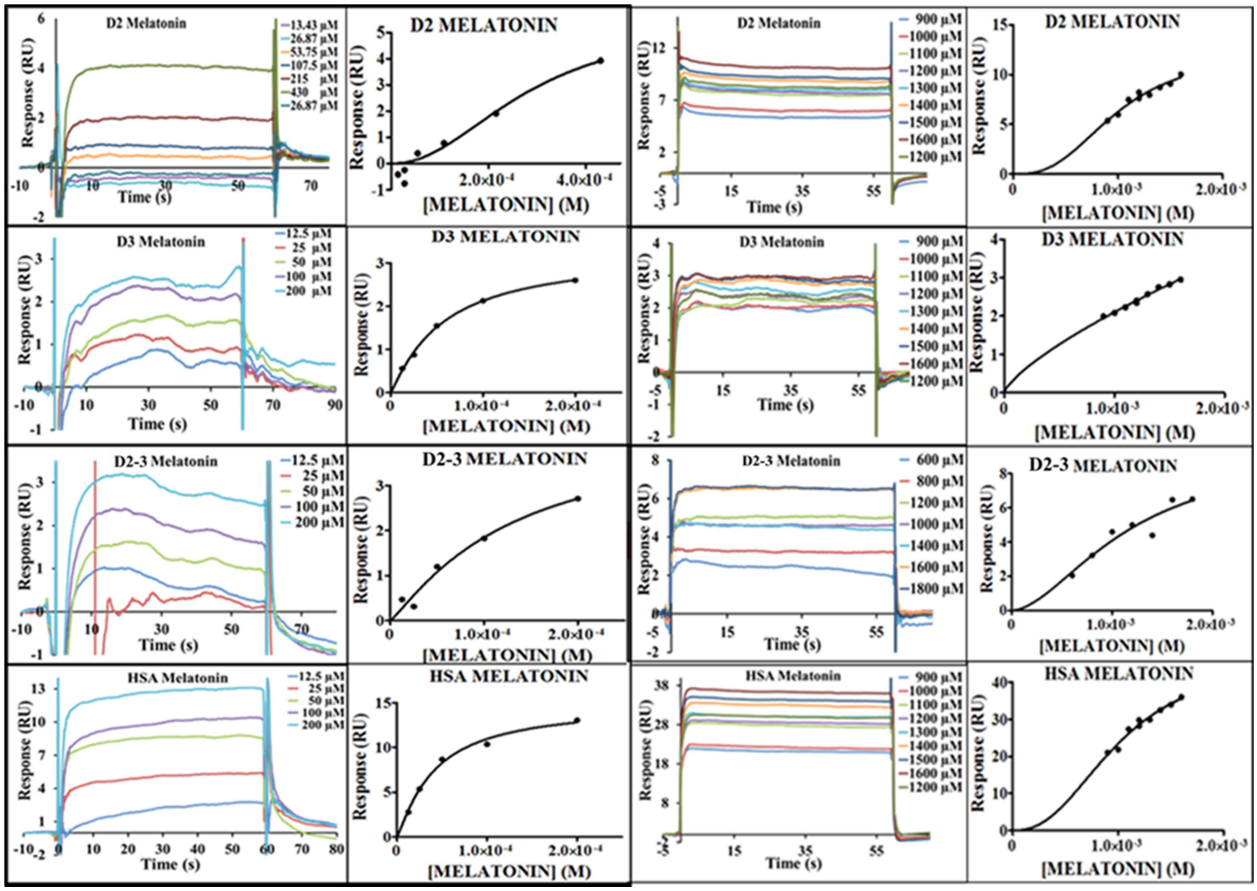

Figure 3.12 Interaction of Melatonin to HSA and its domains. For low concentration range, 12.5µM – 200 µM melatonin was used and for high concentration 900-1600 µM of melatonin, with linear concentration range is used.

Figure 3.13 shows the interaction of CMPF to HSA and its domains. The K_d values obtained for D2, D3, D2-3 and HSA are $1.42 \pm 0.26\times10^{-5}$ M, $8.48 \pm 1.66\times10^{-5}$ M, $7.66 \pm 1.16\times10^{-5}$ M and $4.46 \pm 1.10\times10^{-6}$ M, respectively, and the h values obtained for D2, D3, D2-3 and HSA are 4.5, 4.4, 4.1 and 3.2, respectively. In case of CMPF, D2 is showing high affinity when compared to D3, is in good agreement with the reported data.

Table 3.2: Affinity constant, K_d, values for the interaction of studied PBUTs to HSA and its domains

	HA (M)	IAA (M)	Melatonin (M)	CMPF (M)	
HSA	$4.74\pm1.07\times10^{-5}$	$3.63\pm0.53\times10^{-5}$	$5.19\pm1.10\times10^{-5}$	$4.46\pm1.10\times10^{-6}$	**CMPF > IAA ≥ HA ≥ Melatonin**
D2	$1.05\pm0.11\times10^{-4}$	$1.69\pm0.17\times10^{-4}$	$2.24\pm0.51\times10^{-4}$	$1.42\pm0.26\times10^{-5}$	**CMPF > HA > IAA > Melatonin**
D3	$1.73\pm0.05\times10^{-5}$	$2.15\pm0.22\times10^{-6}$	$3.88\pm1.5\times10^{-5}$	$8.48\pm1.66\times10^{-5}$	**IAA > HA > Melatonin > CMPF**
D2-3	$1.08\pm0.16\times10^{-4}$	$7.97\pm0.89\times10^{-6}$	$1.20\pm0.14\times10^{-4}$	$7.66\pm1.16\times10^{-5}$	**IAA > CMPF > HA > Melatonin**
	D3 > HSA > D2 ≥ D2-3	**D3 > D2-3 > HSA > D2**	**D3 ≥ HSA> D2-3 ≥ D2**	**HSA > D2 > D2-3 ≥ D3**	

Table 3.2 emphasizes the overall comparison of the K_d values. D3 has high affinity for the three PBUTs such as HA, IAA and melatonin, whereas, in case of CMPF, D2 has high affinity to CMPF after HSA. Among the PBUTs studied, melatonin has low affinity for all the proteins except for D3. CD data is showing that the folding of domains was preserved and it is similar to the respective portion of complete HSA indicating that there are no alterations in the binding sites. But, there can be two possibilities for altered ligand binding in case of domains compared to HSA. One is the binding sites may get exposed to solvent and secondly the stabilizing interactions from the residues of neighboring domains may be lost. The high affinity of D3 to HA, IAA and Melatonin compared to HSA indicate that there is no effect of the residues from neighboring domains.

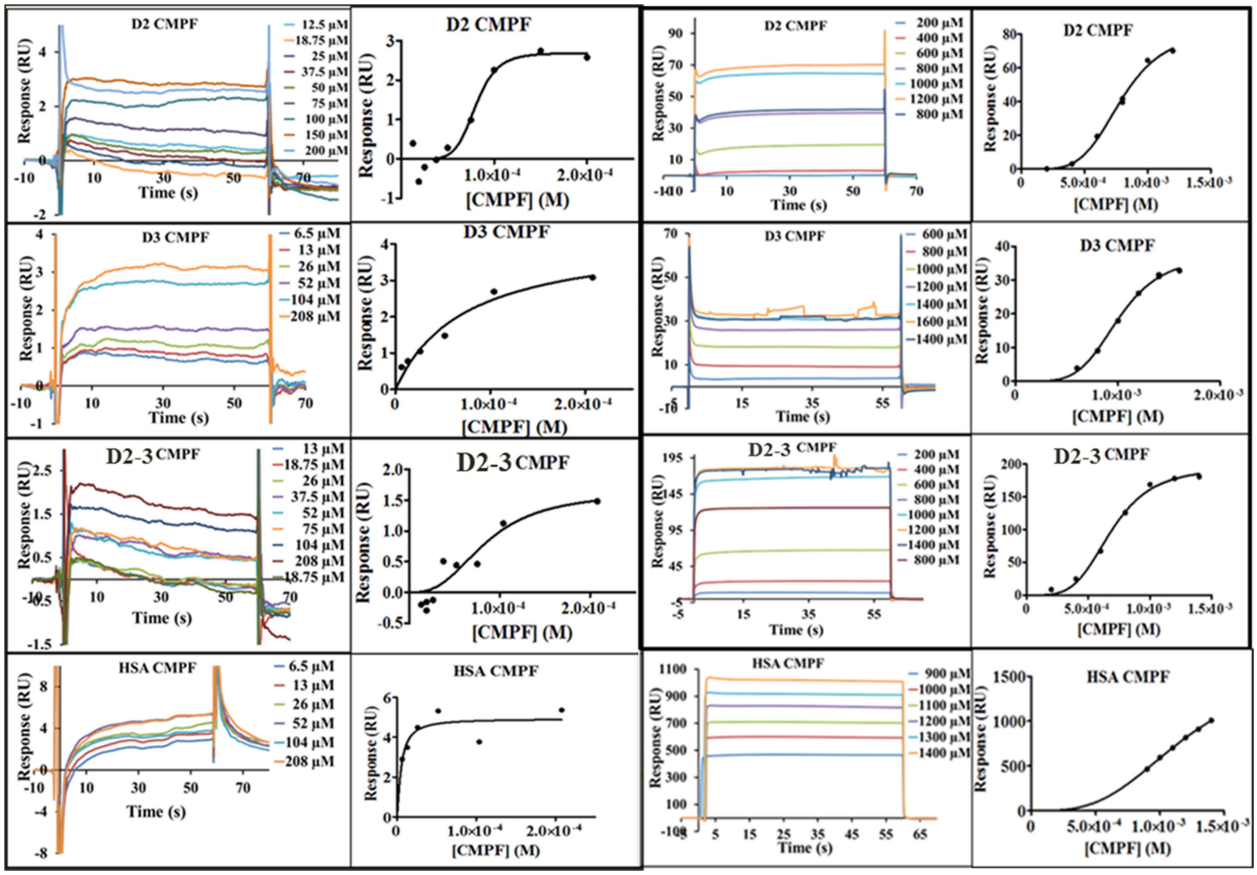

Figure 3.13 Interaction of CMPF to HSA and its domains. For low concentration range, 12.5µM – 200 µM CMPF was used and for high concentration 900-1600 µM of CMPF, with linear concentration range is used.

3.2.4. Molecular Docking

To further understand the complex formation, the residues that are interacting and the type of interactions involved, we have performed the molecular docking studies. He and Carter (He & Carter, 1992) reported the first crystal structure of HSA. Now, there are around seventy crystal structures for HSA and its ligand complexes. This made possible to do several computer-based analyses of this protein, such as molecular docking and molecular simulations studies. Here, we have used the PDB structure of HSA with PDB ID 1AO6 and domains PDB files were prepared by editing this PDB file.

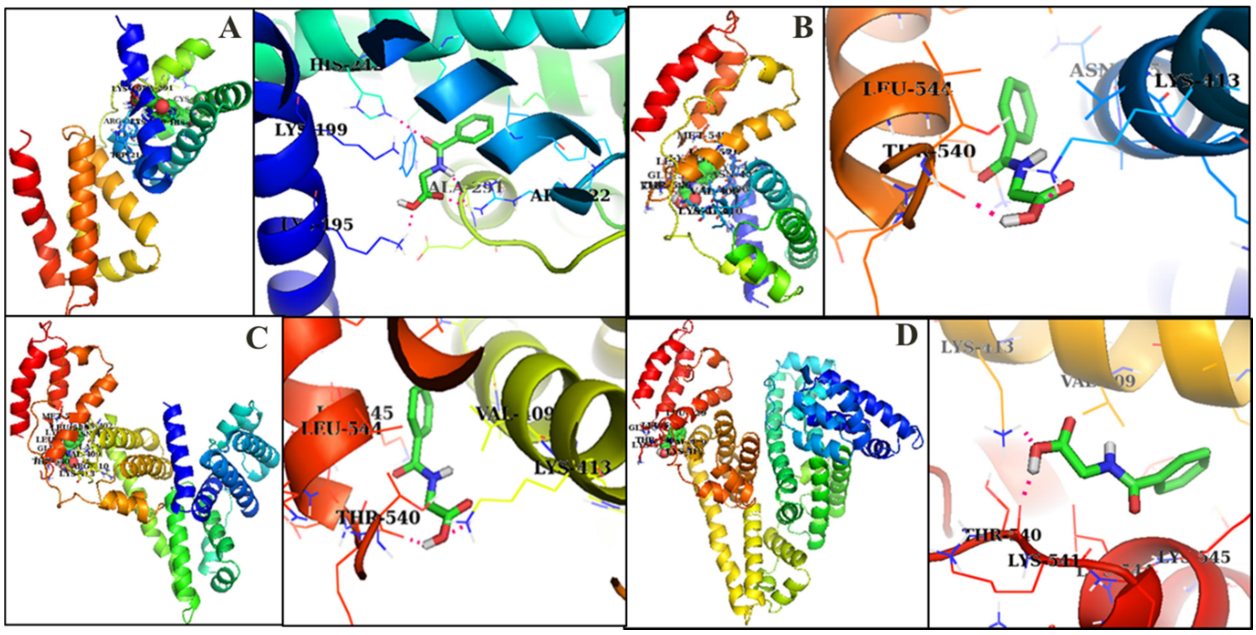

Figure 3.14 Interactions of HA to A) D2, B) D3, C) D2-3 and D) HSA were analyzed using molecular docking studies. The interactions involved in complex formation were visualized using PyMol software.

Figure 3.14 visualizes the interactions in binding of HA to D2, D3, D2-3 and HSA. In case of D2-HA complex, His242, Arg222, Lys195 and Ala291 are forming hydrogen bonds and stabilizing the complex. The carbonyl group of Ala291 is participating in hydrogen bond formation. The binding free energy value obtained for D2-HA complex is -5.13 kcal/mol. In case of D3-HA, the ligand is forming hydrogen bonds with Lys413 and Thr540. Thr540 also interacting with its carbonyl oxygen. The binding free energy value obtained for D3-HA complex is -5.45 kcal/mol. Similar to D3, Lys413 and Thr540 are the players involved in hydrogen bond formation in case of D2-3 and HSA. The binding free energy values obtained for D2-3-HA and HSA-HA complexes are -5.32 and -5.3 kcal/mol, respectively.

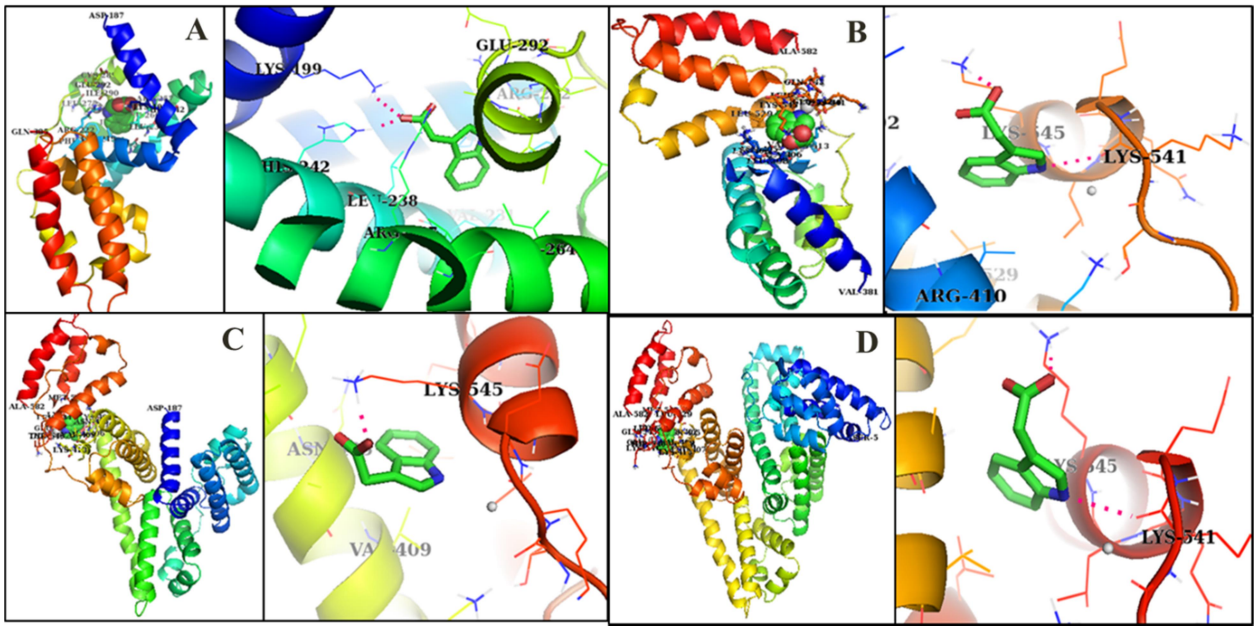

Figure 3.15 Interactions of IAA to A) D2, B) D3, C) D2-3 and D) HSA were analyzed using molecular docking studies. The interactions involved in complex formation were visualized using PyMol software.

The interactions of IAA to HSA and its domains are visualized in Figure 3.15. In case of D2-IAA complex, Lys199 and His242 are forming hydrogen bonds with IAA molecules. The binding free energy value obtained for D2-IAA complex is -6.12 kcal/mol. In D3-IAA complex, Lys541 and Lys545 are forming hydrogen bonds with IAA. Lys541 is interacting through its carbonyl oxygen, whereas Lys545 is interacting through side chain, i.e. ε-amino group. The binding free energy value obtained for D3-IAA complex is -6.35 kcal/mol. Similar to D3-IAA, in case of HSA-IAA also Lys541 and Lys545 are participating in hydrogen bond formation. But, in D2-3-IAA case, only Lys545 is participating. The binding free energy values obtained for D2-3-IAA and HSA-IAA complexes are -6.21 and -6.09 kcal/mol, respectively.

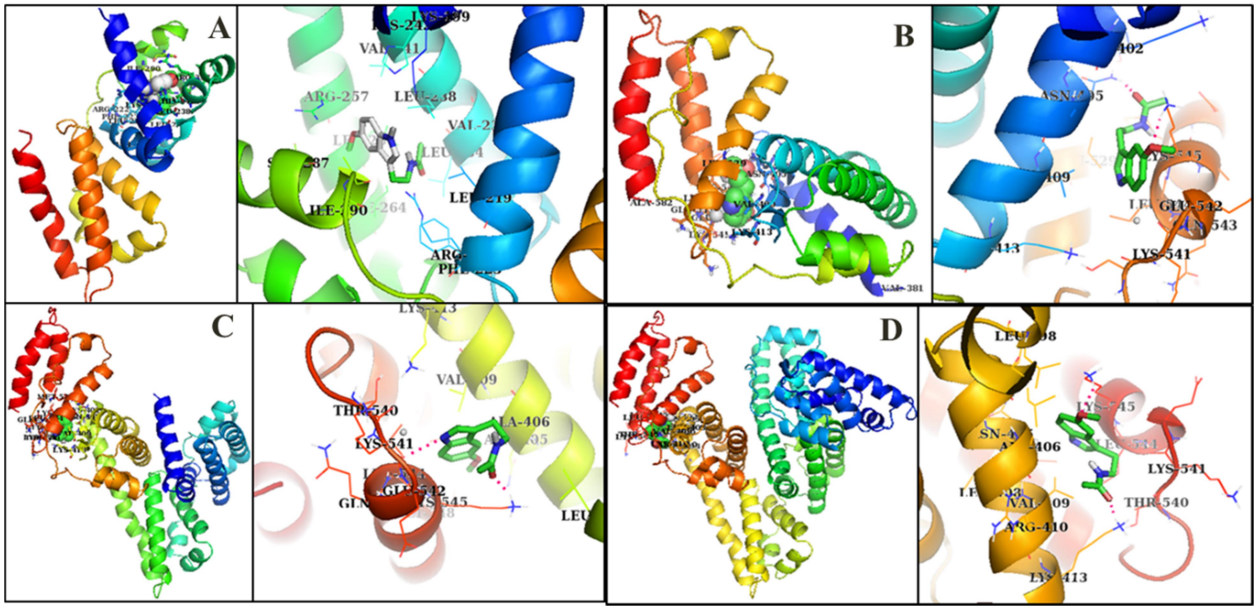

Figure 3.16 Interactions of Melatonin to A) D2, B) D3, C) D2-3 and D) HSA were analyzed using molecular docking studies. The interactions involved in complex formation were visualized using PyMol software.

Figure 3.16 is visualizing the interactions involved in complex formation of melatonin with HSA and its domains. D2-melatonin complex is entirely stabilized by hydrophobic and Van der Waals interactions. The binding free energy value obtained for D2-melatonin complex is -4.98 kcal/mol. Asn405 and Lys545 are interacting to melatonin through hydrogen bond formation in D3-melatonin complex and the binding free energy value is -6. The interaction of melatonin, an indole molecule, to D2-3 is similar to IAA binding in case of D3-IAA complex. Lys541 and Lys545 are forming hydrogen bonds with melatonin in D2-3-melatonin complex and the binding free energy value is -4.51 kcal/mol. In case of HSA-melatonin complex, Lys413 and Lys545 are forming hydrogen bonds with melatonin. The binding free energy value for HSA-melatonin complex is -4.55 kcal/mol.

Figure 3.17 is visualizing the interactions involved in complex formation of CMPF with HSA and its domains. In D2-CMPF complex CMPF is forming hydrogen bonds with Lys199, Arg222, His242 and Arg257. The binding free energy value obtained for D2-CMPF complex is -6.85 kcal/mol. Similar to D2, in case of D2-3, Lys195, Lys199, Arg222, His242 and Arg257 are involved in hydrogen bond formation with CMPF and the binding free energy value obtained for the complex is -6.49 kcal/mol. In HSA-CMPF complex Lys199, Arg222 and His242 are involved in hydrogen bond formation and the binding free energy value is -6.34 kcal/mol. In D3-

CMPF complex, Lys413, Thr540 and Lys545 are forming hydrogen bonds with CMPF and the binding free energy value obtained is -5.7 kcal/mol.

The docking data shows that the combination of basic and aliphatic amino acids are forming favorable binding conditions for the ligands in binding sites. The differential interaction to the domains of HSA could explain the structural differences of the PBUTs molecules. Also, it is evident that all these PBUTs have multiple binding sites to the HSA, as this protein is an allosteric in nature.

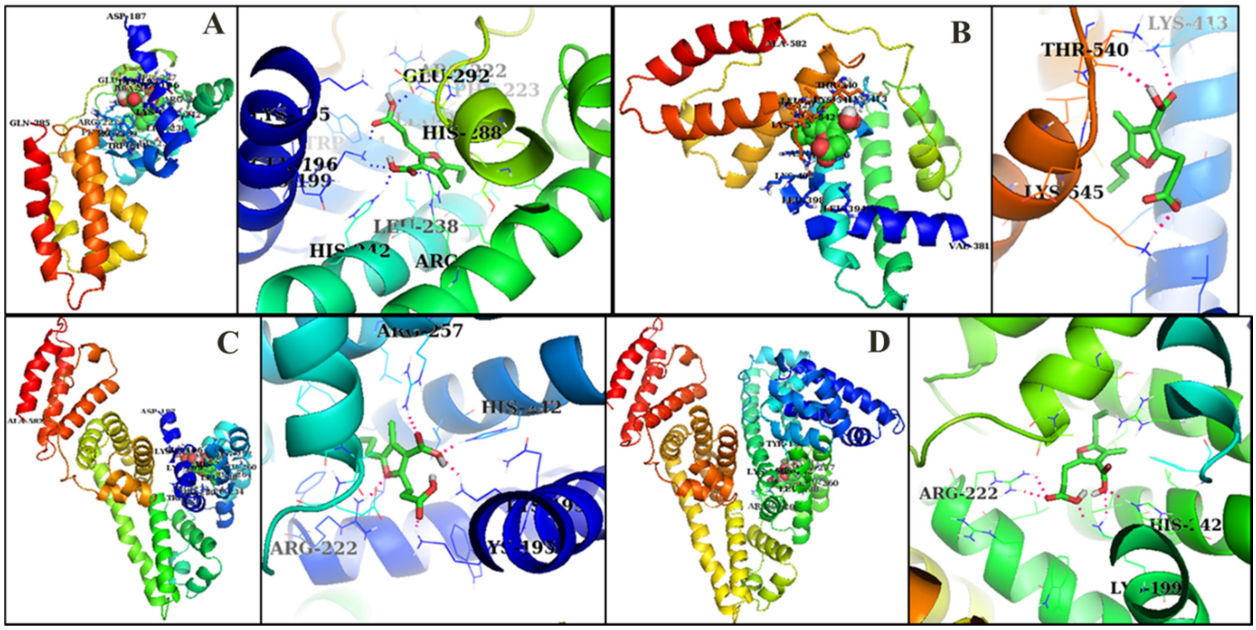

Figure 3.17 Interactions of CMPF to A) D2, B) D3, C) D2-3 and D) HSA were analyzed using molecular docking studies. The interactions involved in complex formation were visualized using PyMol software.

3.3 Conclusions

Our present study emphasized that the expressed domains of HSA D2, D3 and D2-3 are stable enough to the increasing temperature which is a good sign for working on this domains. The selected PBUTs such as HA, IAA, melatonin and CMPF have more than one binding site in HSA. The three PBUTs, HA, IAA and Melatonin can interact with D2, D3 and D2-3, with significant affinity and compared to other domains D3 is having high affinity (Figure 3.18). But CMPF is showing high affinity to D2 than D3. The K_d values obtained for domains of HSA are significantly different from that of complete HSA.

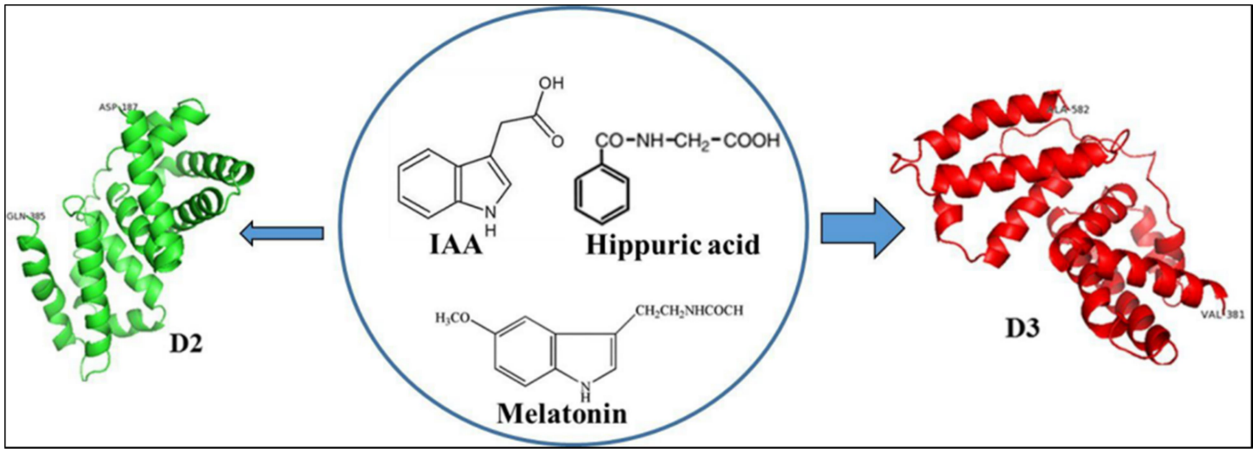

Figure 3.18 Pictorial representation of the final result of the study, showing that D3 has high affinity than D2 towards HA, IAA and Melatonin.

These two findings are useful as albumin can be replaced with its domains as dialysate in extracorporeal dialysis. The K_d value determines the free and protein bound concentration of ligands. The efficiency of dialysate can be improved by increasing the affinity and specificity of dialysate towards PBUTs, as HSA has affinity for several essential molecules, such as metabolites and nutrients in blood plasma. This can be achieved by using the combination of both the domains (i.e. D2 and D3) as dialysate and by playing with the ratios of D2 and D3. Hence, our study is giving a way to develop the therapeutic application to remove the uremic toxins from the kidney failure patients.

Chapter 4

Studying the effect of Herborn (K240E) and Milano Slow (D375H) human serum albumin variants towards binding of phenylbutazone and ibuprofen

4.1 Introduction

Phenylbutazone and Ibuprofen are the non-steroidal anti-inflammatory drugs and can interact with HSA. The interaction of phenylbutazone and ibuprofen to HSA was well characterized. The crystal structure for HSA-phenylbutazone complex (PDB ID: 2BXC) and HSA-ibuprofen (PDB ID: 2BXG) complex are also available (Ghuman et al., 2005). Phenylbutazone binds to site I located in subdomain IIA with high affinity (Curry, 2002, Curry, 2009). The binding of phenylbutazone to HSA was quantified using equilibrium dialysis method and reported that it has more than one binding site in HSA with an association constant of $1.5 \times 10^6\ M^{-1}$ for high affinity binding site (Kragh-Hansen, 1988, Yamasaki et al., 1996). Ibuprofen has two binding sites. One is located in drug site II is the high affinity site and another one is located at the interface between the subdomains IIA and IIB is the secondary binding site. Site II shows stereoselectivity towards ibuprofen binding (Itoh et al., 1997).

Altered drug binding affinity to HSA could be observed in diseased conditions. During this conditions HSA concentration could be altered and consequently structural modifications in HSA were reported (Yamasaki et al., 2013). Thus understanding the changes in drug binding mechanism, in case of modified HSA is useful. There are 67 natural genetic variants of HSA were reported and characterized (Fanali et al., 2012, Kragh-Hansen et al., 2013). The albumin variants include pro-albumin variants and some variants are glycosylated. Most of the HSA variants results from single amino acid substitution and most of them have altered net charge under physiological pH, because most of the point mutations are the result of change in charged amino acids. Along with net charge, the variants showed changes in α -helical content, thermal stability and plasma half-life (Kragh-Hansen et al., 2005, Iwao et al., 2007). Most of the variants were characterized for their ligand binding and altered fatty acid, metal and hormone binding (Kragh-Hansen et al., 1990, Kragh-Hansen et al., 1994, Kragh-Hansen et al., 2004). It was reported that Herborn (K240E) and Milano Slow (D375H) are the two natural variants of HSA (Minchiotti et al., 1993, Galliano et al., 1998). K240E has reduced half-life, α-helical content and thermal stability when compared to native HSA. It shows that reduction in half-life, α-helical content and van't Hoff enthalpy as 1.3%, 4.12% and 21.59% (Kragh-Hansen et al., 2005, Iwao et al., 2007). The effect of the mutation on bilirubin binding was analyzed and the results showed that there was no significant effect of K240E on bilirubin binding (Minchiotti et al., 1993).

D375H also has reduced half-life, α-helical content and van't Hoff enthalpy when compared to native HSA and has 1.54%, 5.3% and 32.23% reduction respectively (Iwao et al., 2007).

The reduction in α-helical content of 4-5% can have significant effect on ligand binding. Studying the binding of various drugs on these two variants would be very important in understanding pharmacokinetics mechanism. In our present study, we have analyzed the binding of K240E and D375H variants with phenylbutazone and ibuprofen. We also studied the interaction with the double mutant harboring two point mutations i.e. K240E/D375H and also with recombinant HSA (rHSA). We have generated the point mutation and the double mutation using site directed mutagenesis. *Pichia pastoris* expression system was used for expression of HSA and its variants. The binding of phenylbutazone and ibuprofen was checked using fluorescence spectroscopy.

4.2 Results and discussion

4.2.1 HSA variants by site directed mutagenesis and their structural analysis

The two point mutations and the double mutant were generated by site directed mutagenesis using *Dpn* I enzyme (Weiner et al., 1994, Vaikuntapu et al., 2018). Figure 4.1 shows the generation of mutants using *Dpn* I. The double mutant was generated by incorporation of single mutation one after the other. The incorporation of the mutations was confirmed by the sequencing analysis. The confirmed clones were transformed to *P. pastoris* and expressed.

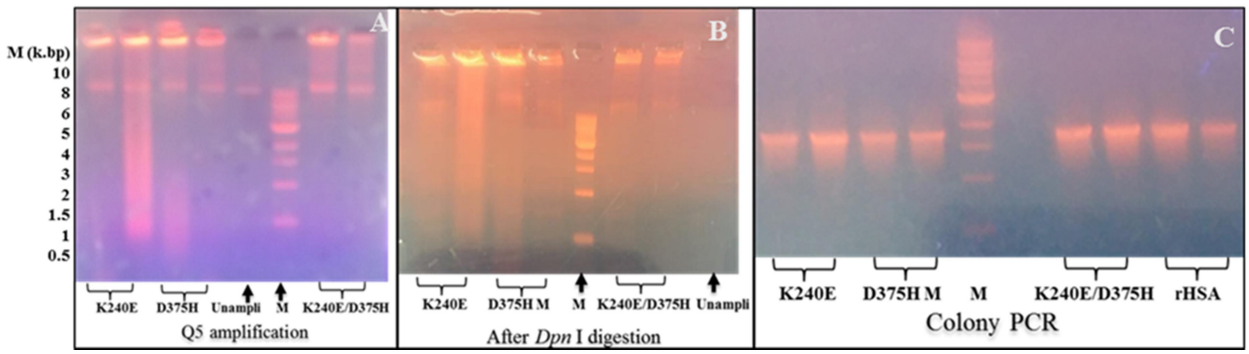

Figure 4.1 A) Q5 amplification of pPIC9K+HSA using primers having mutation. The band corresponds to 11 k.bp is the amplified product and Unamplified (Unampli) is the template plasmid. B) After *Dpn* I digestion the template was digested as there is no band in Unamplified and in case of mutants only PCR amplified product having mutation is there. C) Colony PCR conformation of the mutants.

P. pastoris is a well-known expression system for the production of recombinant HSA (Zhang et al., 2000, Kobayashi et al., 2000). HSA and its variants were expressed extracellularly and the proteins were purified from the culture media. The purity of the proteins was checked using SDS-PAGE. Figure 4.2 shows the SDS-PAGE gel of purified HSA and its variants showing the protein bands corresponding to the molecular weight of HSA (66 kDa).

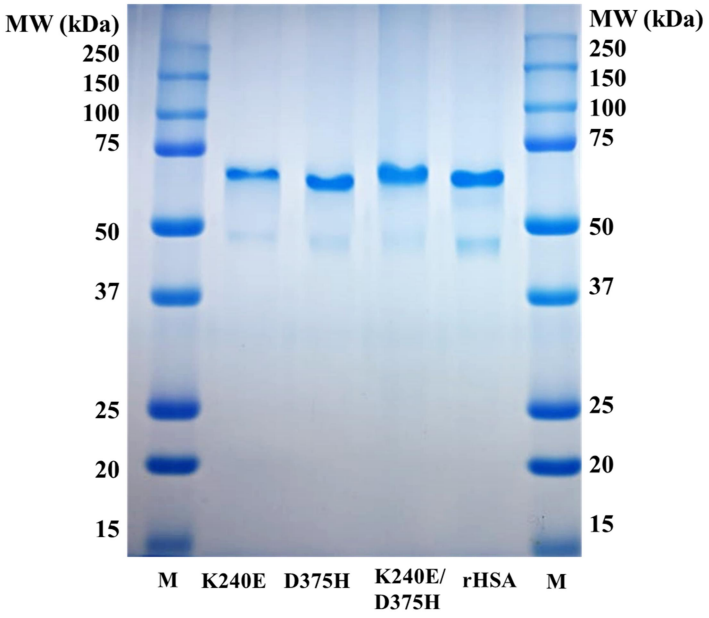

Figure 4.2: SDS-PAGE gel showing migration of HSA and its variants.

The structure of the purified proteins was analyzed using CD spectroscopy. From this spectra the secondary structural elements composition of the protein such as percentage of α-

helix, β-sheets and random coils were obtained (Chen et al., 1974, Kelly et al., 2005). Figure 4.3 shows the CD spectra and the secondary structure element composition of HSA and its variants. α-helical content got reduced in case of heterologous expressed mutant proteins when compared to rHSA as reported in case of plasma derived HSA and its variants (Iwao et al., 2007). K240E showed 2.3% reduction in α-helix and it is 5.6% reduction in case of D375H. The results are in agreement to the reported values where the reduction is high in case of D375H. In K240E, positively charged amino acid got substituted with negatively charged amino acid where as in case of D375H negatively charged amino got changed. This can result in changes in the local interactions between side chains of the residues, leads to the changes in protein structure. In case of K240E/D375H α-helical content got reduced to 9.4%, showing the cumulative effect of both the mutations.

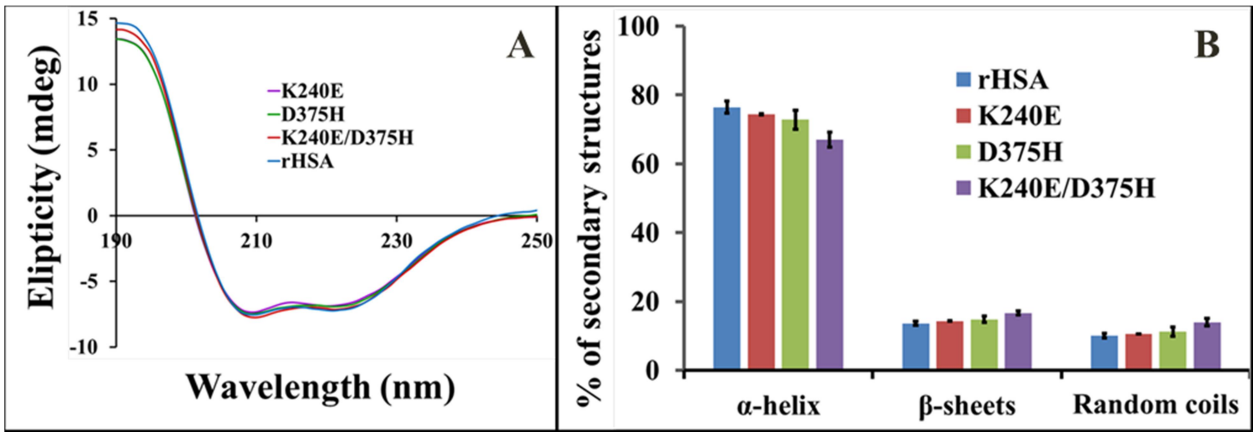

Figure 4.3: Structural analysis of HSA and its variants using CD Spectroscopy. A) The CD spectra of 0.5µM rHSA, K240E, D375H and K240E/D375H. B) % of Secondary structures were obtained using CDNN software.

4.2.2 Interaction of Phenyl butanone to K240E, D375H, K240E/D375H and rHSA

The interaction of phenylbutazone to K240E, D375H, K240E/D375H (variants of HSA) and rHSA was studied using fluorescence spectroscopy. The fluorescence emission of HSA comes from the single tryptophan residue located at 214 position, which is present in site I. Our group previously reported the interaction of various small molecules to HSA using fluorescence quenching phenomenon (Subramanyam et al., 2009, Kallubai et al., 2015, Yeggoni et al., 2015, Nerusu et al., 2017). The emission spectra recorded for the interaction of HSA and its variants with phenylbutazone was given in Figure 4.4. Titration of 0.001mM protein with increasing

concentration of phenylbutazone from 0.001mM to 0.01mM resulted in decrease in fluorescence emission and the quenching of the fluorescence is concentration-dependent. The binding of small molecules to HSA results in the changes of microenvironment of tryptophan residue, which results in the change in emission fluorescence intensity. The fluorescence quenching data can be analyzed using modified Stern − Volmer equation (Lakowicz, 2009a).

$$\frac{\log\ (F_0 - F)}{F} = \log K_a + n\ \log\ [Q]$$

Where n corresponds to the number of binding sites, F_0 represents the fluorescence intensity in the absence of quencher, F represents the fluorescence intensity in the presence of quencher, K_a is the association constant (or) the binding constant and [Q] is the quencher concentration.

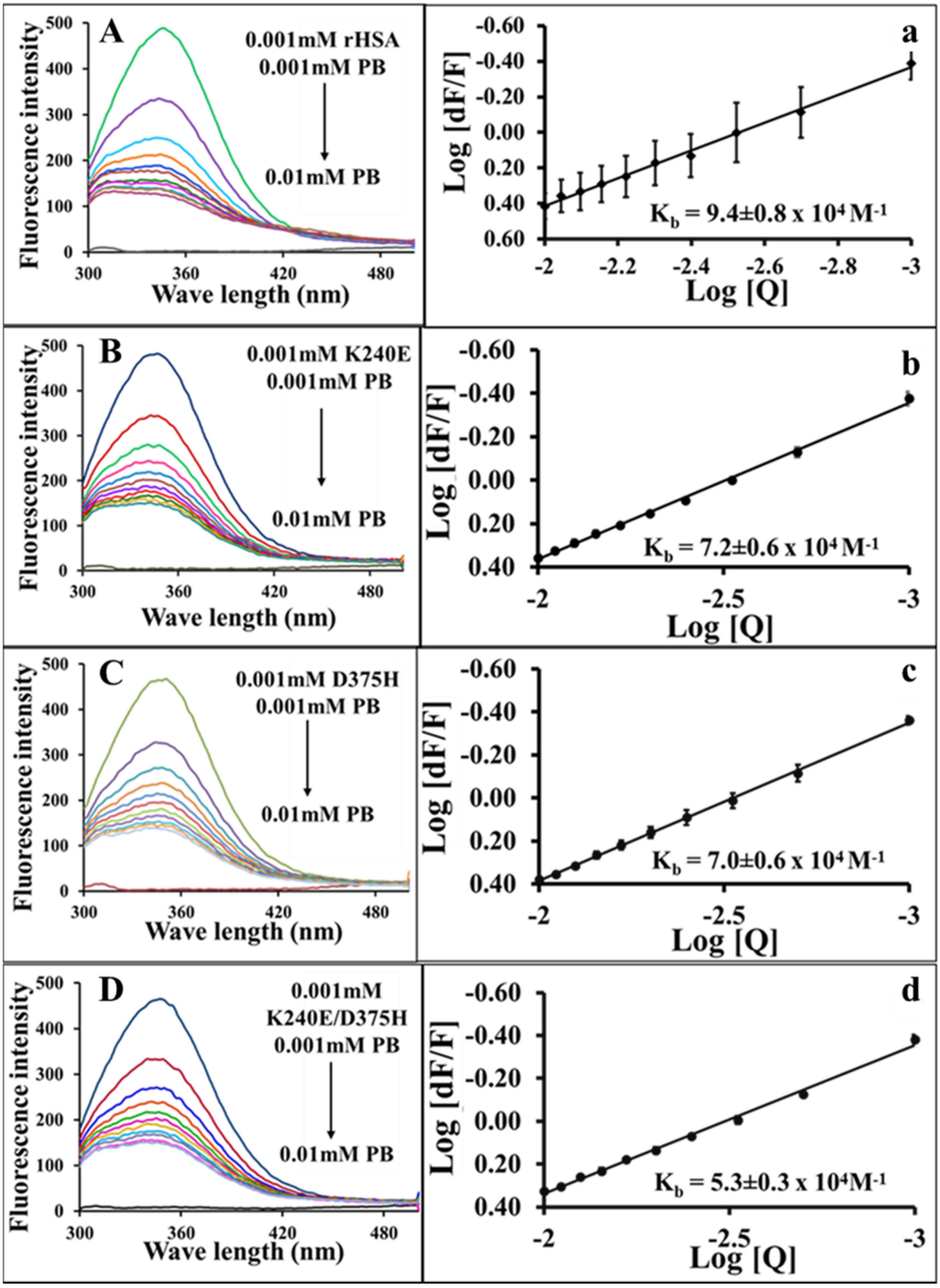

Figure 4.4: Fluorescence emission spectra of A) rHSA, B) K240E, C) D375H and D) K240E/D375H in presence of increasing concentration of phenylbutazone. Modified Stern-Volmer plots for the interaction of phenylbutazone to a) rHSA, b) K240E, c) D375H and d) K240E/D375H

The binding constant values were calculated for the interaction of phenylbutazone with K240E, D375H, K240E/D375H and rHSA as shown in Figure 4.4. The binding constant vales obtained for phenylbutazone binding with K240E, D375H, K240E/D375H and rHSA were found to be 7.2±0.6 x 10^4 M^{-1}, 7.0±0.6 x 10^4 M^{-1}, 5.3±0.3 x 10^4 M^{-1} and 9.4±0.8 x 10^4 M^{-1} respectively. There is a slight decrease in the bindnig constant value incase of K240E and D375H interaction when compared to rHSA. There is an insignificant effect of K240E mutation on phenylbutazone binding. The primary binding site for phenylbutazone is located in site I, where K240 also located. The crystal structure data of HSA-phenylbutazone complex shows that R257 and Y150 are forming hydrogen bonds with phenylbutazone, H242 and R222, are residues forming binding pocket (Ghuman et al., 2005). H242 is very near to K240, but the side chain of K240 is not so near to the binding pocket. Also, the site I is large and flexible region. There by the change of K240 to E240 is not affecting the binding of phenylbutazone significantly. D375 is located distantly from the phenylbutazone binding site. The slight decrease in the binding constant values can be due the presence of other low affinity binding sites. The binding constant value decreased further in case of K240E/D375H, showing the cumulative effect of both the mutations.

The reciprocal of association constant value gives the K_d value from which the binding free energies can be calculated using the following equation.

$$\Delta G^0 = -RT \ln K_d$$

Where ΔG^0 is the free energy change, R is the gas constant at room temperature, and K_d is the dissociation constant which is given by

$$K_a = \frac{1}{K_d}$$

The free energy values obtained for the binding of phenylbutazone to K240E, D375H, K240E/D375H and rHSA are -6.59, -6.58, -6.41 and -6.75 kcal/mol, respectively.

We have also checked the effect of phenylbutazone binding on the protein conformation using CD spectroscopy. The CD spectra of protein were collected with increasing concentration of phenylbutazone. Figure 4.5 shows the CD spectra of K240E, D375H, K240E/D375H and rHSA with increasing concentration of phenylbutazone. The results indicate that there is no effect of phenylbutazone binding on the conformation of HSA and its variants.

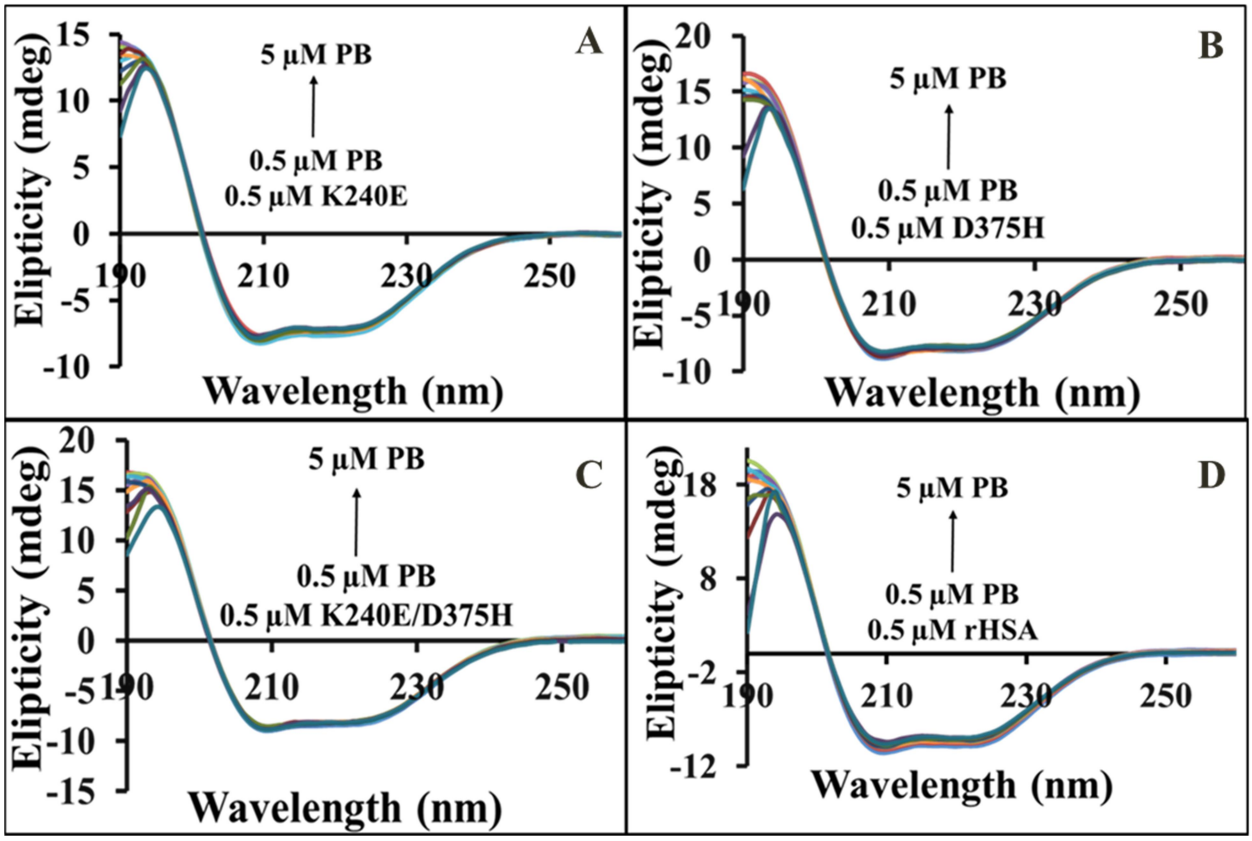

Figure 4.5: CD spectroscopy studies to understand the effect of phenylbutazone binding on structure of A) K240E, B) D375H, C) K240E/D375H and D) rHSA.

4.2.3 Interaction of Ibuprofen to K240E, D375H, K240E/D375H and rHSA

The interaction of ibuprofen to HSA and its variants was also studied using fluorescence spectroscopy. Figure 4.6 shows the interaction of ibuprofen to K240E, D375H, K240E/D375H and rHSA. The binding constant values obtained for ibuprofen binding with K240E, D375H, K240E/D375H and rHSA were found to be 1.4±1.0 x 10^4 M^{-1}, 1.3±0.7 x 10^4 M^{-1}, 7.3±1.0 x 10^3 M^{-1} and 1.2±0.1 x 10^4 M^{-1}, respectively. There is no change in the association constant value of ibuprofen binding to K240E and D375H, but change is observed when both the mutations were there in K240E/D375H. The position of D375 is close to the well-known ibuprofen secondary binding site. Quantum molecular modelling studies allowed to calculate radius of binding pocket residues and showed that F377, the neighboring residue to D375, is located 12 Å distance from ibuprofen (Dantas et al., 2015).

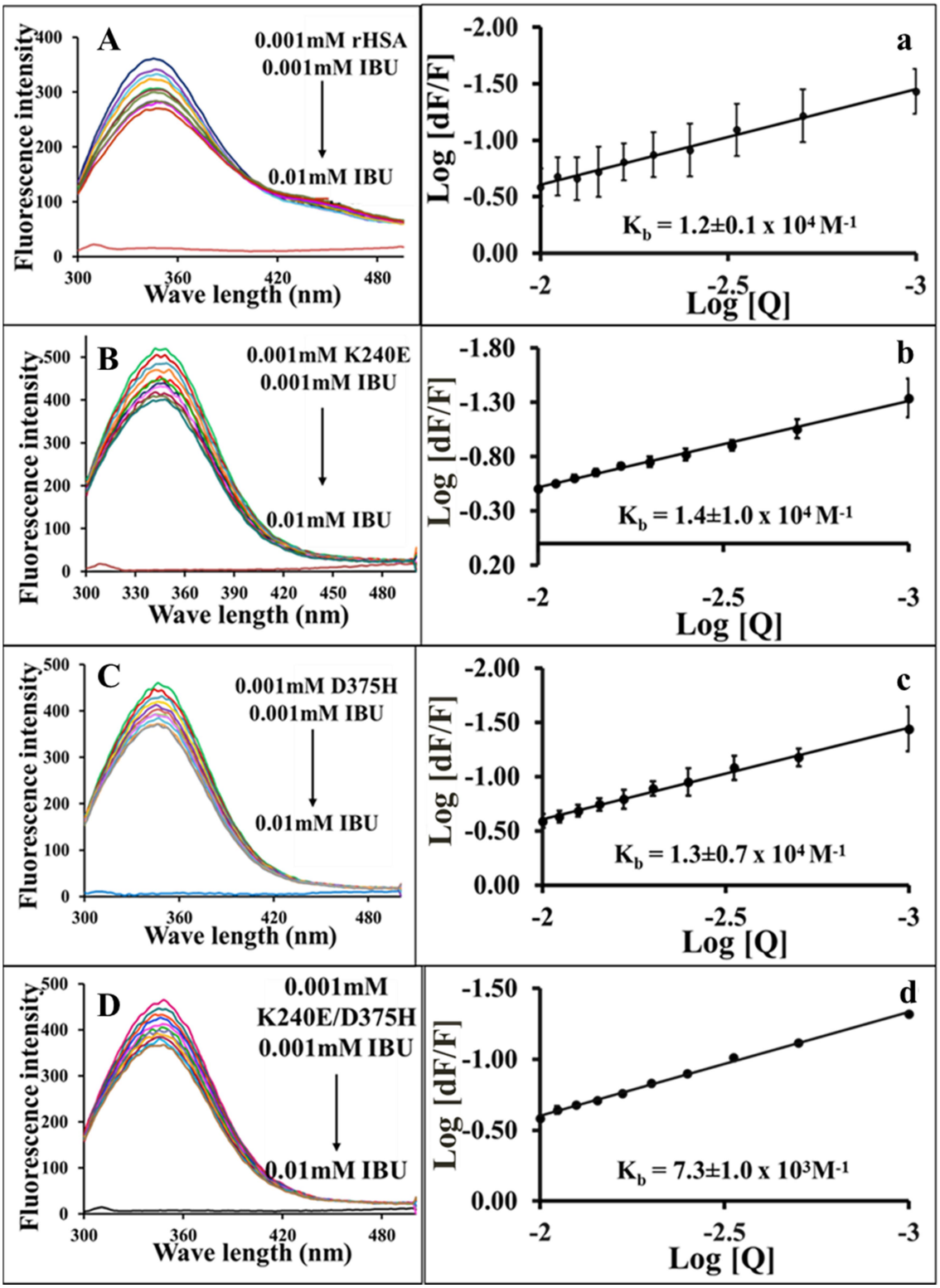

Figure 4.6: Fluorescence emission spectra of A) rHSA, B) K240E, C) D375H and D) K240E/D375H in presence of increasing concentration of ibuprofen. Modified Stern-Volmer plots for the interaction of ibuprofen to a) rHSA, b) K240E, c) D375H and d) K240E/D375H.

Even the D375 residue is distantly present from ibuprofen binding location, the D375H mutation resulted in the significant structural change in the protein which can affect the ibuprofen binding. But the effect is not seen in D375H mutation as the binding constant value obtained is nearer to the binding constant values for K240E and rHSA binding to ibuprofen. But the effect can be observed when both the mutations are there in double mutant (K240E/D375H). This could be because ibuprofen has several other low affinity binding site including site I (Ghuman et al., 2005, Evoli et al., 2016) and also binding of ibuprofen can show allosteric effect on the binding of ligands to the distantly located binding sites. Binding of ibuprofen to HSA can exert allosteric effect on heme binding to the distantly present heme binding site (Nicoletti et al., 2008). Inferring that the presence of both the mutations effecting the binding of ibuprofen significantly to the multiple sites. The binding free energy values were also calculated and the obtained binding free energy values for the binding of ibuprofen to K240E, D375H, K240E/D375H and rHSA are -5.53, -5.54, -5.24 and -5.56 kcal/mol, respectively.

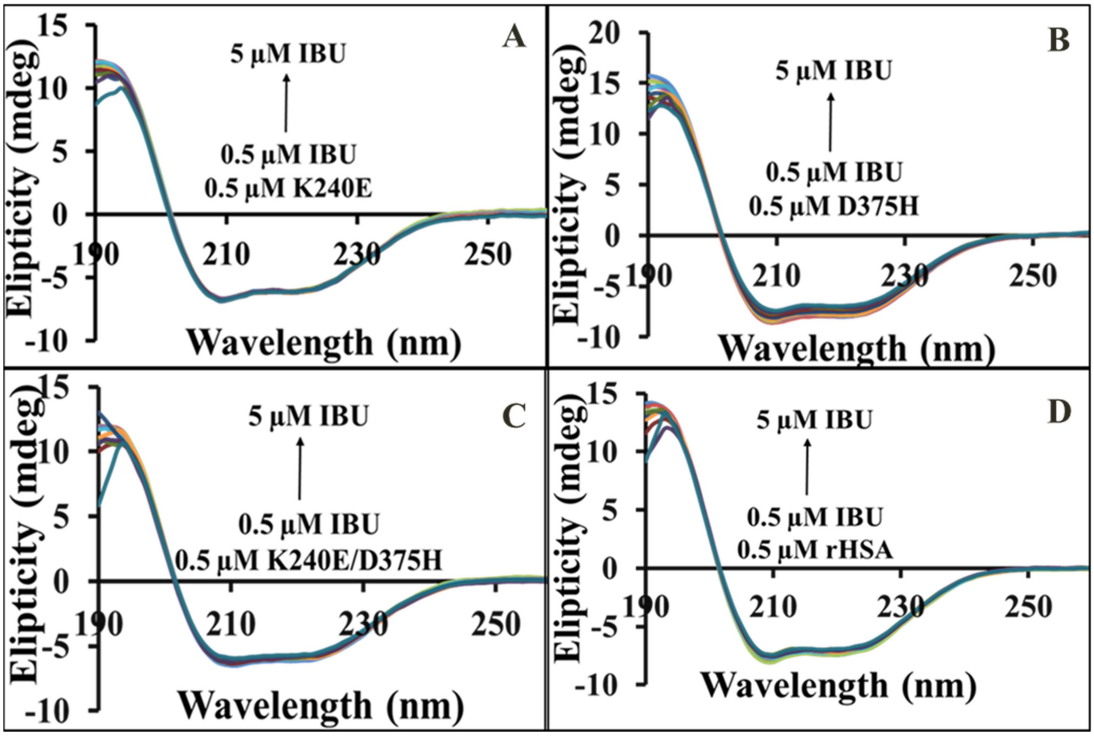

Figure 4.7: CD spectroscopy studies to understand the effect of ibuprofen binding on structure of A) K240E, B) D375H, C) K240E/D375H and D) rHSA.

Table 4.1: Binding constant values for the interaction of Phenylbutazone and Ibuprofen to K240E, D375H, K240E/D375H and rHSA.

	Phenyl butazone K_a (M^{-1})	Ibuprofen K_a (M^{-1})
K240E	$7.2\pm0.6 \times 10^4$	$1.4\pm1.0 \times 10^4$
D375H	$7.0\pm0.6 \times 10^4$	$1.3\pm0.7 \times 10^4$
K240E/D375H	$5.3\pm0.3 \times 10^4$	$7.3\pm1.0 \times 10^3$
rHSA	$9.4\pm0.8 \times 10^4$	$1.2\pm0.1 \times 10^4$
	rHSA >K2 ≥ D3H > K2D	rHSA ≥ K2 ≥ D3H > K2D

We have also checked the effect of ibuprofen binding on protein conformation. Figure 4.7 shows the CD spectra of HSA and its variants in the presence of increasing concentration of ibuprofen. There is no effect of ibuprofen binding on the conformation of the proteins, except in case of D375H. In D375H, there is a marginal change in the structure with ibuprofen binding. We have quantified the changes in secondary structure elements using CDNN software. Figure 4.8 shows the % of α-helix of HSA and its variants in the presence and absence of the phenylbutazone and ibuprofen. We have considered the α-helical content of proteins in absence of ligand as 100 percent. Then the relative percentage of α-helix of the proteins in presence of 5 μM (1:10 of protein to ligand) phenylbutazone and ibuprofen was calculated and shown in Figure 4.8. There is a considerable decrease in the α-helical content in D375H with ibuprofen binding. Which indicates that the conformational rearrangement of the protein to recompense the structural change due to D375H and to accommodate ibuprofen. Overall binding constant values of phenylbutazone and ibuprofen binding to HSA and its variants were shown in table 4.1. In both the cases double mutant (K240E/D375H) is showing decreased binding constant value.

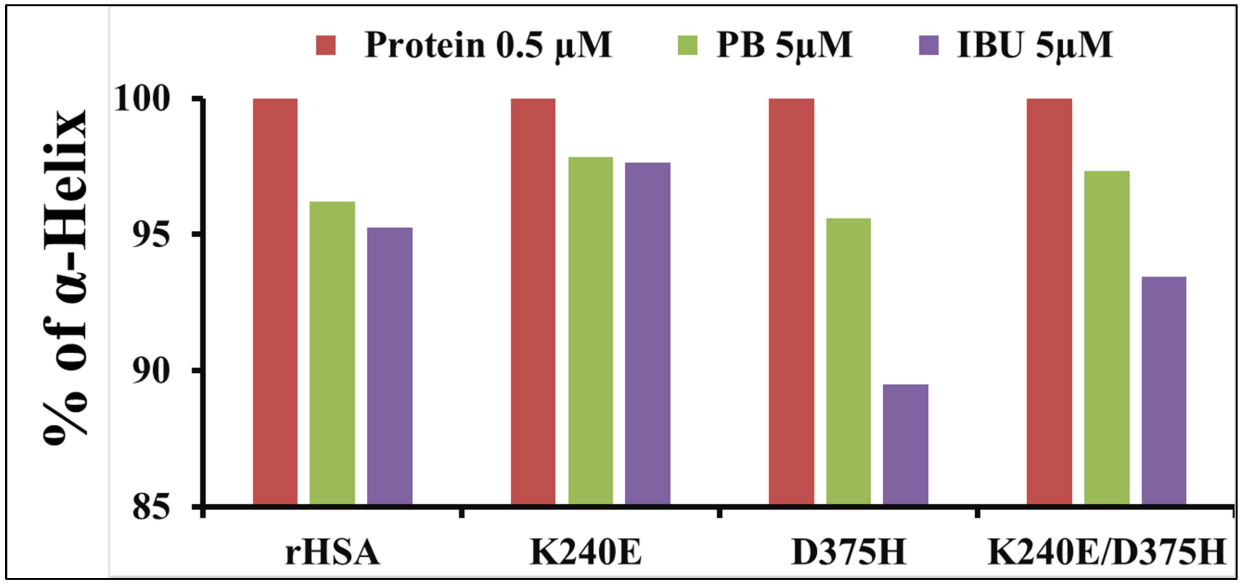

Figure 4.8: α-helical content of rHSA, K240E, D375H and K240E/D375H alone, in presence of 5µM phenylbutazone and in presence of 5µM ibuprofen.

4.3 Conclusion

Studying the effect of albumin modifications on drug binding is useful as the drug binding to HSA determines the pharmacokinetic profile of drugs. In our present study, we have expressed HSA and its variants heterologously and studied the interaction with two non-steroidal anti-inflammatory drugs, phenylbutazone and ibuprofen. From our study it is clear that there is no significant effect of K240E and D375H mutations on phenylbutazone and ibuprofen binding. K240E and D375H are the natural variants of HSA and the insignificant effect of mutation on drug binding is desirable. There is a reduction in the binding constant value in case of double mutant (K240E/D375H) when compared to two individual single point mutations. The effect can be observed in case of double mutant giving that the binding was affected at two sites. Further, CD data showed that phenylbutazone and ibuprofen binding is not affecting the protein conformation, except in D375H, where there is a conformational change in the binding pocket with the ibuprofen binding.

Chapter 5

Unraveling the Stability of Plasma Proteins upon Interaction of Synthesized Androstenedione and its Derivatives - Biophysical and Computational Approach

5.1. Introduction

Steroids get transported in the blood stream with the aid of specific transporter proteins. Even though specific carrier proteins are available for steroids transport, they can also effectively interact with HSA (Pearlman & Crépy, 1967, Varshney et al., 2010). Earlier reports on steroid hormones like testosterone and progesterone show that they can interact with HSA (Pearlman & Crépy, 1967, Westphal & Harding, 1973). Natural variants of HSA like Niigata and Tagliacozzo show high affinity towards prostaglandin and progesterone respectively (Kragh-Hansen et al., 1990). 4-Androstene-3-17-dione (4A) is naturally occurring steroidal hormone, produced in gonads and adrenal glands and is found to be the key metabolic intermediate in steroidal metabolism such as testosterone, estradiol, progesterone, cortisone and cortisol (Malaviya & Gomes, 2008). Synthetically, this compound is also used as a precursor molecule for synthesis of various steroids. It possesses both androgenic and anabolic properties (Bahrke & Yesalis, 2004) and thus, the level of 4A in blood plasma is significant. Also, it is an immediate precursor for testosterone and the enzyme 17-β-hydroxy steroid dehydrogenase converts 4A to testosterone. Further, the enzyme aromatase converts 4A to estrone and estradiol (Jasuja et al., 2005). In this line, 5β-androstane-3-17-dione (5A) was synthesized through organocatalysis method by taking (4A) as starting material (Ramachary et al., 2013). Physiologically, 4A gets convert to 5A in presence of 3-oxo-5-beta-steroid-4-dehydrogenase. Another derivative is (+)-6-methyl-5β androstane-3-17-dione (6M), in which the methyl group is attached at C6 position of 5β-androstane-3-17-dione.

Beside HSA, another plasma protein α 1-acid glycoprotein (AGP), also known as orosomucoid and an acute protein, also interacts with steroids and their derivatives. Perhaps, AGP, acute phase protein plays an important role in binding of drugs. It has a normal range of 0.6–1.2 mg/mL (1–3% of plasma proteins) (Fournier et al., 2000), during inflammation the plasma concentration increases to 2-5 folds. Moreover, this protein has anti-inflammatory and immunomodulatory role. Surprisingly, the levels of AGP elevated in acute inflammation and shows systemic response to local inflammation (Kim et al., 2006). It is a glycoprotein of 183 amino acid residues with 41kDa molecular weight and consists of 45% carbohydrate attached in the form of N-linked glycans, confines to N-terminus of the protein. This protein is negatively charged at physiological pH because of 16 sialic acid residues (Schönfeld et al., 2008). Also, it

has three tryptophan residues, where tryptophan 160 present on the surface of the protein and rest two are located at inner side of the protein (Lupidi et al., 2012). Predominantly, there is only single high affinity basic drug binding site in AGP (Müller & Stillbauer, 1983). Recently, our group reported that there are several molecules specifically bind to the AGP (Kallubai et al., 2015, Yeggoni et al., 2015). Competition for the single basic drug binding site can control the therapeutically effective plasma levels of basic drugs. Because of single binding site, the drugs binding to AGP can attain saturation and are competitively displaceable. Stereo selectivity is also there for single binding site. In case of steroids binding, AGP can interact strongly with progesterone (Kute & Westphal, 1976) and the binding site for the progesterone is located in the N-terminus. Consequently, the binding site for progesterone is near to carbohydrate residue, demonstrated by using calcofluor white as a probe (De Ceukeleire & Albani, 2002).

In the present study we have aimed to understand the following observations like interaction mechanism of the HSA and AGP with synthesized steroid molecules, 4-Androstene-3-17-dione (4A), 5β-androstane-3-17-dione (5A) and (+)-6-methyl-5β-androstane-3-17-dione (6M) (Figure 5.1). Further, the conformational changes and stability of the complexes were emphasized using biophysical and computational approaches.

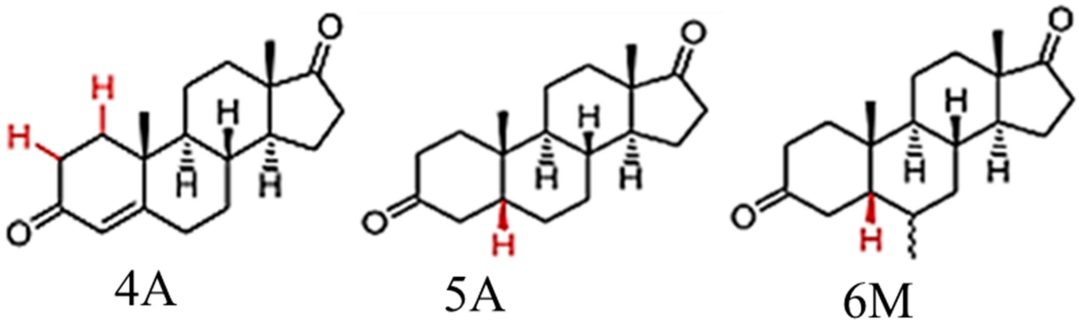

Figure 5.1 Structures of 4A, 5A and 6M. The molecular weight of 4A, 5A and 6M is 286.41, 288.42 and 302.45 Da respectively.

5.2. Results and discussion

5.2.1. Analysis of fluorescence characteristics and quenching mechanism

The phenomenon of fluorescence quenching is an important method to characterize the interaction between a ligand and biological macromolecules. In the present study, the interaction of 4A, 5A and 6M with HSA and AGP was characterized using fluorescence emission spectra. The interaction time was optimized by monitoring the fluorescence emission spectra of HSA and AGP at maximum concentration of the compounds at regular time periods and arrived to the incubation time of 5 minutes. The emission spectra recorded for HSA and AGP with increasing concentrations of the ligands were shown in Figure 5.4 and Figure 5.5, respectively. In presence of increasing concentrations of the 4A, 5A and 6M, the intensity of fluorescence emission decreased gradually with insignificant shift towards shorter wavelength. However, there is no significant fluorescent emission from ligands. Hence, the quenching of the fluorescence is concentration dependent. Our group previously reported the interaction of various phytochemicals with HSA based on fluorescence quenching phenomenon (Subramanyam et al., 2009, Yeggoni et al., 2014).

HSA has a single tryptophan residue (Trp-214) located in the subdomain IIA corresponding to the sudlow's drug binding site I region. The characteristic emission spectrum for HSA has emission maxima at 350 nm (Figure 5.4). In case of AGP it has three tryptophan residues and characteristic florescence emission spectrum shows emission maxima at 340 nm and the peak is narrower compared to HSA (Figure 5.5). When small molecular substances bound to HSA, the changes of intrinsic fluorescence of HSA are induced by the

microenvironment of tryptophan residues. This indicates that microenvironment around tryptophan has been altered due to formation of HSA - 4A (androstenedione), 5A and 6M complexes.

Another important factor which could lead to decrease in emission intensity is the inner filter effect (Yeggoni et al., 2017). The absorption and emission spectra of 4A, 5A and 6M at 10µM concentration were given in Figure 5.2. The emission intensities were corrected for inner filter effect using the following relationship.

$$F_{Cor} = F_{Obs} \times e^{\frac{A_{exi}+A_{emi}}{2}}$$

Where F_{cor} is the corrected fluorescence intensity, A_{exi} and A_{emi} represent the absorbance at the fluorescence excitation (285 nm) and emission wavelengths respectively and F_{obs} is the observed fluorescence.

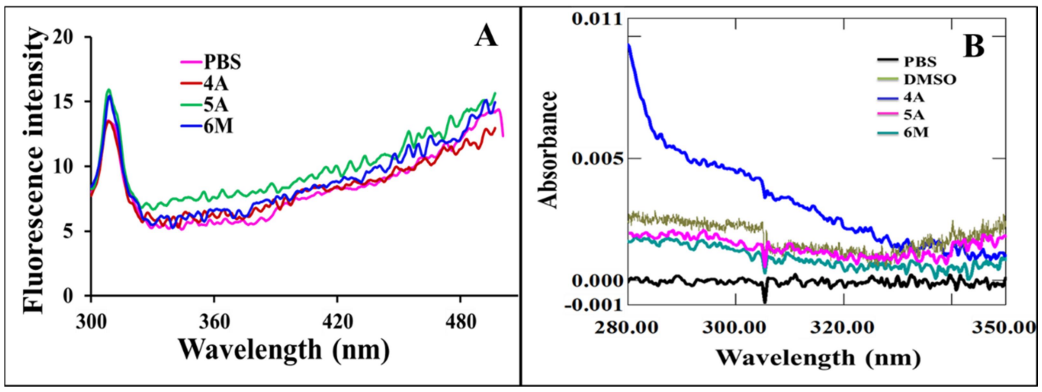

Figure 5.2 A) Fluorescence emission spectra of PBS with pH 7.4, 10µM of 4A, 5A and 6M. B) Absorption spectra of DMSO, 10µM of 4A, 5A and 6M by taking PBS as baseline.

There are two common mechanisms of quenching are well known as dynamic (or) collisional and static quenching (Lakowicz, 2009b), which can be distinguish by temperature, viscosity dependence and by the difference of their fluorescence lifetimes. The relation between the quencher concentration and the fluorescence intensity can be well explained using stern-volmer equation.

$$\frac{F_0}{F} = 1 + K_q \tau_0 [Q] = 1 + K_{SV}[Q]$$

where F_0= fluorescence intensities in the absence of quencher, F = fluorescence intensities in the presence of quencher, [Q] = quencher concentration, k_q = bimolecular quenching rate constant, τ_0 = lifetime of the fluorophore in the absence of quencher and its value is around 10^{-8}s for most of the biomolecules. K_{SV} = Stern–Volmer quenching constant, which can be written as

$$K_q = \frac{K_{SV}}{\tau_0}$$

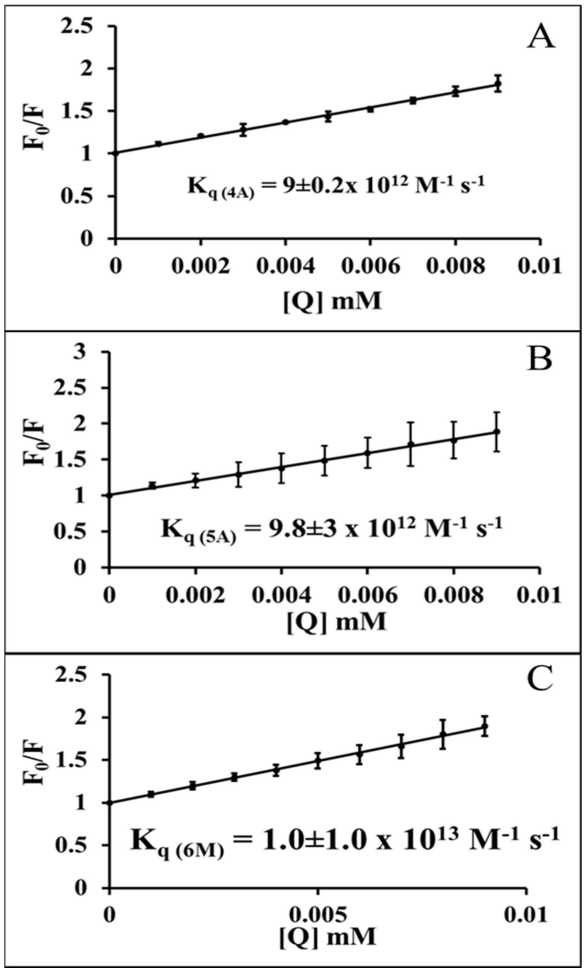

Figure 5.3 Stern–Volmer plot obtained by plotting concentration of A) 4A, B) 5A and C) 6M on X axis and F_0 /F on Y axis. Slope of the graph gives Stern–Volmer quenching constant (K_{SV}), from that bimolecular

quenching rate constant (K_q) was calculated. K_q is more than 2.0×10^{10} M^{-1} s^{-1} for all molecules showing the stable complex formation.

The emission quenching data of HSA was plotted as F_0/F against the concentration of ligand, which was shown in Figure 5.3. It shows that within the investigated concentrations, the Stern– Volmer plot exhibited a good linear relationship. Further the values of Stern–Volmer quenching constant K_{SV} was obtained from the slope, by keeping intercept at 1. The average lifetime (τ_0) of the biopolymer without any quencher has already been reported as ~10^{-8}s (Sharma et al., 2014). From above equation bimolecular quenching rate constant was calculated and that was far greater than the maximum scatter collision quenching constant 2.0×10^{10} $M^{-1}s^{-1}$ (Tabassum et al., 2012) showing the formation of ground state complex between protein and the ligands. It has been well established that for a static quenching process, the quenching constant K_q should be greater than the maximum scatter collision quenching constant. The calculated K_q values are $9.0\pm0.2\times10^{12}M^{-1}s^{-1}$, $9.8\pm3\times10^{12}M^{-1}s^{-1}$ and $1.0\pm1.0\times10^{13}M^{-1}s^{-1}$ respectively for 4A, 5A and 6M with HSA, which are greater than the maximum scatter collision quenching constant. This identification shows that there is a static ground state complex formation between HSA and the ligands. In similar way the interaction between AGP was also identified as ground state complex formation.

The binding constants and the number of binding sites were calculated using modified Stern-Volmer equation.

$$\frac{\log\ (F_0 - F)}{F} = \log K_a + n\ \log\ [Q]$$

Where n corresponds to the number of binding sites, K_a is the binding constant and [Q] is the quencher concentration.

Log K can be calculated from the intercept of the graph $\log(F_0-F)/F$ vs. log[Q] and the slope of the graph gives number of binding sites. The n values of 4A (0.818), 5A (0.911) and 6M (0.963) are nearer to one, showing one to one interaction of the three molecules with HSA. The binding constants were calculated, and they are $5.3\pm2\times10^4M^{-1}$, $5.3\pm1\times10^4M^{-1}$ and $9.5\pm0.2\times10^4M^{-1}$ respectively for 4A, 5A and 6M (Figure 5.4). In similar way the binding constants for 4A, 5A and 6M with AGP were calculated as $7.4\pm4\times10^3M^{-1}$, $2.6\pm0.6\times10^3M^{-1}$ and $2.1\pm0.7\times10^4M^{-1}$, respectively (Figure 5.5). HSA is showing much higher affinity compared to AGP with these

three molecules and however, binding of these three compounds with AGP is also significant. Compared to 4A and 5A, methyl derivative of androstane (6M) is showing higher affinity towards HSA and AGP. These results indicate that both HSA and AGP playing a major role in binding which in turn act as major transporters in blood system.

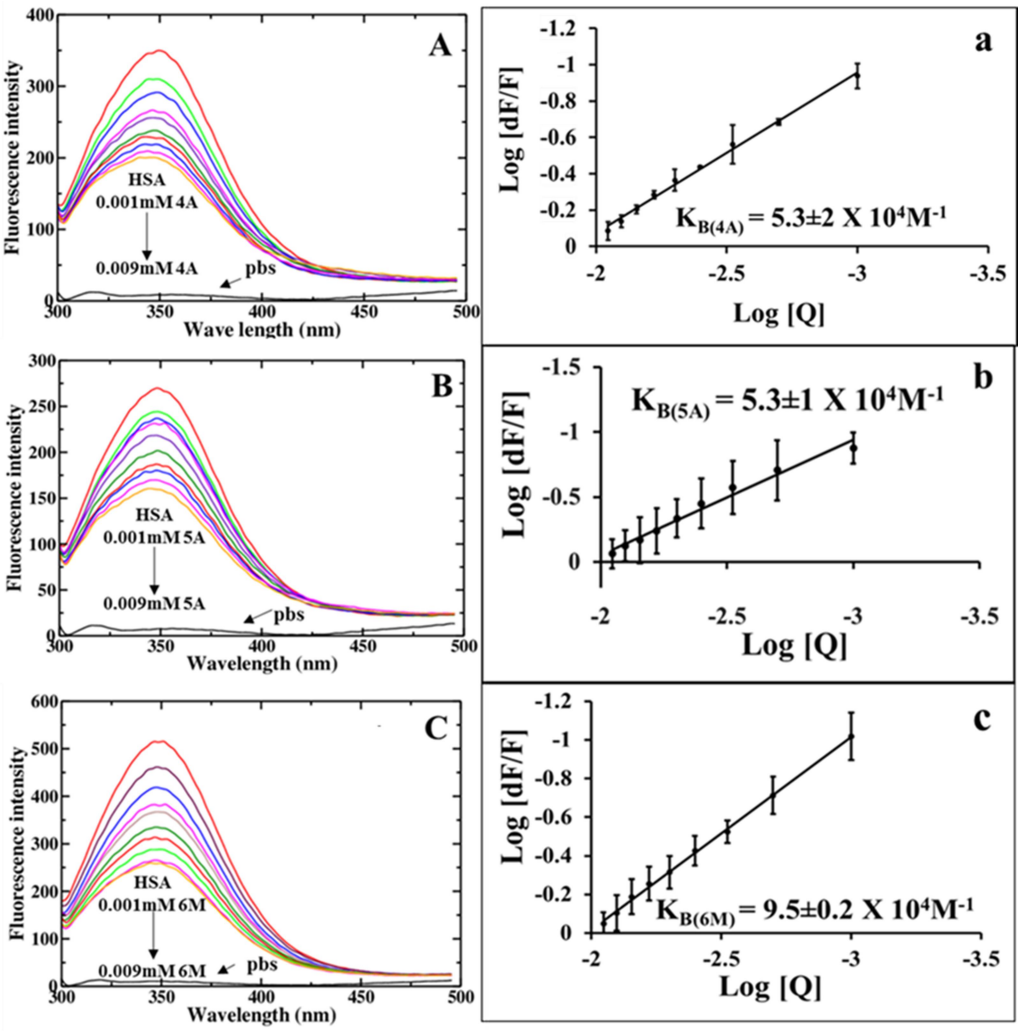

Figure 5.4 Fluorescence emission spectra of HSA in presence of increasing concentrations of A) 4A, B) 5A and C) 6M from 1µM to 9µM. Fluorescence quenching was shown with increasing concentrations of the molecules. There was no fluorescence emission for buffer and the ligands in the given wavelength range from 300-500nm. Modified Stern–Volmer plots for a) 4A, b) 5A and c) 6M respectively, obtained by plotting Log [Q] values on X-axis and Log [dF/F] values on Y-axis. Slope of the plot gives number of binding sites. Y intercept value gives log K values, from those binding constant values were calculated. All three molecules have only one binding site in HSA. Binding constant values are $5.3\pm2X10^{4}\ M^{-1}$, $5.3\pm1X10^{4}\ M^{-1}$ and $9.5\pm0.2X10^{4}\ M^{-1}$ respectively for 4A, 5A and 6M.

Since binding constant (or) association constant value are known, K_d can be calculated from reciprocal of K and from that binding free energies can be calculated using the following equation.

$$\Delta G^0 = -RT \ln K_d$$

Where ΔG° is the free energy change, R is the gas constant at room temperature, and K_d is the dissociation constant which is given by

$$K_a = \frac{1}{K_d}$$

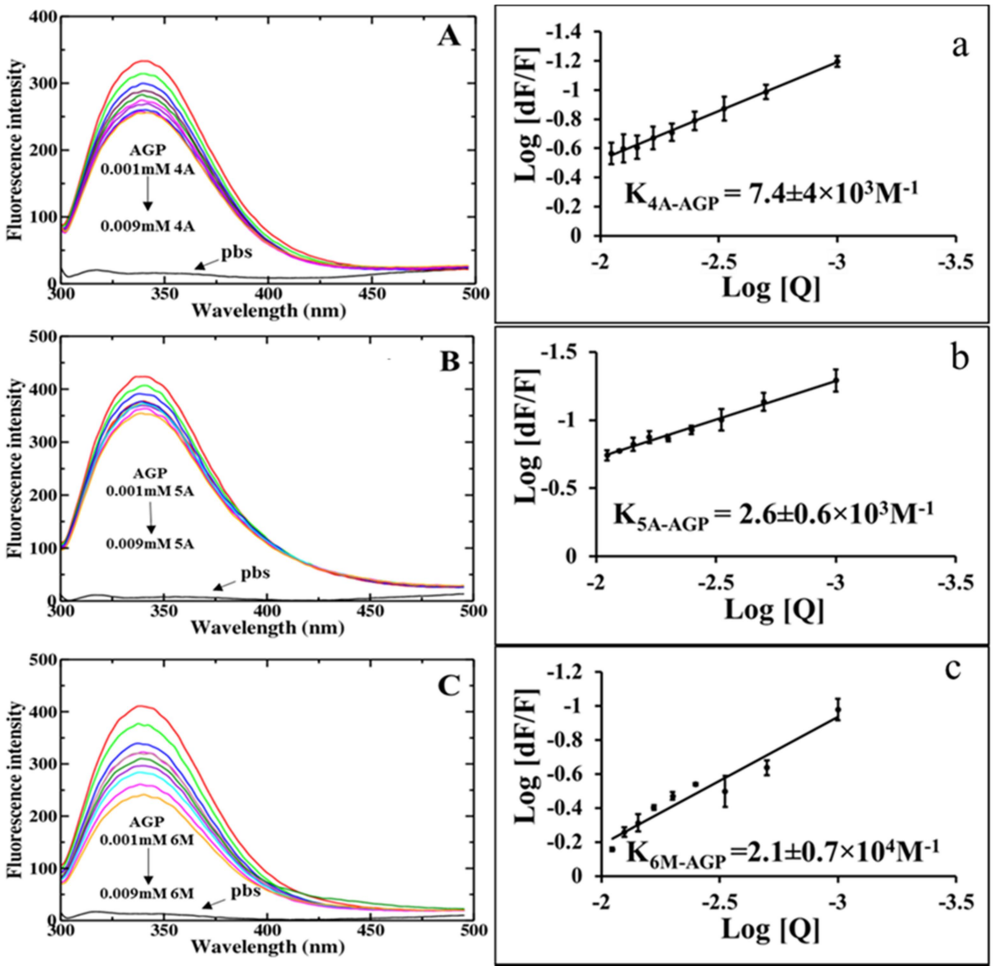

Figure 5.5 Fluorescence emission spectra of AGP with increasing concentrations of A) 4A, B) 5A and C) 6M. Emission maximum for AGP is 340nm. Modified Stern–Volmer plots for a) 4A, b) 5A and c) 6M respectively, obtained by plotting Log [Q] values on X-axis and Log [dF/F] values on Y-axis.

The calculated free energies are -6.59, -6.51 and -6.83 kcal/mol, respectively for 4A, 5A and 6M with HSA. While with AGP the binding free energies were calculated as -5.18, -4.64 and -5.85 kcal/mol, respectively for 4A, 5A and 6M. These results are in agreement with our laboratory on different ligands binding with HSA and AGP (Yeggoni et al., 2014, Kallubai et al., 2015, Yeggoni et al., 2015, Yeggoni et al., 2017). This data infers that 4A (androstenedione), 5A and 6M bind strongly with plasma proteins. Binding of these molecules to AGP is additional importance because it also acts as transporter in some disease conditions like renal failure, pregnancy, burns, etc. Differential binding of these ligands is due to different functional groups attached to the original molecules.

5.2.2. Locating binding site using site specific probes

Several attempts have been made to map the binding sites on HSA, as it can bind to several exogenous and endogenous ligands. Sudlow showed the presence of two specific drug binding sites namely, site I (also called the warfarin binding site) and site II (the benzodiazepine binding site) using a fluorescent probe displacement method (Sudlow et al., 1975). Even though there are two binding sites located in subdomains IIA and IIIA, also other secondary binding site located at subdomain IB in HSA (Yamasaki et al., 2013). Among available list of site specific markers, we have selected phenylbutazone and ibuprofen as site probes for IIA and IIIA, respectively. Equimolar ratio of HSA and site markers was titrated with 4A, 5A and 6M in three different experiments. The binding constant values were calculated as mention above (Figure 5.6). The binding constant for 4A in presence of ibuprofen is $4.6\pm0.1\times10^{4}M^{-1}$. Compared to only HSA, the binding constant value is decreased in presence of site markers and that was lower in case of ibuprofen showing that ligand is competing with ibuprofen to bind to IIIA. Similarly 5A is also showing competence with ibuprofen, however, 6M is competing with phenylbutazone with binding constant values $4.0\pm0.6\times10^{4}M^{-1}$ and $3.5\pm1\times10^{4}M^{-1}$ respectively. Figure 5.6 shows the fluorescence emission spectra of HSA in presence of ibuprofen and phenylbutazone while titrating with increasing concentrations of 4A, 5A and 6M, respectively. Thus, molecular displacement results are in turn determined the specific binding pocket of 4A, 5A and 6M.

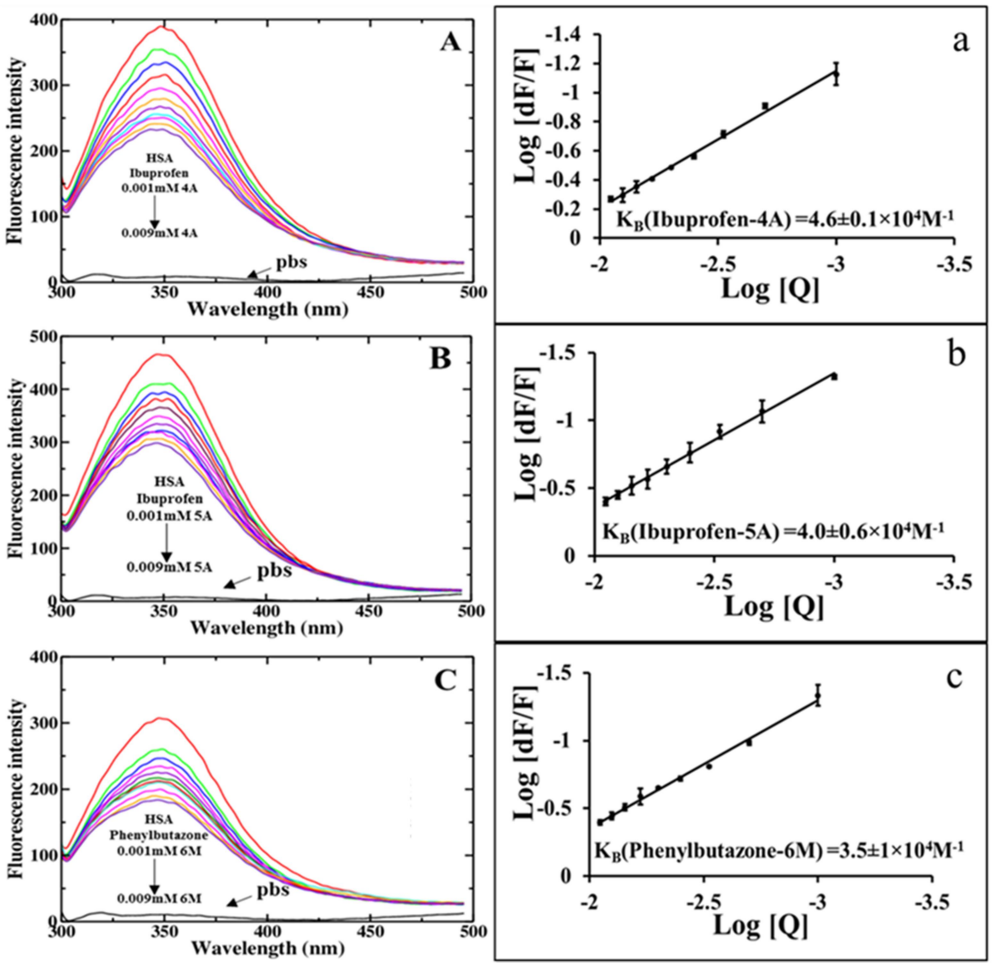

Figure 5.6 Competitive binding analysis of A) 4A, B) 5A and C) 6M. 4A and 5A are competing with ibuprofen towards binding to HSA. 6M is competing with phenylbutazone. Modified Stern–Volmer plots for a) 4A, b) 5A and c) 6M respectively, obtained by plotting Log [Q] values on X-axis and Log [dF/F] values on Y-axis.

5.2.3. Secondary structure analysis from CD data

To understand the influence of ligand binding on the conformation of secondary structure of HSA, CD spectroscopy measurements were performed in the presence of increasing concentrations of 4A, 5A and 6M. The room temperature CD spectra measured in presence of 4A, 5A and 6M were shown in Figure 5.7. The characteristic CD spectra of HSA measured in far-UV region shows two minima at 222nm and 208nm, which are the contributions of n $\rightarrow \pi^*$ transfer of the peptide bonds from α-helix (Anand & Mukherjee, 2013, Gowda & Nandibewoor, 2014, Pan et al., 2014). As shown in Figure 5.7, CD spectra of free HSA exhibit two negative bands in the ultraviolet region at 208 and 222 nm. It was observed that in presence of steroid molecules CD signal of HSA got decreased. The decrease of CD signal indicates decrease of

helical secondary structure content. However, the CD spectra of HSA in the presence or absence of ligands has similar in shape, indicating that there are very minute changes occurred in HSA due to ligand binding. Using CDNN software percentage of secondary structures was quantified for both HSA and HSA in presence of ligands. The percentage of α-helix differed from that of 66.05% in free HSA to 58.1% in 4A-HSA at pH 7.4 while β-turns and random coils were increased from 17.43% to 20.1% and 16.51% to 21.7%, respectively. In case of 5A and 6M α-helix content was decreased to 59.1% and 53.6% respectively. There is a gradual decrease in the α-helical percentage with increasing concentrations of ligands. The percentage changes of secondary structural elements were plotted against concentration of the ligands, which was shown in inset of Figure 5.7. The marginal changes in the percentage of secondary structural elements indicating that 4A, 5A and 6M are interacting with HSA, hence there is a partial unfolding of the protein. Structural change of protein indicates the changes in microenvironment around the binding pocket residues upon binding of these molecules. Similar results were observed from our laboratory work that upon binding of ligands the HSA undergoes conformational change (Yeggoni et al., 2014, Kallubai et al., 2015,Yeggoni et al., 2017).

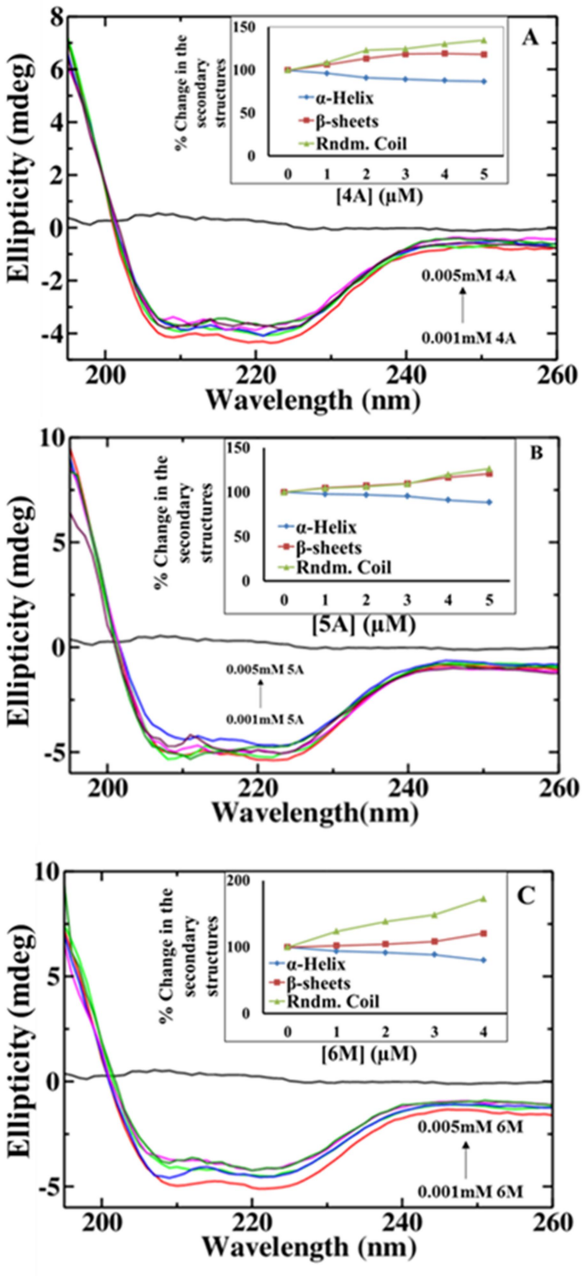

Figure 5.7 Circular Dichroism Spectra of HSA alone (red line) and with increasing concentrations of A) 4A, B) 5A and C) 6M. Characteristic spectrum of protein showing spectral minima at 208 and 222nm, indicating that the HSA is α-helical protein. Inset show the percentage of secondary structural elements of the HSA, obtained by deconvoluting CD spectra using CDNN software.

5.2.4. Mode of ligand binding to HSA using molecular docking approach

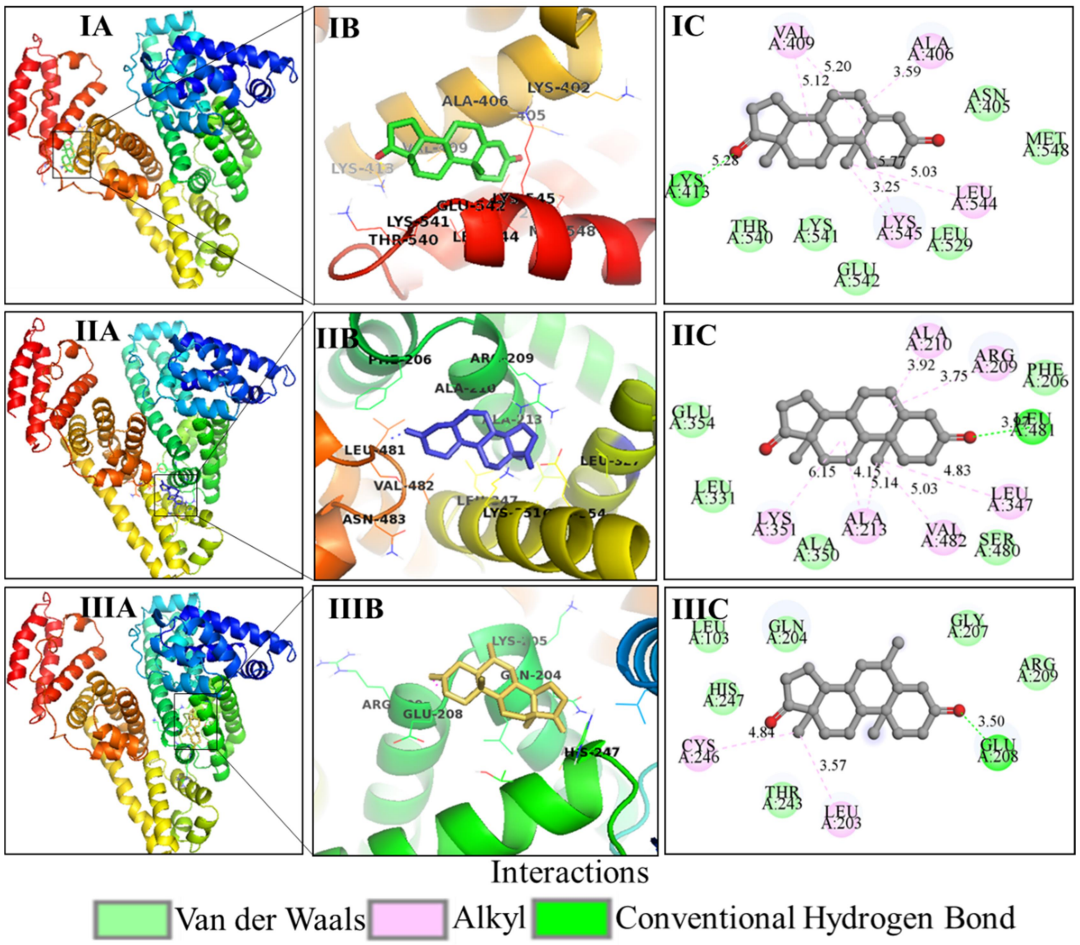

Figure 5.8 Docking of I) 4A, II) 5A and III) 6M with HSA. A), B) and C) from each panel is showing the HSA interaction, 3D view of ligand binding site and 2D view of ligand binding site with the interactions respectively. 4A and 5A are interacting with residues of IIIA domain. 6M is interacting with IIA domain of HSA.

Molecular docking studies were further used to understand the interaction between HSA and the ligands (Gorelik & Goldblum, 2008). The 3D structure (was taken from PBD ID: 1AO6) of HSA consists of three homologous domains, denoted as I, II and III. Each domain contains six-helix and four-helix subdomains. Each domain further subdivided into A and B subdomains that assemble to form heart shaped tertiary structure (Peters Jr, 1995). HSA has two major drug binding sites known as site I and II (Sudlow et al., 1975). Site I is a large, flexible region and has poor stereo selectivity, located in subdomain IIA. The side-chains of Tyr150, His242, and Arg257 located at the bottom of the pocket and Lys195, Lys199, Arg218 and Arg222 on an outer

cluster at the pocket entrance (Yamasaki et al., 2013). Whereas site II is a smaller or narrower site than site I and shows stereo selectivity, located in subdomain IIIA. Site II is largely apolar cavity formed by Leu387, Ser489, Leu453 and a single dominant polar patch at the pocket entrance, having Tyr411 and Arg410 (Curry, 2009).

The docking studies of HSA with 4A (androstenedione), 5A and 6M gives the information about the binding site of these steroid molecules in HSA and the interacting residues that form the binding groove (Figure 5.8). 4A binds in the groove formed by residues of III domain. The residues forming this groove are different from site II. But the groove is located immediately next to the site II, having some of the residues from site II. The electronegative oxygen atom of 4A is forming hydrogen bond with hydrogen from ε-amino group of Lys413, with the bond length of 2.79Å. Further, Thr 540, Lys541, Glu542, Lys545, Leu529 Leu544 Met 548 from subdomain IIIB and Asn405, Ala406, Val409 and Lys413 from subdomain IIIA are forming the binding groove. Val409, Ala406, Leu544 and Lys545 are having hydrophobic interactions and the rest of the residues forming binding groove are interacting with Van der waals interactions there by holding the 4A. Also, 5A is interacting with the residues of III domain. However the binding groove is distinct from that of 4A. Further, binding site of 5A is also overlapping with site II. In this, Phe206, Arg209, Ala210, Ala213, Leu331, Ala350, Lys351, Glu354, Leu347, Ser480, Leu481, and Val482 are the amino acid residues which are forming binding groove for 5A. Moreover, Leu481 is forming hydrogen bond with the electronegative oxygen of 5A and the bond length is 2.91 Å. Further, Ala210, Arg209, Leu347, Val482, Ala213 and Lys351 are forming hydrophobic interactions with 5A and rest is interacting with van der waals interactions. Distinct from 4A and 5A, 6M is interacting with the residues of domain II. Hence, 6M is interacting with Leu203, Thr243, Cys246, His247, Gln204, Gly207, Arg209 and Glu208 of IIA subdomain of HSA. Additionally, Glu208 is forming hydrogen bond with 6M and the bond length is 2.72 Å. From docking results, the binding free energies were calculated to be -7.36, -6.42 and -6.99, respectively for 4A, 5A and 6M respectively. These values are nearer to the experimental values which are obtained from fluorescence emission studies.

5.2.5. Molecular dynamics simulation (MDS) studies

HSA ligand complex formation, complex stability and effect of ligand on HSA conformation with respect to time were analyzed using molecular dynamics and simulation studies.

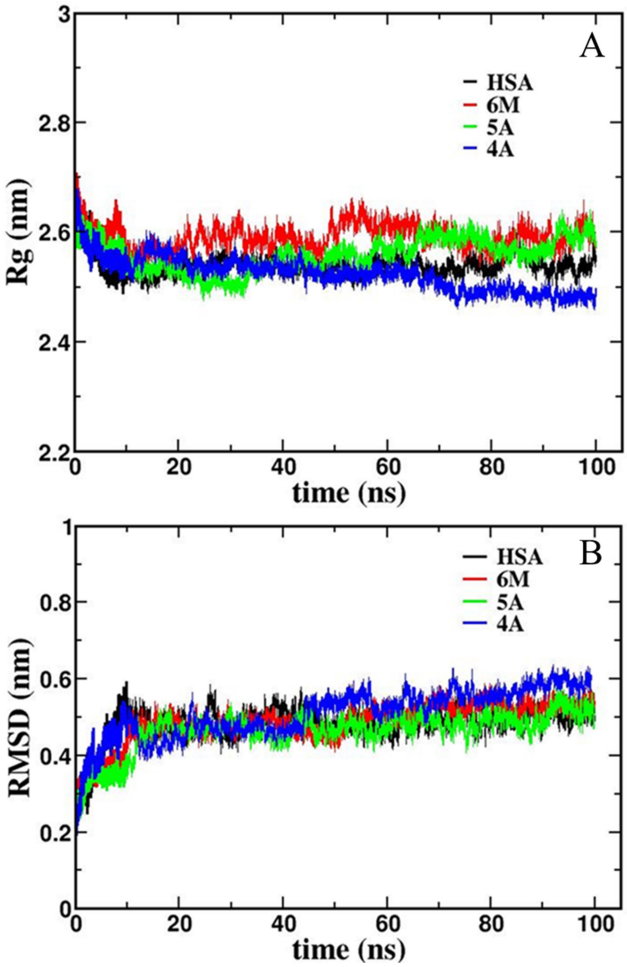

Figure 5.9 A) Time dependent evolution of the radius of gyration and B) RMSD values for free HSA, HSA-4A, HSA-5A and HSA-6M complex during 100ns molecular dynamics (MD) simulation.

The properties such as root mean square deviation (RMSD) of HSA and complexes with respect to initial structures, root mean square fluctuations (RMSF), and radius of gyration (Rg) of protein were obtained from MDS analysis. For the MDS analysis the best conformer was taken from the docking studies for all these molecules (4A, 5A and 6M). RMSD of HSA, HSA-4A, HSA-5A and HSA-6M complexes with respect to initial structure were calculated along 100ns trajectories in GROMACS. RMSD data shows that HSA, HSA-4A, HSA-5A and HSA-6M reaches equilibration after 15ns and later after complexes got stabilized (Figure 5.9). Radius of gyration of free HSA and complexes were also shown in Figure 5.9.

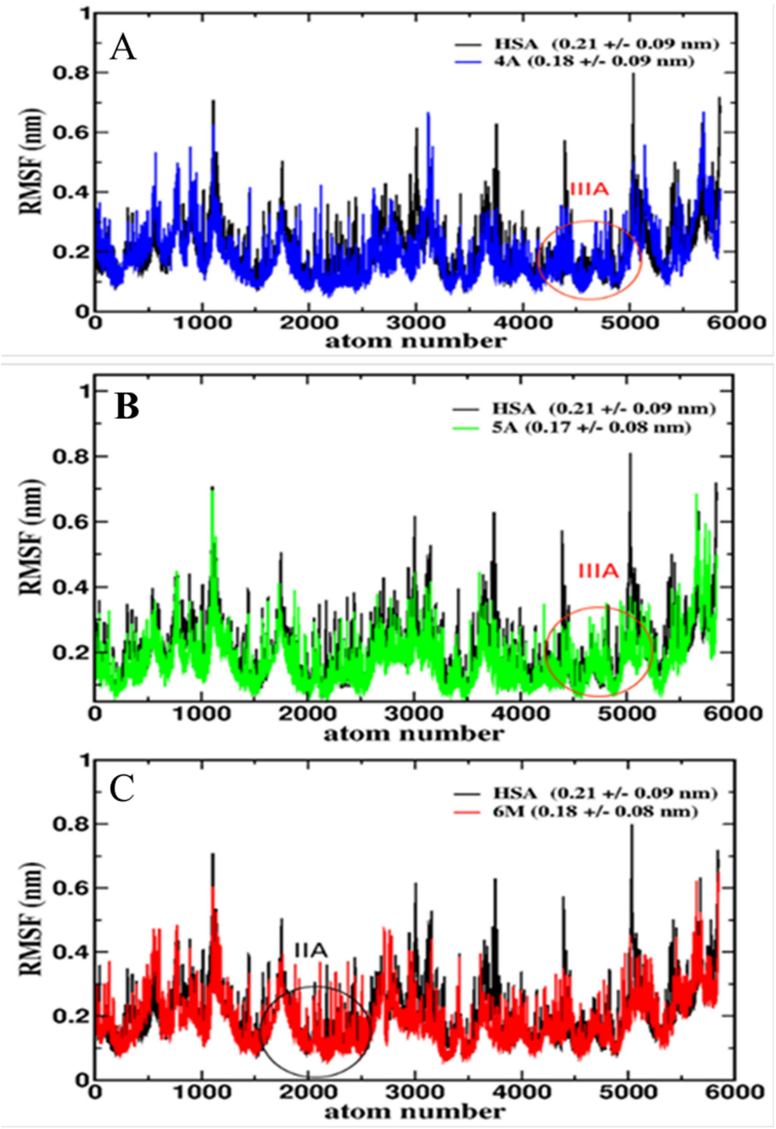

Figure 5.10 Root mean square fluctuations of atoms of HSA in free HSA compared to A) HSA-4A, B) HSA-5A and c) HSA-6M complex.

The initial Rg value of free HSA is 2.68nm and got stabilized at 2.55nm. Experimentally defined Rg value of HSA using small-angle neutron scattering is 2.74 ± 0.035 nm, nearer to the value obtained in present study (Malleda C, 2012, Yeggoni et al., 2014). There is not much difference in the Rg values of HSA-4A and HSA-5A, with respect to HSA alone, up to 60ns. After 60ns there is a decrease in the Rg value of HSA-4A. In case of HSA-6M complex, the Rg value increased slightly, with respect to HSA alone and the variation started from 5ns. Our experimental analysis with CD spectroscopy to understand the influence of ligand on protein

conformation also showed that there is marginal conformational change in the protein during 4A, 5A and 6M binding (Figure 5.7) and it is high in case of 6M. The CD data is further supporting the Rg data.

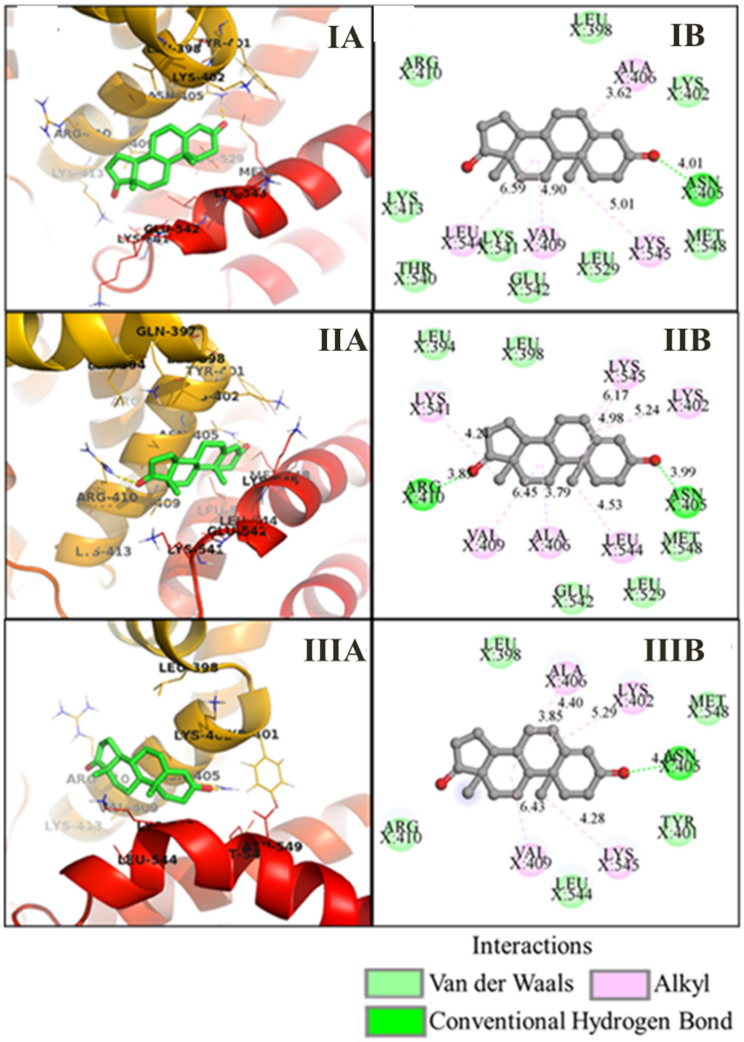

Figure 5.11 Interactions of 4A to HSA were shown after I) 3 ns, II) 6 ns and III) 10 ns from the 100ns molecular dynamics simulations. The 3D and 2D view of interactions were shown in panel A and B respectively. The 3D figure is showing the orientation of the molecule in the binding groove and the nature of the interactions were shown in 2D visualization.

Local protein mobility was analyzed by plotting RMS fluctuations of HSA and the ligands against the atom number. Figure 5.10 shows the RMSF data of HSA and HSA-4A, where RMSF value of HSA is 0.21nm with 0.09nm standard deviation and that is 0.18±0.09nm for HSA-4A. Comparative RMSF in 4A binding region i.e. IIIB shows that RMSF values of HSA-

4A is similar to that of HSA alone with little fluctuations, showing the rigidity of the residues because of ligand binding. The RMSF of HSA-5A and HSA-6M are 0.17±0.08 and 0.18±0.08, respectively. The IIIA region and IIA region of HSA showing less RMS fluctuations in case of 5A and 6M binding respectively compared to HSA protein alone.

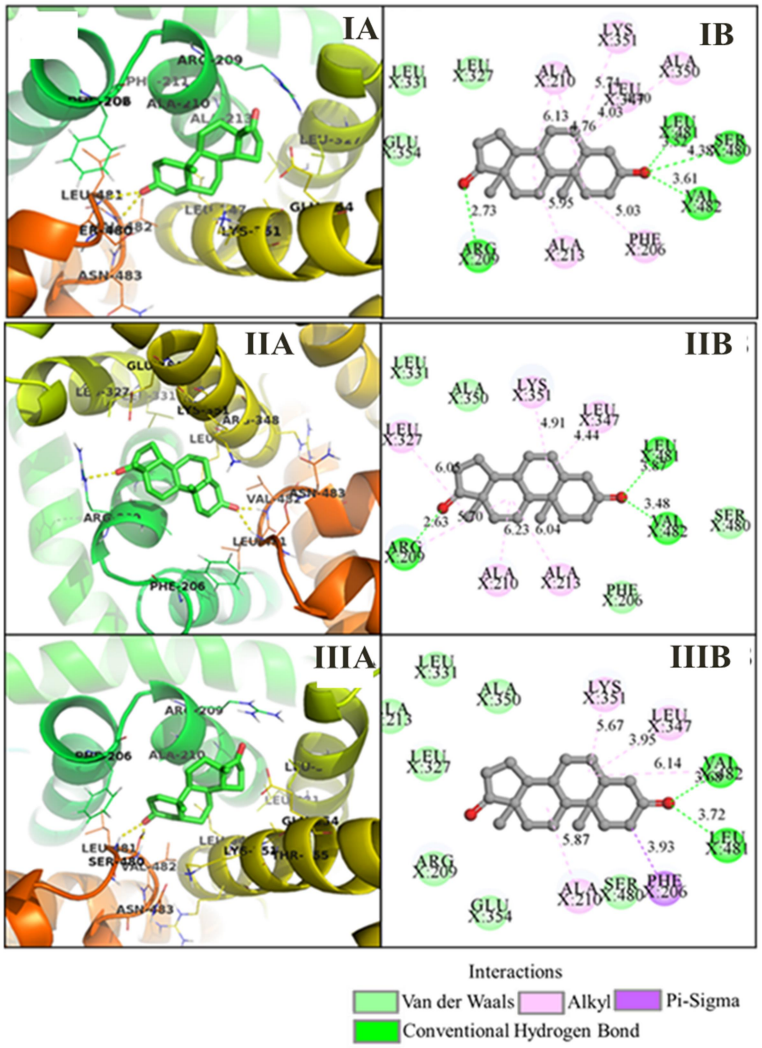

Figure 5.12 Interactions of 5A to HSA were shown after I) 3 ns, II) 6 ns and III) 10 ns from the 100ns molecular dynamics simulations. The 3D and 2D view of interactions were shown in panel A and B respectively. The 3D figure is showing the orientation of the molecule in the binding groove and the nature of the interactions were shown in 2D visualization.

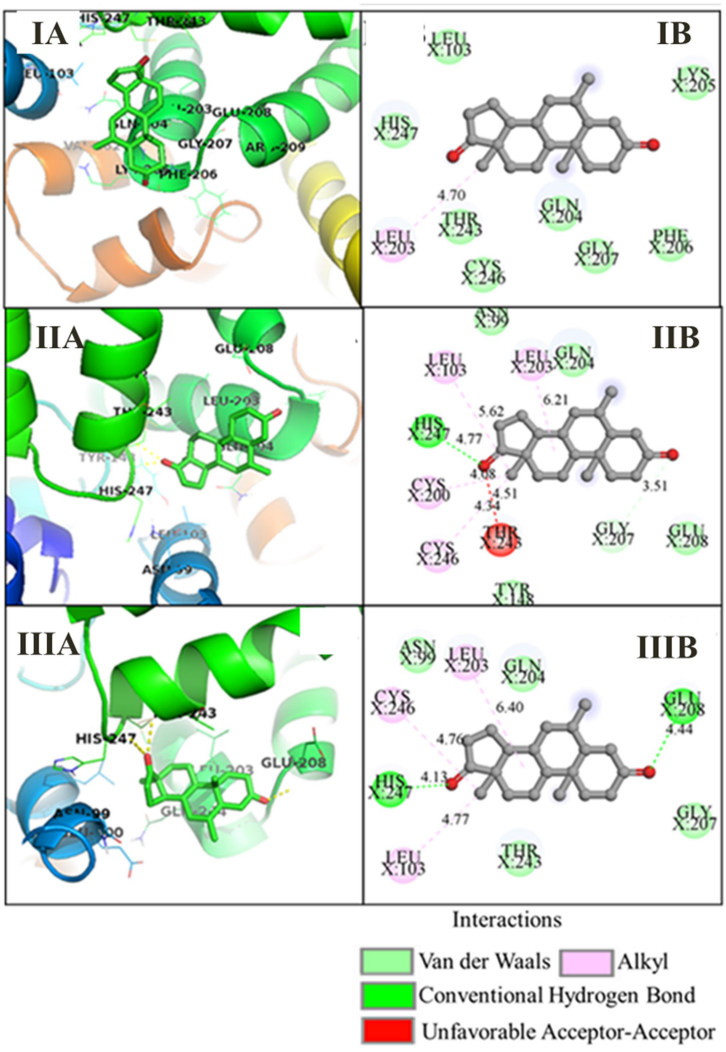

Figure 5.13 Interactions of 6M to HSA were shown after I) 3 ns, II) 6 ns and III) 10 ns from the 100ns molecular dynamics simulations. The 3D and 2D view of interactions were shown in panel A and B respectively. The 3D figure is showing the orientation of the molecule in the binding groove and the nature of the interactions were shown in 2D visualization.

Further, the interactions of 4A, 5A and 6M to HSA were visualized at every 3ns, 6ns and 10ns time points from the 100ns MDS data, to get better insight into the complex stability. Initially 4A is interacting to Lys413 by hydrogen bond (Figure 5.8) and in time course reoriented towards Asn405 in the binding groove itself and forming hydrogen bond with Asn405. From 3ns time point, 4A is interacting with Asn405 by hydrogen bond and this is stable up to 10ns (Figure 5.11). The molecule is held by Van der Waal interactions and hydrophobic interactions given by

the binding site residues (Figure 5.8, 5.11). In the similar way stability of 5A (Figure 5.12) and 6M (Figure 5.13) were shown by plotting the interactions at 3ns, 6ns and 10ns.

5.3. Conclusion

The present study gives the detailed description about the binding mechanism of androstenedione and its derivatives to the HSA and AGP with various biophysical techniques. Fluorescence studies show that the synthesized compounds (4A, 5A and 6M) can interact with both HSA and AGP, however with more affinity towards HSA. The association constants and free energies were found to be $5.3\pm2\times10^{4}M^{-1}$, $5.3\pm1\times10^{4}M^{-1}$ and $9.5\pm0.2\times10^{4}M^{-1}$ and -6.59, -6.51 and -6.83 kcal/mole respectively with HSA. Among 4A, 5A and 6M, the methyl derivative (6M) has high affinity towards HSA and AGP. Competitive binding studies by site specific markers indicate that the compounds 4A and 5A are binding to domain III of HSA whereas 6M is binding to domain II of HSA. Conformational changes in protein upon ligand binding were observed by CD spectroscopy, indicates that there is partial unfolding of the protein upon binding of 4A, 5A and 6M. Further, these studies were corroborated by *in silico* studies wherein hydrogen bonding, hydrophobic interactions and van der waals interactions are major driving forces towards high affinities to HSA. Furthermore, the RMSD values from MDS data show that the complexes are stabilized after 15ns. The Rg data, calculated using MDS further supports the partial unfolding of the protein during ligand binding as observed in CD spectroscopy.

The synthesized molecule 6M is a methyl derivative of 5A showed approximately 2 fold and 10 fold increased affinity towards HSA and AGP respectively due to the presence of additional methyl group wherein hydrophobic interactions slightly dominate over other forces. The present study reiterates the importance of synthetic molecules in the drug discovery that enhances the drug distribution at the target sites without sacrificing the drug activity.

Summary

The main goal of this study reveals in chapter 3, the interaction of individual domains of human serum albumin (HSA) to protein bound uremic toxins (PBUTs). PBUTs are the endogenous substances that get accumulate in renal failure patients leading to the toxic effects on normal physiological functions. Removal of PBUTs from patients by means of external devices is needed for the survival of the patients. Albumin is the dialysate in some of the extracorporeal devices. Studying the interaction of PBUTs to HSA domains gives valuable information to improve the efficacy of dialysate in such devices. The dialysate should specifically remove the PBUTs and should not remove the essential molecules from blood. In such case the dialysate should have more affinity and specificity towards PBUTs. We have selected the uremic toxins such as hippuric acid, indole acetic acid, melatonin and CMPF and studied their affinity to domains of HSA. The obtained results showed that, all four PBUTs have more than one binding site in HSA and have significant affinity to D2, D3 and D2-3 of HSA, which has been cloned and expressed. Hippuric acid, indole acetic acid and melatonin have high affinity to domain 3 of HSA. CMPF has high affinity to domain 2 of HSA. The K_d value determines the free and protein bound concentration of ligands. The K_d values obtained for domains of HSA are significantly different from that of complete HSA. These findings are useful as albumin can be replaced with its domains as dialysate in extracorporeal dialysis. The efficiency of dialysate can be improved by increasing the affinity and specificity of dialysate towards PBUTs and this can be achieved by using the combination of both the domains (i.e. D2 and D3) as dialysate and by playing with the ratios of D2 and D3. Hence, our study is giving a way to develop the therapeutic application to remove the uremic toxins from the kidney failure patients.

In 4^{th} chapter we have studied the interaction of phenylbutazone and ibuprofen to the Herborn (K240E) and Milano Slow (D375H) natural variants of HSA. Studying the effect of albumin modifications on drug binding is useful as the drug binding to HSA determines the pharmacokinetic profile of drugs. For our study, we have expressed HSA, K240E, D375H and the double mutant (K240E/D375H) heterologously in *Pichia pastoris* and studied interaction with the two non-steroidal anti-inflammatory drugs phenylbutazone and ibuprofen. From our study it is clear that there is no significant effect of K240E and D375H mutations on phenylbutazone and ibuprofen binding. As, K240E and D375H are the natural variants of HSA,

the insignificant effect of mutation on drug binding is desirable. But, the effect can be observed in case of double mutant (K240E/D375H). This is showing that the binding was affected at two sites. Further, the results showed that phenylbutazone and ibuprofen binding is not affecting the protein conformation, except in D375H, where there is a conformational change in the binding pocket with the ibuprofen binding.

In 5th chapter we have analyzed the binding mechanism of synthesized androstenedione and its derivatives to HSA using biophysical and computational tools. We have analyzed the binding of 4-Androstene-3-17-dione (4A), 5β-androstane-3-17-dione (5A) and (+)-6-methyl-5β androstane-3-17-dione (6M) to HSA. The results gave detailed description about binding mechanism. The association constants values obtained for interaction of 4A, 5A and 6M to HSA were found to be $5.3\pm2\times10^{4}M^{-1}$, $5.3\pm1\times10^{4}M^{-1}$ and $9.5\pm0.2\times10^{4}M^{-1}$, respectively. Among all three, the methyl derivative (6M) has high affinity towards HSA. 6M has one additional methyl group, when compared to other two molecules. The high affinity of 6M to hydrophobic binding pocket is because of the additional methyl group. Giving that addition of hydrophobic groups can enhances the binding of molecules to HSA and is useful in design of new therapeutic molecules. Competitive binding studies by site specific markers gave additional information about the binding site. The compounds 4A and 5A are binding to domain III of HSA whereas 6M is binding to domain II of HSA. Further, these studies were corroborated by *in silico* docking studies wherein hydrogen bonding, hydrophobic interactions and van der waals interactions are major driving forces towards high affinities to HSA. Furthermore, the RMSD values from MDS data show that the complexes are stabilized after 15ns. The Rg data, calculated using MDS further supports the partial unfolding of the protein during ligand binding as observed from CD spectroscopy data. Comparative binding analysis with other plasma protein AGP showed that HSA has high affinity when compared to AGP. In case of AGP also 6M is sowing high affinity.

The results obtained from this work gives valuable information regarding the binding nature of HSA and its applications in various fields of medicine. Understanding the binding mechanism of PBUTs to HSA domains is very much useful to address the problem of PBUTs. Studying the binding mechanism of natural variants of HSA to drugs is useful to understand the pharmacokinetic profile of drugs. Studying the interaction mechanism of synthesized androstenedione molecules with small changes in molecule structure gives information that the addition of hydrophobic groups to the molecules can increase the binding affinity to HSA and

this understanding is helpful in case drug design. It is our hope that our study will give a vital solution to kidney failure patients to remove the uremic toxins by dialysis method using the domains of HSA and further studies like natural mutants with drugs would give clue to understand the pharmacokinetics role in various clinical situations.

Bibliography

Abraham M, Van Der Spoel D, Lindahl E, Hess B, 2014. the GROMACS development team. *GROMACS user manual version* **5**.

Aggeler PM, O'reilly RA, Leong L, Kowitz PE, 1967. Potentiation of anticoagulant effect of warfarin by phenylbutazone. *New England Journal of Medicine* **276**, 496-501.

Albanese DC, Gaggero N, 2015. Albumin as a promiscuous biocatalyst in organic synthesis. *RSC Advances* **5**, 10588-98.

An F-F, Zhang X-H, 2017. Strategies for preparing albumin-based nanoparticles for multifunctional bioimaging and drug delivery. *Theranostics* **7**, 3667- 89.

Anand U, Mukherjee S, 2013. Binding, unfolding and refolding dynamics of serum albumins. *Biochimica et Biophysica Acta - General Subjects* **1830**, 5394-404.

Andersen JT, Cameron J, Plumridge A, Evans L, Sleep D, Sandlie I, 2013. Single-chain variable fragment albumin fusions bind the neonatal Fc receptor (FcRn) in a species dependent manner: implications for in vivo half-life evaluation of albumin-fusion therapeutics. *Journal of Biological Chemistry* **288**, 24277-85.

Andersen JT, Dalhus B, Cameron J*,* Daba MB, Plumridge A, Evans L, Brennan SO, Gunnarsen KS, Bjørås M, Sleep D, Sandlie I, 2012. Structure-based mutagenesis reveals the albumin-binding site of the neonatal Fc receptor. *Nature Communications* **3**, 610.

Anraku M, Chuang VTG, Maruyama T, Otagiri M, 2013. Redox properties of serum albumin. *Biochimica et Biophysica Acta - General Subjects* **1830**, 5465-72.

Bahrke MS, Yesalis CE, 2004. Abuse of anabolic androgenic steroids and related substances in sport and exercise. *Current opinion in pharmacology* **4**, 614-20.

Bal W, Sokołowska M, Kurowska E, Faller P, 2013. Binding of transition metal ions to albumin: sites, affinities and rates. *Biochimica et Biophysica Acta - General Subjects* **1830**, 5444-55.

Banères-Roquet F, Gualtieri M, Villain-Guillot P, Pugnière M, Leonetti J-P, 2009. Use of a surface plasmon resonance method to investigate antibiotic and plasma protein interactions. *Antimicrobial agents and chemotherapy* **53**, 1528-31.

Barnett JP, Blindauer CA, Kassaar O*,* Khazaipoul S, Martin EM, Sadler PJ, Stewart AJ, 2013. Allosteric modulation of zinc speciation by fatty acids. *Biochimica et Biophysica Acta - General Subjects* **1830**, 5456-64.

Benedetti F, Berti F, Bidoggia S, 2011. Aldolase activity of serum albumins. *Organic & biomolecular chemistry* **9**, 4417-20.

Berendsen HJ, Van Der Spoel D, Van Drunen R, 1995. GROMACS: a message-passing parallel molecular dynamics implementation. *Computer physics communications* **91**, 43-56.

Bertuzzi A, Mingrone G, Gandolfi A, Greco AV, Ringoir S, Vanholder R, 1997. Binding of indole-3-acetic acid to human serum albumin and competition with L-tryptophan. *Clinica chimica acta* **265**, 183-92.

Biacore manual. Biacore™ Assay Handbook. *GE Healthcare Life Sciences*.

Bos OJ, Fischer MJ, Wilting J, Janssen LH, 1988a. Drug-binding and other physicochemical properties of a large tryptic and a large peptic fragment of human serum albumin. *Biochimica et Biophysica Acta - Protein Structure and Molecular Enzymology* **953**, 37-47.

Bos OJ, Remijn JP, Fischer MJ, Wilting J, Janssen LH, 1988b. Location and characterization of the warfarin binding site of human serum albumin: a comparative study of two large fragments. *Biochemical pharmacology* **37**, 3905-9.

Brogioni B, Berti F, 2014. Surface plasmon resonance for the characterization of bacterial polysaccharide antigens: a review. *MedChemComm* **5**, 1058-66.

Bruschi M, Candiano G, Santucci L, Ghiggeri GM, 2013. Oxidized albumin. The long way of a protein of uncertain function. *Biochimica et Biophysica Acta - General Subjects* **1830**, 5473-9.

Chen Y-H, Yang JT, Chau KH, 1974. Determination of the helix and β form of proteins in aqueous solution by circular dichroism. *Biochemistry* **13**, 3350-9.

Chen Z, He Y, Shi B, Yang D, 2013. Human serum albumin from recombinant DNA technology: challenges and strategies. *Biochimica et Biophysica Acta - General Subjects* **1830**, 5515-25.

Curry S, 2002. Beyond expansion: structural studies on the transport roles of human serum albumin. *Vox sanguinis* **83**, 315-9.

Curry S, 2009. Lessons from the crystallographic analysis of small molecule binding to human serum albumin. *Drug metabolism and pharmacokinetics* **24**, 342-57.

Dantas DS, Oliveira JI, Neto JXL, Costa RFD, Bezerra EM, Freire VN, Caetano EWS, Fulco UL, Albuquerque EL, 2015. Quantum molecular modelling of ibuprofen bound to human serum albumin. *RSC Advances* **5**, 49439-50.

De Ceukeleire M, Albani JR, 2002. Interaction between carbohydrate residues of α1-acid glycoprotein (orosomucoid) and progesterone. A fluorescence study. *Carbohydrate research* **337**, 1405-10.

Dhondt A, Vanholder R, Van Biesen W, Lameire N, 2000. The removal of uremic toxins. *Kidney International* **58**, S47-S59.

Dockal M, Carter DC, Rüker F, 1999. The three recombinant domains of human serum albumin structural characterization and ligand binding properties. *Journal of Biological Chemistry* **274**, 29303-10.

Dockal M, Carter DC, Rüker F, 2000a. Conformational transitions of the three recombinant domains of human serum albumin depending on pH. *Journal of Biological Chemistry* **275**, 3042-50.

Dockal M, Chang M, Carter DC, Rüker F, 2000b. Five recombinant fragments of human serum albumin—tools for the characterization of the warfarin binding site. *Protein Science* **9**, 1455-65.

Drmanovic Z, Voyatzi S, Kouretas D, Sahpazidou D, Papageorgiou A, Antonoglou O, 1999. Albumin possesses intrinsic enolase activity towards dihydrotestosterone which can differentiate benign from malignant breast tumors. *Anticancer research* **19**, 4113-24.

Duranton F, Cohen G, De Smet R, Rodriguez M, Jankowski J, Vanholder R, Argiles A, European Uremic Toxin Work Group, 2012. Normal and pathologic concentrations of uremic toxins. *Journal of the American Society of Nephrology* **23**, 1258-70.

Elsadek B, Kratz F, 2012. Impact of albumin on drug delivery—new applications on the horizon. *Journal of controlled release* **157**, 4-28.

Evoli S, Mobley DL, Guzzi R, Rizzuti B, 2016. Multiple binding modes of ibuprofen in human serum albumin identified by absolute binding free energy calculations. *Physical Chemistry Chemical Physics* **18**, 32358-68.

Fabini E, Fiori GML, Tedesco D, Lopes NP, Bertucci C, 2016. Surface plasmon resonance and circular dichroism characterization of cucurbitacins binding to serum albumins for early pharmacokinetic profiling. *Journal of pharmaceutical and biomedical analysis* **122**, 166-72.

Fanali G, Di Masi A, Trezza V, Marino M, Fasano M, Ascenzi P, 2012. Human serum albumin: from bench to bedside. *Molecular Aspects of Medicine* **33**, 209-90.

Fournier T, Medjoubi-N N, Porquet D, 2000. Alpha-1-acid glycoprotein. *Biochimica et Biophysica Acta - Protein Structure and Molecular Enzymology* **1482**, 157-71.

Frostell-Karlsson Å, Remaeus A, Roos H, Andersson K, Borg P, Hämäläinen M, Karlsson R, 2000. Biosensor analysis of the interaction between immobilized human serum albumin and drug compounds for prediction of human serum albumin binding levels. *Journal of medicinal chemistry* **43**, 1986-92.

Fujiwara S-I, Amisaki T, 2013. Fatty acid binding to serum albumin: molecular simulation approaches. *Biochimica et Biophysica Acta - General Subjects* **1830**, 5427-34.

Galliano M, Watkins S, Madison J, Putnam FW, Kragh-Hansen U, Cesati R, Minchiotti L, 1998. Structural characterization of three genetic variants of human serum albumin modified in subdomains IIB and IIIA. *European journal of biochemistry* **251**, 329-34.

Georges H, Presle N, Buronfosse T, Fournel-Gigleux S, Netter P, Magdalou J, Lapicque F, 2000. In vitro stereoselective degradation of carprofen glucuronide by human serum albumin. Characterization of sites and reactive amino acids. *Chirality* **12**, 53-62.

Gerasimova YV, Bobik TV, Ponomarenko NA,Shakirov MM, Zenkova MA, Tamkovich NV, Popova TV, Knorre DG, Godovikova TS, 2010. RNA-hydrolyzing activity of human serum albumin and its recombinant analogue. *Bioorganic & medicinal chemistry letters* **20**, 1427-31.

Ghuman J, Zunszain PA, Petitpas I, Bhattacharya AA, Otagiri M, Curry S, 2005. Structural basis of the drug-binding specificity of human serum albumin. *Journal of Molecular Biology* **353**, 38-52.

Giri J, Diallo MS, Simpson AJ, Liu Y, Goddard WA, Kumar R, Woods GC, 2011. Interactions of poly (amidoamine) dendrimers with human serum albumin: binding constants and mechanisms. *ACS nano* **5**, 3456-68.

Glatz J, Veerkamp J, 1983. Removal of fatty acids from serum albumin by Lipidex 1000 chromatography. *Journal of biochemical and biophysical methods* **8**, 57-61.

Gokara M, Malavath T, Kalangi SK, Reddana P, Subramanyam R, 2014. Unraveling the binding mechanism of asiatic acid with human serum albumin and its biological implications. *Journal of Biomolecular Structure and Dynamics* **32**, 1290-302.

Gokara M, Sudhamalla B, Amooru DG, Subramanyam R, 2010. Molecular interaction studies of trimethoxy flavone with human serum albumin. *PLoS One* **5**, e8834.

Gorelik B, Goldblum A, 2008. High quality binding modes in docking ligands to proteins. *Proteins* **71**, 1373-86.

Gowda JI, Nandibewoor ST, 2014. Binding and conformational changes of human serum albumin upon interaction with 4-aminoantipyrine studied by spectroscopic methods and cyclic voltammetry. *Spectrochimica Acta Part A: Molecular and Biomolecular Spectroscopy* **124**, 397-403.

Gupta D, Lis CG, 2010. Pretreatment serum albumin as a predictor of cancer survival: a systematic review of the epidemiological literature. *Nutrition journal* **9**, 69.

Hamilton JA, 2013. NMR reveals molecular interactions and dynamics of fatty acid binding to albumin. *Biochimica et Biophysica Acta - General Subjects* **1830**, 5418-26.

He XM, Carter DC, 1992. Atomic structure and chemistry of human serum albumin. *Nature* **358**, 209.

Huey R, Morris GM, Olson AJ, Goodsell DS, 2007. A semiempirical free energy force field with charge-based desolvation. *Journal of computational chemistry* **28**, 1145-52.

Invitrogen, 2010a. EasySelect™Pichia Expression Kit. *Manual part no. 25-0172*.

Invitrogen, 2010b. pPIC9K, A Pichia Vector for Multicopy Integration and Secreted Expression. *Manual part no. 25-0106*.

Itoh T, Saura Y, Tsuda Y, Yamada H, 1997. Stereoselectivity and enantiomer-enantiomer interactions in the binding of ibuprofen to human serum albumin. *Chirality* **9**, 643-9.

Iwao Y, Hiraike M, Kragh-Hansen U, Mera K, Noguchi T, Anraku M, Kawai K, Maruyama T, Otagiri M, 2007. Changes of net charge and α-helical content affect the pharmacokinetic properties of human serum albumin. *Biochimica et Biophysica Acta -Proteins and Proteomics* **1774**, 1582-90.

Iwao Y, Ishima Y, Yamada J, Noguchi T, Kragh-Hansen U, Mera K, Honda D, Suenaga A, Maruyama T, Otagiri M, 2012. Quantitative evaluation of the role of cysteine and methionine residues in the antioxidant activity of human serum albumin using recombinant mutants. *IUBMB life* **64**, 450-4.

Jasuja R, Ramaraj P, Mac RP, Singh AB, Storer TW, Artaza J, Miller A, Singh R, Taylor WE, Lee ML, Davidson T, Sinha-Hikim I, Gonzalez-Cadavid N, Bhasin S, 2005. Δ-4-androstene-3, 17-dione binds androgen receptor, promotes myogenesis in vitro, and increases serum testosterone levels, fat-free mass, and muscle strength in hypogonadal men. *The Journal of Clinical Endocrinology & Metabolism* **90**, 855-63.

Kallubai M, Rachamallu A, Yeggoni DP, Subramanyam R, 2015. Comparative binding mechanism of lupeol compounds with plasma proteins and its pharmacological importance. *Molecular BioSystems* **11**, 1172-83.

Kelly SM, Jess TJ, Price NC, 2005. How to study proteins by circular dichroism. *Biochimica et Biophysica Acta - Proteins and Proteomics* **1751**, 119-39.

Kenanova VE, Olafsen T, Salazar FB, Williams LE, Knowles S, Wu AM, 2010. Tuning the serum persistence of human serum albumin domain III: diabody fusion proteins. *Protein Engineering, Design & Selection* **23**, 789-98.

Kim KA, Lee EY, Kang JH, Lee HG, Kim JW, Kwon DH, Jang YJ, Yeom Y-II, Chung TW, Kim YD, Yoon DY, Song EY, 2006. Diagnostic accuracy of serum asialo-α1-acid glycoprotein concentration for the differential diagnosis of liver cirrhosis and hepatocellular carcinoma. *Clinica chimica acta* **369**, 46-51.

Kobayashi K, 2006. Summary of recombinant human serum albumin development. *Biologicals* **34**, 55-9.

Kobayashi K, Kuwae S, Ohya T, Ohda T, Ohyama M, Ohi H, Tomomitsu K, Ohmura T, 2000. High-level expression of recombinant human serum albumin from the methylotrophic yeast Pichia pastoris with minimal protease production and activation. *Journal of bioscience and bioengineering* **89**, 55-61.

Komatsu T, 2012. Protein-based nanotubes for biomedical applications. *Nanoscale* **4**, 1910-8.

Komatsu T, Nakagawa A, Zunszain PA, Curry S, Tsuchida E, 2007. Genetic engineering of the heme pocket in human serum albumin: modulation of O2 binding of iron protoporphyrin

IX by variation of distal amino acids. *Journal of the American Chemical Society* **129**, 11286-95.

Komatsu T, Ohmichi N, Nakagawa A, Zunszain PA, Curry S, Tsuchida E, 2005. O2 and CO binding properties of artificial hemoproteins formed by complexing iron protoporphyrin IX with human serum albumin mutants. *Journal of the American Chemical Society* **127**, 15933-42.

Komatsu T, Ohmichi N, Zunszain PA, Curry S, Tsuchida E, 2004. Dioxygenation of human serum albumin having a prosthetic heme group in a tailor-made heme pocket. *Journal of the American Chemical Society* **126**, 14304-5.

Komatsu T, Wang R-M, Zunszain PA, Curry S, Tsuchida E, 2006. Photosensitized Reduction of Water to Hydrogen Using Human Serum Albumin Complexed with Zinc− Protoporphyrin IX. *Journal of the American Chemical Society* **128**, 16297-301.

Kragh-Hansen U, 1988. Evidence for a large and flexible region of human serum albumin possessing high affinity binding sites for salicylate, warfarin, and other ligands. *Molecular pharmacology* **34**, 160-71.

Kragh-Hansen U, 2013. Molecular and practical aspects of the enzymatic properties of human serum albumin and of albumin-ligand complexes. *Biochimica et Biophysica Acta - General Subjects* **1830**, 5535-44.

Kragh-Hansen U, Brennan S, Minchiotti L, Galliano M, 1994. Modified high-affinity binding of Ni2+, Ca2+ and Zn2+ to natural mutants of human serum albumin and proalbumin. *Biochemical Journal* **301**, 217-23.

Kragh-Hansen U, Campagnoli M, Dodig S, Nielsen H, Benko B, Raos M, Cesati R, Sala A, Galliano M, Minchiotti L, 2004. Structural analysis and fatty acid-binding properties of two Croatian variants of human serum albumin. *Clinica chimica acta* **349**, 105-12.

Kragh-Hansen U, Chuang VTG, Otagiri M, 2002. Practical aspects of the ligand-binding and enzymatic properties of human serum albumin. *Biological and Pharmaceutical Bulletin* **25**, 695-704.

Kragh-Hansen U, Minchiotti L, Brennan SO, Sugita O, 1990. Hormone binding to natural mutants of human serum albumin. *European journal of biochemistry* **193**, 169-74.

Kragh-Hansen U, Minchiotti L, Galliano M, Peters T, Jr., 2013. Human serum albumin isoforms: genetic and molecular aspects and functional consequences. *Biochimica et Biophysica Acta - General Subjects* **1830**, 5405-17.

Kragh-Hansen U, Saito S, Nishi K, Anraku M, Otagiri M, 2005. Effect of genetic variation on the thermal stability of human serum albumin. *Biochimica et Biophysica Acta - Proteins and Proteomics* **1747**, 81-8.

Kratz F, 2008. Albumin as a drug carrier: design of prodrugs, drug conjugates and nanoparticles. *Journal of controlled release* **132**, 171-83.

Krenzel ES, Chen Z, Hamilton JA, 2013. Correspondence of fatty acid and drug binding sites on human serum albumin: a two-dimensional nuclear magnetic resonance study. *Biochemistry* **52**, 1559-67.

Krisper P, Stadlbauer V, Stauber RE, 2011. Clearing of toxic substances: are there differences between the available liver support devices? *Liver International* **31**, 5-8.

Kute T, Westphal U, 1976. Steroid-protein interactions. XXXIV. Chemical modification of α1-acid glycoprotein for characterization of the progesterone binding site. *Biochimica et Biophysica Acta - Protein Structure* **420**, 195-213.

Kwon C-H, Maddison K, Locastro L, Borch RF, 1987. Accelerated decomposition of 4-hydroxycyclophosphamide by human serum albumin. *Cancer research* **47**, 1505-8.

Laemmli UK, 1970. Cleavage of structural proteins during the assembly of the head of bacteriophage T4. *Nature* **227**, 680.

Lakowicz JR, 2009. Principles of fl uorescence spectroscopy. Third Edition. *Springer: New York,* , 277-318.

Lee KC, Baker LA, Stanzani G, Alibhai H, Chang YM, Palacios CJ, Leckie PJ, Giordano P, Priestnall SL, Antoine DJ, Jenkins RE, Goldring CE, Park BK, Andreola F, Agarwal B, Mookerjee RP, Davies NA, Jalan R, 2015. Extracorporeal liver assist device to exchange albumin and remove endotoxin in acute liver failure: Results of a pivotal pre-clinical study. *Journal of hepatology* **63**, 634-42.

Lee SS-Y, Li J, Tai JN, Ratliff TL, Park K, Cheng J-X, 2015. Avasimibe encapsulated in human serum albumin blocks cholesterol esterification for selective cancer treatment. *ACS nano* **9**, 2420-32.

Lejon S, Frick I-M, Björck L, Wikström M, Svensson S, 2004. Crystal structure and biological implications of a bacterial albumin binding module in complex with human serum albumin. *Journal of Biological Chemistry* **279**, 42924-8.

Li X, Wang S, 2015. Binding of glutathione and melatonin to human serum albumin: a comparative study. *Colloids and Surfaces B: Biointerfaces* **125**, 96-103.

Lisowska-Myjak B, 2014. Uremic toxins and their effects on multiple organ systems. *Nephron Clinical Practice* **128**, 303-11.

Lomis N, Westfall S, Farahdel L, Malhotra M, Shum-Tim D, Prakash S, 2016. Human serum albumin nanoparticles for use in cancer drug delivery: process optimization and in vitro characterization. *Nanomaterials* **6**, 116.

Lupidi G, Camaioni E, Khalifé H, Avenali L, Damiani E, Tanfani F, Scirè A, 2012. Characterization of thymoquinone binding to human α1-acid glycoprotein. *Journal of pharmaceutical sciences* **101**, 2564-73.

Mahammed A, Gross Z, 2005. Albumin-conjugated corrole metal complexes: extremely simple yet very efficient biomimetic oxidation systems. *Journal of the American Chemical Society* **127**, 2883-7.

Malaviya A, Gomes J, 2008. Androstenedione production by biotransformation of phytosterols. *Bioresource Technology* **99**, 6725-37.

Malleda C AN, Gokara M, Subramanyam R, 2012. Molecular Dynamics Simulation Studies of Betulinic Acid with Human Serum Albumin. *Journal of Molecular Modeling* **18**, 2589 − 97.

Mandal S, Hossain M, Devi PS, Kumar GS, Chaudhuri K, 2013. Interaction of carbon nanoparticles to serum albumin: elucidation of the extent of perturbation of serum albumin conformations and thermodynamical parameters. *Journal of hazardous materials* **248**, 238-45.

Mao H, Gunasekera AH, Fesik SW, 2000. Expression, refolding, and isotopic labeling of human serum albumin domains for NMR spectroscopy. *Protein expression and purification* **20**, 492-9.

Matsushita S, Isima Y, Chuang VTG, Watanabe H, Tanase S, Maruyama T, Otagiri M, 2004. Functional analysis of recombinant human serum albumin domains for pharmaceutical applications. *Pharmaceutical research* **21**, 1924-32.

Mendez CM, Mcclain CJ, Marsano LS, 2005. Albumin therapy in clinical practice. *Nutrition in clinical practice* **20**, 314-20.

Minchiotti L, Galliano M, Zapponi MC, Tenni R, 1993. The structural characterization and bilirubin-binding properties of albumin Herborn, a [Lys240→ Glu] albumin mutant. *European journal of biochemistry* **214**, 437-44.

Minomo A, Ishima Y, Chuang VT, Suwa Y, Kragh-Hansen U, Narisoko T, Morioka H, Maruyama T, Otagiri M, 2013. Albumin domain II mutant with high bilirubin binding affinity has a great potential as serum bilirubin excretion enhancer for hyperbilirubinemia treatment. *Biochimica et Biophysica Acta - General Subjects* **1830**, 2917-23.

Mitzner SR, 2011. Extracorporeal liver support-albumin dialysis with the Molecular Adsorbent Recirculating System (MARS). *Annals of hepatology* **10**, 21-8.

Mitzner SR, Stange J, Klammt S, Peszynski P, Schmidt R, Nöldge-Schomburg G, 2001. Extracorporeal detoxification using the molecular adsorbent recirculating system for critically ill patients with liver failure. *Journal of the American Society of Nephrology* **12**, S75-S82.

Morris GM, Goodsell DS, Halliday RS, Huey R, Hart WE, Belew RK, Olson AJ, 1998. Automated docking using a Lamarckian genetic algorithm and an empirical binding free energy function. *Journal of computational chemistry* **19**, 1639-62.

Morris GM, Huey R, Lindstrom W, Sanner MF, Belew RK, Goodsell DS, Olson AJ, 2009. AutoDock4 and AutoDockTools4: Automated docking with selective receptor flexibility. *Journal of computational chemistry* **30**, 2785-91.

Müller WE, Stillbauer AE, 1983. Characterization of a common binding site for basic drugs on human α 2-acid glycoprotein (orosomucoid). *Naunyn-Schmiedeberg's archives of pharmacology* **322**, 170-3.

Naveenraj S, Anandan S, 2013. Binding of serum albumins with bioactive substances–nanoparticles to drugs. *Journal of Photochemistry and Photobiology C: Photochemistry Reviews* **14**, 53-71.

Nerusu A, Reddy PS, Ramachary DB, Subramanyam R, 2017. Unraveling the Stability of Plasma Proteins upon Interaction of Synthesized Androstenedione and Its Derivatives- A Biophysical and Computational Approach. *ACS Omega* **2**, 6514-24.

Nicoletti FP, Howes BD, Fittipaldi M, Fanali G, Fasano M, Ascenzi P, Smulevich G, 2008. Ibuprofen induces an allosteric conformational transition in the heme complex of human serum albumin with significant effects on heme ligation. *Journal of the American Chemical Society* **130**, 11677-88.

Pan F, Xu T, Yang L, Jiang X, Zhang L, 2014. Probing the binding of an endocrine disrupting compound-Bisphenol F to human serum albumin: insights into the interactions of harmful chemicals with functional biomacromolecules. *Spectrochimica Acta Part A: Molecular and Biomolecular Spectroscopy* **132**, 795-802.

Paris G, Kraszewski S, Ramseyer C, Enescu M, 2012. About the structural role of disulfide bridges in serum albumins: evidence from protein simulated unfolding. *Biopolymers* **97**, 889-98.

Park DS, Petersen CE, Ha CE, Harohalli K, Feix JB, Bhagavan NV, 1999. Expression of a human serum albumin fragment (consisting of subdomains IA, IB, and IIA) and a study of its properties. *IUBMB life* **48**, 169-74.

Pearlman WH, Crépy O, 1967. Steroid-protein interaction with particular reference to testosterone binding by human serum. *Journal of Biological Chemistry* **242**, 182-9.

Pedersen AO, Jacobsen J, 1980. Reactivity of the thiol group in human and bovine albumin at pH 3–9, as measured by exchange with 2, 2′-dithiodipyridine. *European journal of biochemistry* **106**, 291-5.

Peters Jr T, 1995. *All about albumin: biochemistry, genetics, and medical applications*. Academic press.

Petitpas I, Grüne T, Bhattacharya AA, Curry S, 2001. Crystal structures of human serum albumin complexed with monounsaturated and polyunsaturated fatty acids1. *Journal of molecular biology* **314**, 955-60.

Qu X, Komatsu T, 2009. Molecular capture in protein nanotubes. *ACS nano* **4**, 563-73.

Qu X, Komatsu T, Sato T, Glatter O, Horinouchi H, Kobayashi K, Tsuchida E, 2008. Structure, photophysical property, and cytotoxicity of human serum albumin complexed with tris (dicarboxymethylene)[60] fullerene. *Bioconjugate chemistry* **19**, 1556-60.

Ramachary DB, Sakthidevi R, Reddy PS, 2013. Direct organocatalytic stereoselective transfer hydrogenation of conjugated olefins of steroids. *RSC Advances* **3**, 13497-506.

Reetz MT, Jiao N, 2006. Copper–phthalocyanine conjugates of serum albumins as enantioselective catalysts in Diels–Alder reactions. *Angewandte Chemie International Edition* **45**, 2416-9.

Rempel B, Gui B, Maley J, Reaney M, Sammynaiken R, 2010. Biomolecular interaction study of cyclolinopeptide A with human serum albumin. *Journal of Biomedicine and Biotechnology* **737289**.

Rich RL, Day YS, Morton TA, Myszka DG, 2001. High-resolution and high-throughput protocols for measuring drug/human serum albumin interactions using BIACORE. *Analytical biochemistry* **296**, 197-207.

Sakai T, Takadate A, Otagiri M, 1995. Characterization of binding site of uremic toxins on human serum albumin. *Biological and Pharmaceutical Bulletin* **18**, 1755-61.

Sakurai Y, Ma S-F, Watanabe H, Yamaotsu N, Hirono S, Kurono Y, Kragh-Hansen U, Otagiri M, 2004. Esterase-like activity of serum albumin: characterization of its structural chemistry using p-nitrophenyl esters as substrates. *Pharmaceutical research* **21**, 285-92.

Sand KMK, Bern M, Nilsen J, Noordzij HT, Sandlie I, Andersen JT, 2015. Unraveling the interaction between FcRn and albumin: opportunities for design of albumin-based therapeutics. *Frontiers in immunology* **5**, 682.

Sandblad P, Arnell R, Samuelsson J, Fornstedt T, 2009. Approach for reliable evaluation of drug proteins interactions using surface plasmon resonance technology. *Analytical chemistry* **81**, 3551-9.

Santagostino E, Negrier C, Klamroth R, Tiede A, Pabinger-Fasching I, Voigt C, Jacobs I, Morfini M, 2012. Safety and pharmacokinetics of a novel recombinant fusion protein linking coagulation factor IX with albumin (rIX-FP) in hemophilia B patients. *Blood* **120**, 2405-11

Satoh M, Hayashi H, Watanabe M, Ueda K, Yamato H, Yoshioka T, Motojima M, 2003. Uremic toxins overload accelerates renal damage in a rat model of chronic renal failure. *Nephron Experimental Nephrology* **95**, e111-e8.

Sbarouni E, Georgiadou P, Voudris V, 2011. Ischemia modified albumin changes–review and clinical implications. *Clinical Chemistry and Laboratory Medicine* **49**, 177-84.

Schönfeld DL, Ravelli RB, Mueller U, Skerra A, 2008. The 1.8-Å crystal structure of α1-acid glycoprotein (orosomucoid) solved by UV RIP reveals the broad drug-binding activity of this human plasma lipocalin. *Journal of molecular biology* **384**, 393-405.

Schrodinger L, 2015. PyMOL: The PyMOL Molecular Graphics System, version 1.8.

Schüttelkopf AW, Van Aalten DM, 2004. PRODRG: a tool for high-throughput crystallography of protein–ligand complexes. *Acta Crystallographica Section D: Biological Crystallography* **60**, 1355-63.

Sengupta D, Kannan M, Reddy AR, 2011. A root proteomics-based insight reveals dynamic regulation of root proteins under progressive drought stress and recovery in Vigna radiata (L.) Wilczek. *Planta* **233**, 1111-27.

Setoguchi N, Takamura N, Fujita KI, Ogata K, Tokunaga J, Nishio T, Chosa E, Arimori K, Kawai K, Yamamoto R, 2013. A diclofenac suppository–nabumetone combination therapy for arthritic pain relief and a monitoring method for the diclofenac binding capacity of HSA site II in rheumatoid arthritis. *Biopharmaceutics & drug disposition* **34**, 125-36.

Sharma AS, Anandakumar S, Ilanchelian M, 2014. A combined spectroscopic and molecular docking study on site selective binding interaction of Toluidine blue O with Human and Bovine serum albumins. *Journal of Luminescence* **151**, 206-18.

Sharma UK, Sharma N, Kumar R, Sinha AK, 2013. Biocatalysts for multicomponent Biginelli reaction: bovine serum albumin triggered waste-free synthesis of 3, 4-dihydropyrimidin-2-(1H)-ones. *Amino Acids* **44**, 1031-7.

Sheng Z, Hu D, Zheng M, Zhao P, Liu H, Gao D, Gong P, Gao G, Zhang P, Ma Y, Cai L, 2014. Smart human serum albumin-indocyanine green nanoparticles generated by programmed assembly for dual-modal imaging-guided cancer synergistic phototherapy. *ACS nano* **8**, 12310-22.

Shi D, Jin Y-X, Tang Y-H, Hu H-H, Xu S-Y, Yu L-S, Jiang H-D, Zeng S, 2012. Stereoselective binding of mexiletine and ketoprofen enantiomers with human serum albumin domains. *Acta Pharmacologica Sinica* **33**, 710-6.

Shim YY, Reaney MJ, 2015. Kinetic interactions between cyclolinopeptides and immobilized human serum albumin by surface plasmon resonance. *Journal of agricultural and food chemistry* **63**, 1099-106.

Simard JR, Zunszain PA, Hamilton JA, Curry S, 2006. Location of high and low affinity fatty acid binding sites on human serum albumin revealed by NMR drug-competition analysis. *Journal of molecular biology* **361**, 336-51.

Sleep D, Cameron J, Evans LR, 2013. Albumin as a versatile platform for drug half-life extension. *Biochimica et Biophysica Acta - General Subjects* **1830**, 5526-34.

Sogorb MA, García-ArgüElles S, Carrera V, Vilanova E, 2008. Serum albumin is as efficient as paraxonase in the detoxication of paraoxon at toxicologically relevant concentrations. *Chemical research in toxicology* **21**, 1524-9.

Sogorb MA, Vilanova E, 2010. Serum albumins and detoxication of anti-cholinesterase agents. *Chemico-biological interactions* **187**, 325-9.

Spotnitz WD, Burks S, 2008. Hemostats, sealants, and adhesives: components of the surgical toolbox. *Transfusion* **48**, 1502-16.

Stanyon HF, Viles JH, 2012. Human Serum Albumin Can Regulate Amyloid-β Peptide Fiber Growth in the Brain Interstitium Implications for alzheimer disease. *Journal of Biological Chemistry* **287**, 28163-8.

Subramanyam R, Gollapudi A, Bonigala P, Chinnaboina M, Amooru DG, 2009a. Betulinic acid binding to human serum albumin: A study of protein conformation and binding affinity. *Journal of Photochemistry and Photobiology B: Biology* **94**, 8-12.

Subramanyam R, Goud M, Sudhamalla B, Reddeem E, Gollapudi AK, Nellaepalli S, Yadavalli V, Chinnaboina M, Amooru DG, 2009b. Novel binding studies of human serum albumin with trans-feruloyl maslinic acid. *Journal of Photochemistry and Photobiology B: Biology* **95**, 81-8.

Sudhamalla B, Gokara M, Ahalawat N, Amooru DG, Subramanyam R, 2010. Molecular dynamics simulation and binding studies of β-sitosterol with human serum albumin and its biological relevance. *The Journal of Physical Chemistry B* **114**, 9054-62.

Sudlow G, Birkett DJ, Wade DN, 1975. The Characterization of Two Specific Drug Binding Sites on Human Serum Albumin. *Molecular pharmacology* **11**, 824-32.

Sudlow G, Birkett D, Wade D, 1976. Further characterization of specific drug binding sites on human serum albumin. *Molecular pharmacology* **12**, 1052-61.

Tabassum S, Al-Asbahy WM, Afzal M, Arjmand F, 2012. Synthesis, characterization and interaction studies of copper based drug with human serum albumin (HSA):

spectroscopic and molecular docking investigations. *Journal of Photochemistry and Photobiology B: Biology* **114**, 132-9.

Takamura N, Maruyama T, Otagiri M, 1997. Effects of uremic toxins and fatty acids on serum protein binding of furosemide: possible mechanism of the binding defect in uremia. *Clinical chemistry* **43**, 2274-80.

Tao X, Thijssen S, Kotanko P, Ho C-H, Henrie M, Stroup E, Handelman G, 2016. Improved dialytic removal of protein-bound uraemic toxins with use of albumin binding competitors: an in vitro human whole blood study. *Scientific reports* **6**, 23389.

Tian S, Li Q, Yao W, Xu C, 2013. Construction and characterization of a potent, long-lasting recombinant human serum albumin-interferon α1 fusion protein expressed in Pichia pastoris. *Protein expression and purification* **90**, 124-8.

Vaikuntapu PR, Mallakuntla MK, Das SN, Bhuvanachandra B, Ramakrishna B, Nadendla SR, Podile AR, 2018. Applicability of endochitinase of Flavobacterium johnsoniae with transglycosylation activity in generating long-chain chitooligosaccharides. *International journal of biological macromolecules* **117**, 62-71.

Vanholder R, Baurmeister U, Brunet P, Cohen G, Glorieux G, Jankowski J, 2008. A bench to bedside view of uremic toxins. *Journal of the American Society of Nephrology* **19**, 863-70.

Vanholder R, De Smet R, Glorieux G, Argile´ A, Baurmeister U, Brunet P, Clark W, Cohen G, De Deyn PP, Deppisch R, Descamps-latscha B, Henle T, Jorres A, Lemke HD, Massy ZA, Passlick-deetjen J, Rodriguez M, Stegmayr B, Stenvinkel P, Tetta C, Wanner C, Zidek W, 2003. Review on uremic toxins: classification, concentration, and interindividual variability. *Kidney International* **63**, 1934-43.

Varshney A, Sen P, Ahmad E, Rehan M, Subbarao N, Khan RH, 2010. Ligand binding strategies of human serum albumin: how can the cargo be utilized? *Chirality: The Pharmacological, Biological, and Chemical Consequences of Molecular Asymmetry* **22**, 77-87.

Walker JE, 1976. Lysine residue 199 of human serum albumin is modified by acetylsalicylic acid. *FEBS letters* **66**, 173-5.

Wang ZM, Ho JX, Ruble JR, Rose J, Rüker F, Ellenburg M, Murphy R, Click J, Soistman E, Wilkerson L, Carter DC, 2013. Structural studies of several clinically important oncology

drugs in complex with human serum albumin. *Biochimica et Biophysica Acta - General Subjects* **1830**, 5356-74.

Wei Y, Thyparambil AA, Latour RA, 2014. Protein helical structure determination using CD spectroscopy for solutions with strong background absorbance from 190 to 230 nm. *Biochimica et Biophysica Acta - Proteins and Proteomics* **1844**, 2331-7.

Weiner MP, Costa GL, Schoettlin W, Cline J, Mathur E, Bauer JC, 1994. Site-directed mutagenesis of double-stranded DNA by the polymerase chain reaction. *Gene* **151**, 119-23.

Westphal U, Harding GB, 1973. Steroid-protein interactions XXVII. Progesterone binding to polymers of human serum albumin. *Biochimica et Biophysica Acta -Protein Structure* **310**, 518-27.

Yamasaki K, Chuang VT, Maruyama T, Otagiri M, 2013. Albumin-drug interaction and its clinical implication. *Biochimica et Biophysica Acta - General Subjects* **1830**, 5435-43.

Yamasaki K, Maruyama T, Kragh-Hansen U, Otagiri M, 1996. Characterization of site I on human serum albumin: concept about the structure of a drug binding site. *Biochimica et Biophysica Acta - Protein Structure and Molecular Enzymology* **1295**, 147-57.

Yamasaki K, Maruyama T, Takadate A, Suenaga A, Kragh-Hansen U, Otagiri M, 2004. Characterization of site I of human serum albumin using spectroscopic analyses: locational relations between regions Ib and Ic of site I. *Journal of pharmaceutical sciences* **93**, 3004-12.

Yeggoni DP, Gokara M, Mark Manidhar D, Rachamallu A, Nakka S, Reddy CS, Subramanyam R, 2014. Binding and molecular dynamics studies of 7-hydroxycoumarin derivatives with human serum albumin and its pharmacological importance. *Molecular pharmaceutics* **11**, 1117-31.

Yeggoni DP, Kuehne C, Rachamallu A, Subramanyam R, 2017. Elucidating the binding interaction of andrographolide with the plasma proteins: biophysical and computational approach. *RSC Advances* **7**, 5002-12.

Yeggoni DP, Rachamallu A, Dubey S, Mitra A, Subramanyam R, 2018. Probing the interaction mechanism of menthol with blood plasma proteins and its cytotoxicity activities. *Journal of Biomolecular Structure and Dynamics* **36**, 465-74.

Yeggoni DP, Rachamallu A, Kallubai M, Subramanyam R, 2015. Cytotoxicity and comparative binding mechanism of piperine with human serum albumin and α-1-acid glycoprotein. *Journal of Biomolecular Structure and Dynamics* **33**, 1336-51.

Yeggoni DP, Rachamallu A, Subramanyam R, 2016a. A comparative binding mechanism between human serum albumin and α-1-acid glycoprotein with corilagin: biophysical and computational approach. *RSC Advances* **6**, 40225-37.

Yeggoni DP, Rachamallu A, Subramanyam R, 2016b. Protein stability, conformational change and binding mechanism of human serum albumin upon binding of embelin and its role in disease control. *Journal of Photochemistry and Photobiology B: Biology* **160**, 248-59.

Yeggoni DP, Subramanyam R, 2014. Binding studies of l-3, 4-dihydroxyphenylalanine with human serum albumin. *Molecular BioSystems* **10**, 3101-10.

Yu J, Ju Y, Zhao L, Chu X, Yang W, Tian Y, Sheng F, Lin J, Liu F, Dong Y, Hou Y, 2015. Multistimuli-regulated photochemothermal cancer therapy remotely controlled via Fe5C2 nanoparticles. *ACS nano* **10**, 159-69.

Yvon M, Wal J-M, 1988. Identification of lysine residue 199 of human serum albumin as a binding site for benzylpenicilloyl groups. *FEBS letters* **239**, 237-40.

Zaidi N, Ajmal MR, Rabbani G, Ahmad E, Khan RH, 2013. A comprehensive insight into binding of hippuric acid to human serum albumin: a study to uncover its impaired elimination through hemodialysis. *PLoS One* **8**, e71422.

Zhang Q, Yu H, Zhang F-Z, Shen Z-C, 2013. Expression and purification of recombinant human serum albumin from selectively terminable transgenic rice. *Journal of Zhejiang University SCIENCE B* **14**, 867-74.

Zhang W, Inan M, Meagher MM, 2000. Fermentation strategies for recombinant protein expression in the methylotrophic yeastPichia pastoris. *Biotechnology and Bioprocess Engineering* **5**, 275-87.

Zheng Y-R, Suntharalingam K, Johnstone TC, Yoo H, Lin W, Brooks JG, Lippard SJ, 2014. Pt (IV) prodrugs designed to bind non-covalently to human serum albumin for drug delivery. *Journal of the American Chemical Society* **136**, 8790-8.

Zunszain PA, Ghuman J, Komatsu T, Tsuchida E, Curry S, 2003. Crystal structural analysis of human serum albumin complexed with hemin and fatty acid. *BMC Structural biology* **3**, 6.

Publication

Aparna Nerusu, P. Srinivasa Reddy, Dhevalapally B. Ramachary, Rajagopal Subramanyam, 2017. Unraveling the Stability of Plasma Proteins upon Interaction of Synthesized Androstenedione and Its Derivatives- A Biophysical and Computational Approach. *ACS Omega,* **2**, 6514-24.

ACS OMEGA

Article

http://pubs.acs.org/journal/acsodf

Unraveling the Stability of Plasma Proteins upon Interaction of Synthesized Androstenedione and Its Derivatives—A Biophysical and Computational Approach

Aparna Nerusu,[†] P. Srinivasa Reddy,[‡] Dhevalapally B. Ramachary,[‡] and Rajagopal Subramanyam*[,†]

[†]Department of Plant Science, School of Life Sciences, University of Hyderabad, Gachibowli, Hyderabad, Telangana 500046, India
[‡]Catalysis Laboratory, School of Chemistry, University of Hyderabad, Gachibowli, Hyderabad, Telangana 500046, India

Supporting Information

ABSTRACT: 4-Androstene-3-17-dione (4A), also known as androstenedione, is the key intermediate of steroid metabolism. 5β-Androstane-3-17-dione (5A) and (+)-6-methyl-5β-androstane-3-17-dione (6M) are the steroid derivatives of androstenedione. The interactions of androstenedione and its derivatives with plasma proteins are important in understanding the distribution and bioavailability of these molecules. In our present study, we have studied the binding affinity of androstenedione and its derivatives with plasma proteins such as human serum albumin (HSA) and α1-acid glycoprotein (AGP). Our results showed that the 4A, 5A, and 6M steroid molecules can form stable complexes with HSA and AGP. The affinity of the studied steroid molecules with HSA is high compared to that with AGP, and the binding constants obtained for 4A, 5A, and 6M with HSA are $5.3 \pm 2 \times 10^4$, $5.3 \pm 1 \times 10^4$, and $9.5 \pm 0.2 \times 10^4$ M^{-1}, respectively. Further, binding sites of these steroid molecules in HSA are identified using molecular displacement and docking studies: it is found that 4A and 5A bind to domain III while 6M binds to domain II of HSA. Furthermore, the circular dichroism data revealed that there is a partial unfolding of the protein while interacting with androstenedione and its derivatives. Also, molecular dynamics simulations were carried out for HSA−androstenedione and its derivative complexes to understand their stability; hence, these results yielded that HSA−androstenedione and its derivative complexes were stabilized after 15 ns and maintained their stable structures.

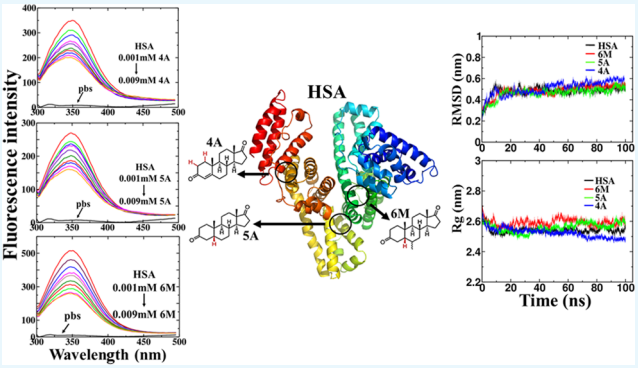

1. INTRODUCTION

Plasma proteins bind reversibly to drugs, hormones, and metabolites, which are hydrophobic in nature and circulate in the bloodstream. The binding affinity of plasma proteins determines free and effective concentrations, thereby regulating the pharmacokinetics and pharmacodynamics of the drugs. Hence, understanding the interaction mechanisms of various drugs and metabolites with these plasma proteins is of clinical significance. The major carrier proteins in plasma include human serum albumin (HSA), α1-acid glycoprotein (AGP), and lipoproteins.[1] Among the aforementioned plasma proteins, HSA is one of the most abundant proteins in human plasma, and it acts as a carrier for most drugs. Drugs that interact with HSA are acidic/neutral in nature, but they are basic in the case of AGP.[2]

Steroids get transported in the bloodstream with the aid of specific transporter proteins. Even though specific carrier proteins are available for the transport of steroids, they can also effectively interact with HSA.[3,4] Earlier reports on steroid hormones such as testosterone and progesterone show that they can interact with HSA.[3,5] Natural variants of HSA such as Niigata and Tagliacozzo show a high affinity toward prostaglandin and progesterone, respectively.[6] Besides HSA, another plasma protein AGP, an acute protein, also interacts with steroids and their derivatives. AGP can interact strongly with progesterone,[7] and the binding site for the progesterone is located in the N-terminus. Consequently, the binding site for progesterone is near to carbohydrate residue, demonstrated by using calcofluor white as a probe.[8]

4-Androstene-3-17-dione (4A) is a naturally occurring steroidal hormone, which is produced in gonads and adrenal glands, and is found to be the key metabolic intermediate in the metabolism of steroids such as testosterone, estradiol, progesterone, cortisone, and cortisol.[9] Synthetically, this compound is also used as a precursor molecule for the synthesis of various steroids. It possesses both androgenic and anabolic properties,[10] and thus, the level of 4A in blood plasma is significant. Also, it is an immediate precursor for testosterone, and the enzyme 17-β-hydroxysteroid dehydrogenase converts 4A to testosterone. Further, the enzyme aromatase converts 4A

Received: June 14, 2017
Accepted: September 20, 2017
Published: October 9, 2017

DOI: 10.1021/acsomega.7b00577
ACS Omega 2017, 2, 6514−6524

to estrone and estradiol.[11] In this line, we have synthesized 5β-androstane-3-17-dione (5A) through an organocatalysis method by taking 4A as the starting material.[12] Physiologically, 4A gets converted to 5A in the presence of 3-oxo-5-β-steroid-4-dehydrogenase. Another derivative is (+)-6-methyl-5β-androstane-3-17-dione (6M), in which the methyl group is attached at the C6 position of 5β-androstane-3-17-dione.

Structurally, HSA is a nonglycosylated 585-amino-acid polypeptide chain, predominantly made up of α-helix (67%).[13,14] It possess multidomain organization with three homologous domains, domain I (1−195), II (196−383), and III (384−585), forming a three-dimensional (3D) heart-shaped globular molecule. It is a negatively charged protein and has 17 highly cross-linked disulfide bonds.[15,16] It contains a single tryptophan residue at position 214. The protein mainly functions as a regulator of plasma colloid oncotic pressure, and it also acts as a carrier for many exogenous and endogenous metabolites and drugs.[17] In addition to drug-carrying properties, this protein possesses several other properties such as antioxidant and (pseudo)enzymatic properties.[18,19] It has a wide range of biochemical properties and interactions with several kinds of molecules such as fatty acids, porphyrins, bilirubin, thyroxin, and metal ions;[20−24] hence, this protein can be exploited for various applications. There are two major binding sites in HSA, site I and site II, located in domain IIA and IIIA, respectively.[25] Further, domain IB is also named a drug-binding site.[25] It has an important role as drugs/ligands compete for the same binding site. Also, it is an allosteric protein and can accommodate more than one molecule at a time. Thus, understanding of these complex mechanisms of ligand interactions can help to understand the clinical outcome.

Perhaps, AGP also known as orosomucoid and acute phase protein plays an important role in binding of drugs. It has a normal range of 0.6−1.2 mg/mL (1−3% of plasma proteins);[26] during inflammation, the plasma concentration increases to 2−5 folds. Moreover, this protein has antiinflammatory and immunomodulatory roles. Surprisingly, the levels of AGP elevated in acute inflammation and show systemic response to local inflammation.[27] It is a glycoprotein of 183 amino acid residues with 41 kDa molecular weight, consists of 45% carbohydrate attached in the form of N-linked glycans, and confines to the N-terminus of the protein. This protein is negatively charged at physiological pH because of 16 sialic acid residues.[28] Also, it has three tryptophan residues, where tryptophan 160 is present on the surface of the protein and rest two are located at the inner side of the protein.[29] Predominantly, there is only a single high-affinity basic drug-binding site in AGP.[30] Recently, our group reported that there are several molecules specifically bind to AGP.[31,32] Competition for the single basic drug-binding site can control the therapeutically effective plasma levels of basic drugs. Because of the single binding site, the drugs binding to AGP can attain saturation and are competitively displaceable. Stereo selectivity also exists for the single binding site.

In the present study, we have aimed to understand the following observations such as interaction mechanism of HSA and AGP with the synthesized steroid molecules, 4-androstene-3-17-dione (4A), 5β-androstane-3-17-dione (5A), and (+)-6-methyl-5β-androstane-3-17-dione (6M) (Scheme 1). Further, the conformational changes and stability of the complexes were emphasized using biophysical and computational approaches.

Scheme 1. Structures of 4A, 5A, and 6M[a]

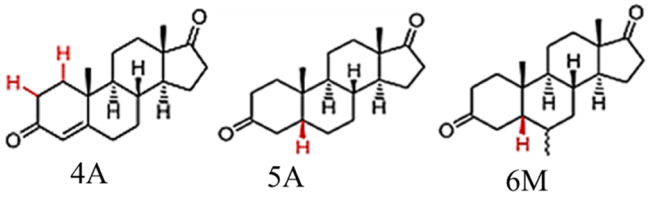

[a]The molecular weights of 4A, 5A, and 6M are 286.41, 288.42, and 302.45 Da, respectively.

2. RESULTS AND DISCUSSION

2.1. Analysis of Fluorescence Characteristics and Quenching Mechanism. The phenomenon of fluorescence quenching is an important method to characterize the interaction between a ligand and biological macromolecules. In the present study, the interaction of 4A, 5A, and 6M with HSA and AGP was characterized using fluorescence emission spectra. The interaction time was optimized by monitoring the fluorescence emission spectra of HSA and AGP at maximum concentrations of the compounds at regular time periods and the interaction time of 5 minutes was obtained. The emission spectra recorded for HSA and AGP with increasing concentrations of the ligands are shown in Figures 1 and 2, respectively. In the presence of increasing concentrations of 4A, 5A, and 6M, the intensity of fluorescence emission decreased gradually with an insignificant shift toward shorter wavelengths. However, there is no significant fluorescence emission from the ligands. Hence, the quenching of the fluorescence is concentration-dependent. Quenching can occur by a variety of molecular interactions such as excited-state reactions, molecular rearrangements, energy transfer, ground-state complex formation, and collisional quenching.[33] Our group previously reported the interaction of various phytochemicals with HSA based on the fluorescence quenching phenomenon.[34,35]

Usually, in protein, aromatic amino acids such as tryptophan, tyrosine, and phenylalanine act as intrinsic fluorophores.[33] Among all three aromatic amino acids, tryptophan has much stronger fluorescence intensity and higher quantum yield because of its indole ring. Tyrosine also has a quantum yield similar to that of tryptophan, but in native proteins, its fluorescence emission usually gets quenched by tryptophan or if it is ionized. Further, phenylalanine gives a very low quantum yield, and hence the intrinsic fluorescence of a protein is the solely contribution from tryptophan residues. Usually, microenvironment of the protein affects the emission spectra of the tryptophan residues. The fluorescence emission maxima shift toward shorter wavelength if the tryptophan residue is surrounded by hydrophobic residues so that each and every protein shows its own characteristic fluorescence emission spectra based on the number and surrounding environment of the tryptophan residues. HSA has a single tryptophan residue (Trp-214) located in the subdomain IIA corresponding to the Sudlow's drug-binding site I region. The characteristic emission spectrum for HSA has emission maxima at 350 nm (Figure 1). In the case of AGP, it has three tryptophan residues, its characteristic fluorescence emission spectrum shows emission maxima at 340 nm, and the peak is narrower compared to that of HSA (Figure 2). When small molecules are bound to HSA, the changes of intrinsic fluorescence of HSA are induced by the microenvironment of tryptophan residues. This indicates that

DOI: 10.1021/acsomega.7b00577
ACS Omega 2017, 2, 6514−6524

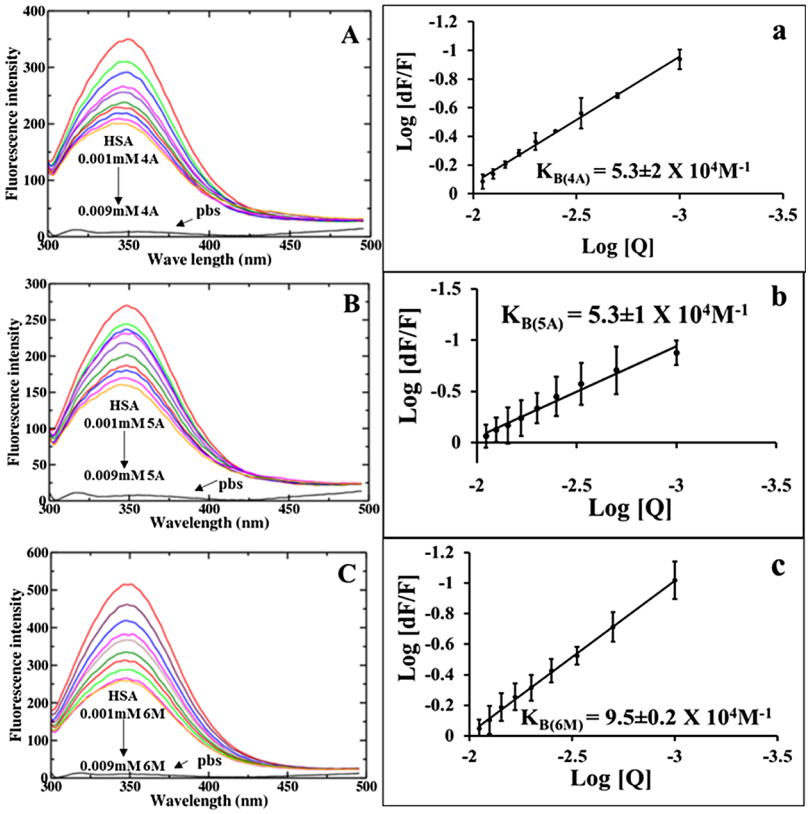

Figure 1. Fluorescence emission spectra of HSA in the presence of increasing concentrations of (A) 4A, (B) 5A, and (C) 6M from 1 to 9 μM. Fluorescence quenching was shown with increasing concentrations of the molecules. There was no fluorescence emission for buffer and the ligands in the given wavelength ranging from 300 to 500 nm. Modified Stern−Volmer plots for (a) 4A, (b) 5A, and (c) 6M obtained by plotting log [Q] values on the *X*-axis and log [d*F*/*F*] values on the *Y*-axis. The slope of the plot gives the number of binding sites. The *Y* intercept value gives log *K* values, from which the binding constant values were calculated. All three molecules have only one binding site in HSA. The binding constant values are 5.3 ± 2 × 10^4, 5.3 ± 1 × 10^4, and 9.5 ± 0.2 × 10^4 M^{-1}, respectively, for 4A, 5A, and 6M.

the microenvironment around tryptophan has been altered because of the formation of HSA−4A (androstenedione), HSA−5A, and HSA−6M complexes.

Another important factor that could lead to a decrease in emission intensity is the inner filter effect.[36] The inner filter effect refers to the absorbance of light at the excitation or emission wavelength by the ligands present in the solution. The absorption and emission spectra of 4A, 5A, and 6M at 10 μM concentration are given in Figure S1. The emission intensities were corrected for the inner filter effect using the following relationship:

$$F_{Cor} = F_{Obs} \times e^{(A_{exi}+A_{emi})/2}$$

where F_{Cor} is the corrected fluorescence intensity, A_{exi} and A_{emi} represent the absorbance at the fluorescence excitation (285 nm) and emission wavelengths, respectively, and F_{Obs} is the observed fluorescence.

Two common mechanisms of quenching are well-known: dynamic (or) collisional and static quenching,[33] which can be distinguished by temperature, viscosity dependence, and the difference of their fluorescence lifetimes. The relation between the quencher concentration and the fluorescence intensity can be well-explained using the Stern−Volmer equation.

$$F_0/F = 1 + K_q\tau_0[Q] = 1 + K_{SV}[Q]$$

where F_0 represents the fluorescence intensity in the absence of quencher, F represents the fluorescence intensity in the presence of quencher, [Q] is the quencher concentration, K_q is the bimolecular quenching rate constant, τ_0 is the lifetime of the fluorophore in the absence of quencher and its value is around 10^{-8} s for most of the biomolecules, and K_{SV} is the Stern−Volmer quenching constant, which can be written as

$$K_q = K_{SV}/\tau_0$$

The emission quenching data of HSA were plotted as F_0/F against the concentration of ligands, which is shown in Figure S2. It shows that within the investigated concentrations, the Stern−Volmer plot exhibited a good linear relationship. Further, the values of the Stern−Volmer quenching constant K_{SV} were obtained from the slope, by keeping the intercept at 1. The average lifetime (τ_0) of the biopolymer without any quencher has already been reported as ∼10^{-8} s.[37] From the above equation, bimolecular quenching rate constant was calculated and was far greater than the maximum scatter collision quenching constant 2.0 × 10^{10} M^{-1} s^{-1},[38] showing the formation of a ground-state complex between the protein and the ligands. It has been well-established that for a static quenching process, the quenching constant K_q should be greater than the maximum scatter collision quenching constant. The calculated K_q values are 9.0 ± 0.2 × 10^{12}, 9.8 ± 3 × 10^{12}, and 1.0 ± 1.0 × 10^{13} M^{-1} s^{-1}, respectively, for 4A, 5A, and 6M with HSA, which are greater than the maximum scatter collision quenching constant. This identification shows that there is a static ground-state complex formation between HSA and the ligands. In a similar way, the interaction between AGP and the

DOI: 10.1021/acsomega.7b00577
ACS Omega 2017, 2, 6514−6524

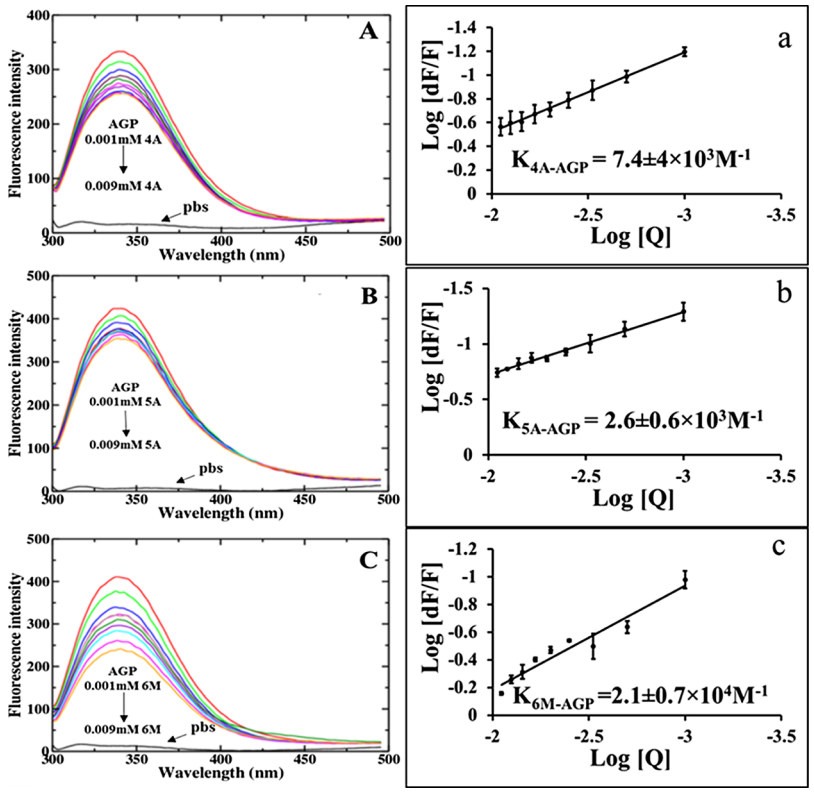

Figure 2. Fluorescence emission spectra of AGP with increasing concentrations of (A) 4A, (B) 5A, and (C) 6M. The emission maximum for AGP is 340 nm. Modified Stern–Volmer plots for (a) 4A, (b) 5A, and (c) 6M obtained by plotting log [Q] values on the *X*-axis and log [d*F*/*F*] values on the *Y*-axis.

ligands was also identified as the ground-state complex formation.

The binding constants and the number of binding sites were calculated using the modified Stern–Volmer equation.

$$\log(F_0 - F)/F = \log K + n \log[\mathrm{Q}]$$

where n corresponds to the number of binding sites, K is the binding constant, and [Q] is the quencher concentration.

log K can be calculated from the intercept of the graph of $\log(F_0 - F)/F$ versus log [Q], and the slope of the graph gives the number of binding sites. The n values of 4A (0.818), 5A (0.911), and 6M (0.963) are nearer to 1, showing the one-to-one interaction of the three molecules with HSA. The binding constants were calculated, and they are $5.3 \pm 2 \times 10^4$, $5.3 \pm 1 \times 10^4$, and $9.5 \pm 0.2 \times 10^4$ M^{-1}, respectively, for 4A, 5A, and 6M (Figure 1). In a similar way, the binding constants for 4A, 5A, and 6M with AGP were calculated as $7.4 \pm 4 \times 10^3$, $2.6 \pm 0.6 \times 10^3$, and $2.1 \pm 0.7 \times 10^4$ M^{-1}, respectively (Figure 2). HSA is showing much higher affinity compared to AGP with these three molecules; however, binding of these three compounds with AGP is also significant. Compared to 4A and 5A, the methyl derivative of androstane (6M) is showing higher affinity toward HSA and AGP. These results indicate that both HSA and AGP play a major role in binding which in turn act as major transporters in the blood system.

Because the binding constant (or) association constant value is known, K_d can be calculated from the reciprocal of K, and from that, binding free energies can be calculated using the following equation:

$$\Delta G^0 = -RT \ln K_d$$

where ΔG^0 is the free energy change, R is the gas constant at room temperature, and K_d is the dissociation constant which is given by

$$K_a = 1/K_d$$

The calculated free energies are −6.59, −6.51, and −6.83 kcal/mol, respectively, for 4A, 5A, and 6M with HSA, whereas with AGP, the binding free energies are calculated as −5.18, −4.64, and −5.85 kcal/mol, respectively, for 4A, 5A, and 6M. These results are in agreement with those from our laboratory work on different ligands binding with HSA and AGP.[31,32,34,36] These data infer that 4A (androstenedione), 5A, and 6M bind strongly with plasma proteins. Binding of these molecules to AGP is of additional importance because it also acts as a transporter in some disease conditions such as renal failure, pregnancy, burns, and so forth. Differential binding of these ligands is due to different functional groups attached to the original molecules.

2.2. Locating the Binding Site Using Site-Specific Probes. Several attempts have been made to map the binding sites on HSA, as it can bind to several exogenous and endogenous ligands. Sudlow showed the presence of two specific drug-binding sites, namely, site I (also called the warfarin binding site) and site II (the benzodiazepine binding site) using a fluorescent probe displacement method.[39] Even though there are two binding sites located in subdomains IIA and IIIA, other secondary binding site is also located at subdomain IB in HSA.[25] Among the available list of site-specific markers, we selected phenylbutazone and ibuprofen as site probes for IIA and IIIA, respectively. An equimolar ratio of HSA and site markers was titrated with 4A, 5A, and 6M in three

DOI: 10.1021/acsomega.7b00577
ACS Omega 2017, 2, 6514–6524

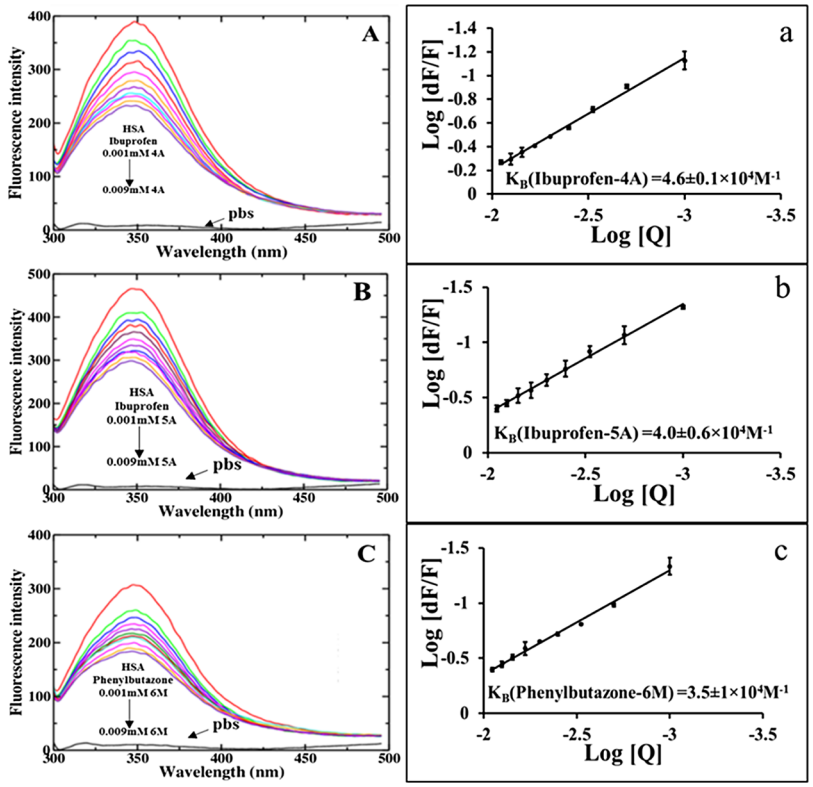

Figure 3. Competitive binding analysis of (A) 4A, (B) 5A, and (C) 6M. 4A and 5A are competing with ibuprofen toward binding to HSA. 6M is competing with phenylbutazone. Modified Stern−Volmer plots for (a) 4A, (b) 5A, and (c) 6M obtained by plotting log [Q] values on the *X*-axis and log [d*F*/*F*] values on the *Y*-axis.

different experiments. The binding constant values were calculated as mentioned above (Figure 3). The binding constant for 4A in the presence of ibuprofen is 4.6 ± 0.1 × 10^4 M^{-1}. Compared to only HSA, the binding constant value is decreased in the presence of site markers and is lower in the case of ibuprofen, showing that the ligand is competing with ibuprofen to bind to IIIA. Similarly, 5A is also competes with ibuprofen; however, 6M is competing with phenylbutazone, with binding constant values 4.0 ± 0.6 × 10^4 and 3.5 ± 1 × 10^4 M^{-1}, respectively. Figure 3 shows the fluorescence emission spectra of HSA in the presence of ibuprofen and phenylbutazone while titrating with increasing concentrations of 4A, 5A, and 6M. Thus, molecular displacement results in turn determined the specific binding pockets of 4A, 5A, and 6M.

2.3. Secondary Structure Analysis from Circular Dichroism Data. To understand the influence of ligand binding on the conformation of secondary structure of HSA, circular dichroism (CD) spectroscopy measurements were performed in the presence of increasing concentrations of 4A, 5A, and 6M. The room-temperature CD spectra measured in the presence of 4A, 5A, and 6M are shown in Figure 4. The characteristic CD spectra of HSA measured in the far-UV region show two minima at 222 and 208 nm, which are the contributions of n → π^* transfer of the peptide bonds from α-helix.[40−42] As shown in Figure 4, CD spectra of free HSA exhibit two negative bands in the ultraviolet region at 208 and 222 nm. It was observed that in the presence of steroid molecules, the CD signal of HSA got decreased. The decrease of the CD signal indicates a decrease of helical secondary structure content. However, the CD spectra of HSA in the presence or absence of ligands are similar in shape, indicating that there are very minute changes occurred in HSA due to ligand binding. Using CDNN software, the percentage of secondary structures was quantified for both free HSA and HSA in the presence of ligands. The percentage of α-helix differed from 66.05% in free HSA to 58.1% in 4A−HSA at pH 7.4 while β-turns and random coils were increased from 17.43 to 20.1% and from 16.51 to 21.7%, respectively. In the cases of 5A and 6M, the α-helix content was decreased to 59.1 and 53.6%, respectively. There is a gradual decrease in the α-helical percentage with increasing concentrations of ligands. The percentage changes of secondary structural elements were plotted against the concentration of the ligands, which is shown in the inset of Figure 4. The marginal changes in the percentage of secondary structural elements indicate that 4A, 5A, and 6M are interacting with HSA; hence, there is a partial unfolding of the protein. Structural changes of the protein indicate the changes in the microenvironment around the binding pocket residues upon binding of these molecules. Similar results were observed from our laboratory work that upon binding of ligands, HSA undergoes conformational changes.[31,34,36] To understand the stability of HSA in various temperatures, CD spectra were recorded for HSA with increasing temperature from 25 to 85 °C. The temperature influence is not significant up to 65 °C, consistent with the fact that HSA alone is stable up to 65 °C (data not shown).

2.4. Mode of Ligand Binding to HSA Using the Molecular Docking Approach. Molecular docking studies were further used to understand the interaction between HSA and the ligands.[43] The 3D structure (taken from PDB ID: 1AO6) of HSA consists of three homologous domains, denoted as I, II, and III. Each domain contains six-helix and four-helix subdomains. Each domain further subdivided into A and B subdomains that assemble to form a heart-shaped tertiary

DOI: 10.1021/acsomega.7b00577
ACS Omega 2017, 2, 6514−6524

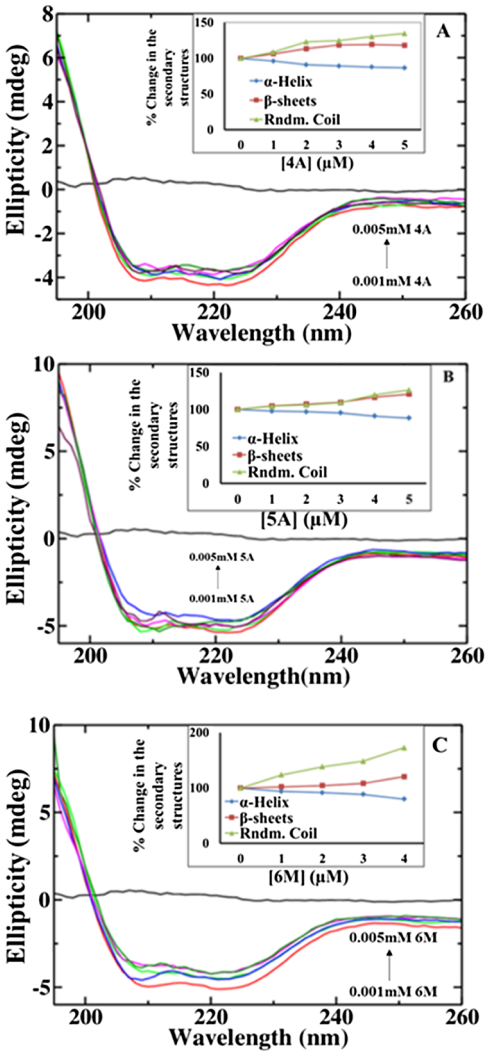

Figure 4. CD spectra of HSA alone (red line) and with increasing concentrations of (A) 4A, (B) 5A, and (C) 6M. The characteristic spectrum of protein shows spectral minima at 208 and 222 nm, indicating that HSA is an α-helical protein. The inset shows the percentage of secondary structural elements of HSA, obtained by deconvoluting the CD spectra using CDNN software.

structure.[1] HSA has two major drug-binding sites known as site I and II.[39] Site I is a large, flexible region, has poor stereo selectivity, and is located in subdomain IIA. The side chains of Tyr150, His242, and Arg257 are located at the bottom of the pocket, and Lys195, Lys199, Arg218, and Arg222 are located on an outer cluster at the pocket entrance.[25] On the other hand, site II is a smaller or narrower site than site I, shows stereo selectivity, and is located in subdomain IIIA. Site II is a largely apolar cavity formed by Leu387, Ser489, Leu453, and a single dominant polar patch at the pocket entrance, having Tyr411 and Arg410.[44]

The docking studies of HSA with 4A (androstenedione), 5A, and 6M give the information about the binding site of these steroid molecules in HSA and the interacting residues that form the binding groove (Figure 5). 4A binds in the groove formed by the residues of domain III. The residues forming this groove are different from those of site II. However, the groove is located immediately next to site II, having some of the residues from site II. The electronegative oxygen atom of 4A is forming a hydrogen bond with hydrogen from the ε-amino group of Lys413, with a bond length of 2.79 Å. Further, Thr540, Lys541, Glu542, Lys545, Leu529, Leu544, and Met548 from subdomain IIIB and Asn405, Ala406, Val409, and Lys413 from subdomain IIIA are forming the binding groove. Val409, Ala406, Leu544, and Lys545 are having hydrophobic interactions, and the rest of the residues forming the binding groove are interacting with van der Waals interactions, thereby holding 4A. Also, 5A is interacting with the residues of domain III. However, the binding groove is distinct from that of 4A. Further, the binding site of 5A is also overlapping with site II. In this, Phe206, Arg209, Ala210, Ala213, Leu331, Ala350, Lys351, Glu354, Leu347, Ser480, Leu481, and Val482 are the amino acid residues that form a binding groove for 5A. Moreover, Leu481 is forming a hydrogen bond with the electronegative oxygen of 5A, and the bond length is 2.91 Å. Further, Ala210, Arg209, Leu347, Val482, Ala213, and Lys351 are forming hydrophobic interactions with 5A, and the rest are interacting with van der Waals interactions. Distinct from 4A and 5A, 6M is interacting with the residues of domain II. Hence, 6M is interacting with Leu203, Thr243, Cys246, His247, Gln204, Gly207, Arg209, and Glu208 of subdomain IIA of HSA. Additionally, Glu208 is forming a hydrogen bond with 6M, and the bond length is 2.72 Å. From docking results, the binding free energies were calculated to be −7.36, −6.42, and −6.99 kcal/mol, respectively, for 4A, 5A, and 6M. These values are nearer to the experimental values that are obtained from fluorescence emission studies.

2.5. Molecular Dynamics Simulation Studies. HSA−ligand complex formation, complex stability, and the effect of ligands on HSA conformation with respect to time were analyzed using molecular dynamics and simulation studies. The properties such as root-mean-square deviation (rmsd) of HSA and complexes with respect to their initial structures, root-mean-square fluctuations (RMSFs), and radius of gyration (Rg) of the protein were obtained from molecular dynamics simulation (MDS) analysis. For the MDS analysis, the best conformer was taken from the docking studies for all of these molecules (4A, 5A, and 6M).

The rmsd values of HSA, HSA−4A, HSA−5A, and HSA−6M complexes with respect to their initial structure were calculated along 100 ns trajectories in GROMACS. The rmsd data show that HSA, HSA−4A, HSA−5A, and HSA−6M reach equilibration after 15 ns and later after the complexes got stabilized (Figure 6). Rg values of free HSA and complexes are also shown in Figure 6. The initial Rg value of free HSA is 2.68 nm and got stabilized at 2.55 nm. Experimentally defined Rg value of HSA using small-angle neutron scattering is 2.74 ± 0.035 nm, nearer to the value obtained in the present study.[34,45] There is not much difference in the Rg values of HSA−4A and HSA−5A, with respect to that of HSA alone, up to 60 ns. After 60 ns, there is a decrease in the Rg value of HSA−4A. In the case of HSA−6M complex, the Rg value increased slightly, with respect to that of HSA alone, and the variation started from 5 ns. Our experimental analysis with CD spectroscopy to understand the influence of ligands on protein conformation also showed that there is a marginal conformational change in the protein during 4A, 5A, and 6M binding (Figure 4) and it is high in the case of 6M. The CD data are further supporting the Rg data.

Local protein mobility was analyzed by plotting the RMSFs of HSA and the ligands against the atom number. Figure 7 shows the RMSF data of HSA and HSA−4A, where the RMSF value of HSA is 0.21 nm with 0.09 nm standard deviation and is

DOI: 10.1021/acsomega.7b00577
ACS Omega 2017, 2, 6514−6524

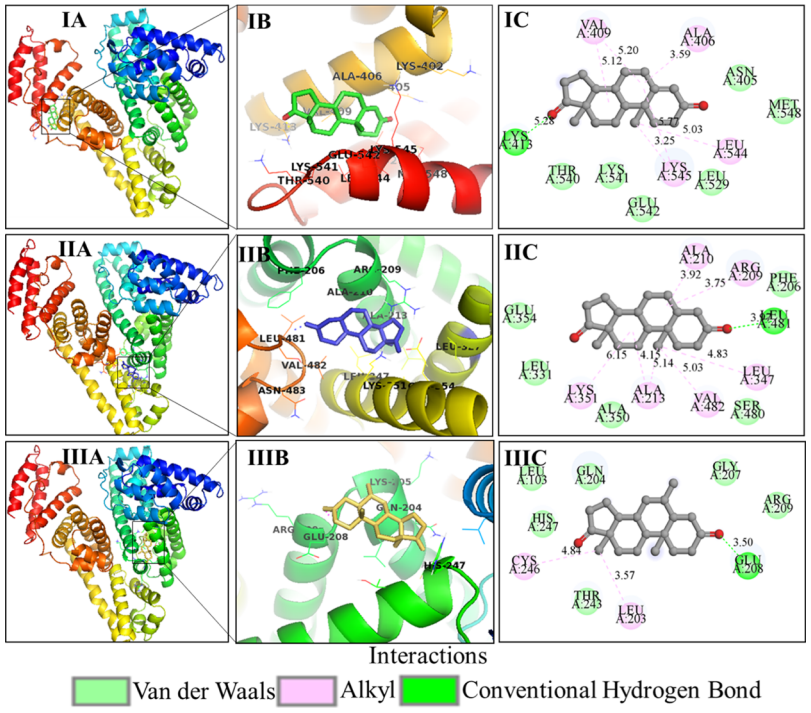

Figure 5. Docking of (I) 4A, (II) 5A, and (III) 6M with HSA. HSA interaction, 3D view of the ligand binding site, and 2D view of the ligand binding site with the interactions are shown in panels A, B, and C, respectively. 4A and 5A are interacting with the residues of domain IIIA. 6M is interacting with domain IIA of HSA.

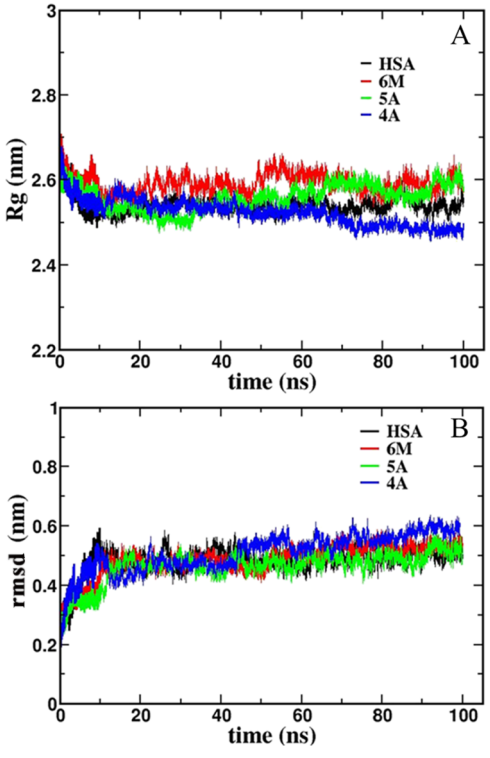

Figure 6. (A) Time-dependent evolution of the Rg and (B) rmsd values for free HSA, HSA−4A, HSA−5A, and HSA−6M complexes during 100 ns MDS.

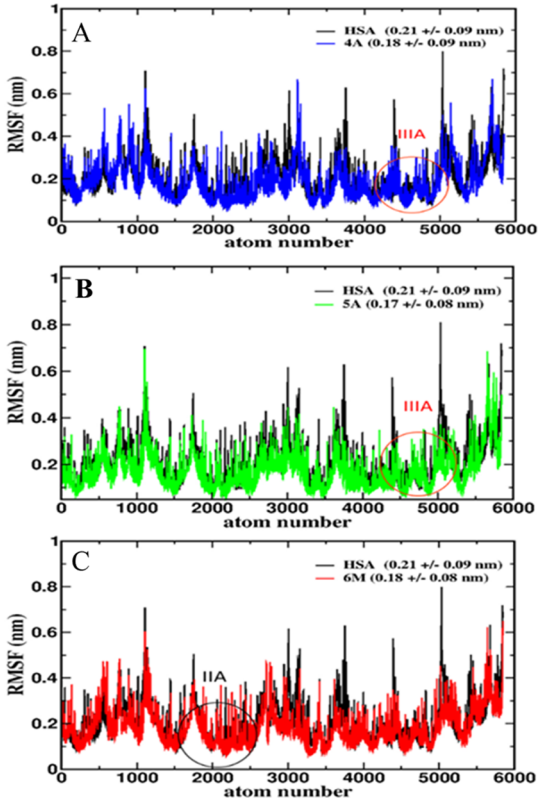

Figure 7. RMSFs of atoms of HSA in free HSA compared to those of (A) HSA−4A, (B) HSA−5A, and (c) HSA−6M complexes.

0.18 ± 0.09 nm for HSA−4A. Comparative RMSF in the 4A binding region, that is, IIIB shows that the RMSF values of HSA−4A are similar to those of HSA alone with little fluctuations, showing the rigidity of the residues because of ligand binding. The RMSF values of HSA−5A and HSA−6M are 0.17 ± 0.08 and 0.18 ± 0.08, respectively. The IIIA region

DOI: 10.1021/acsomega.7b00577
ACS Omega 2017, 2, 6514−6524

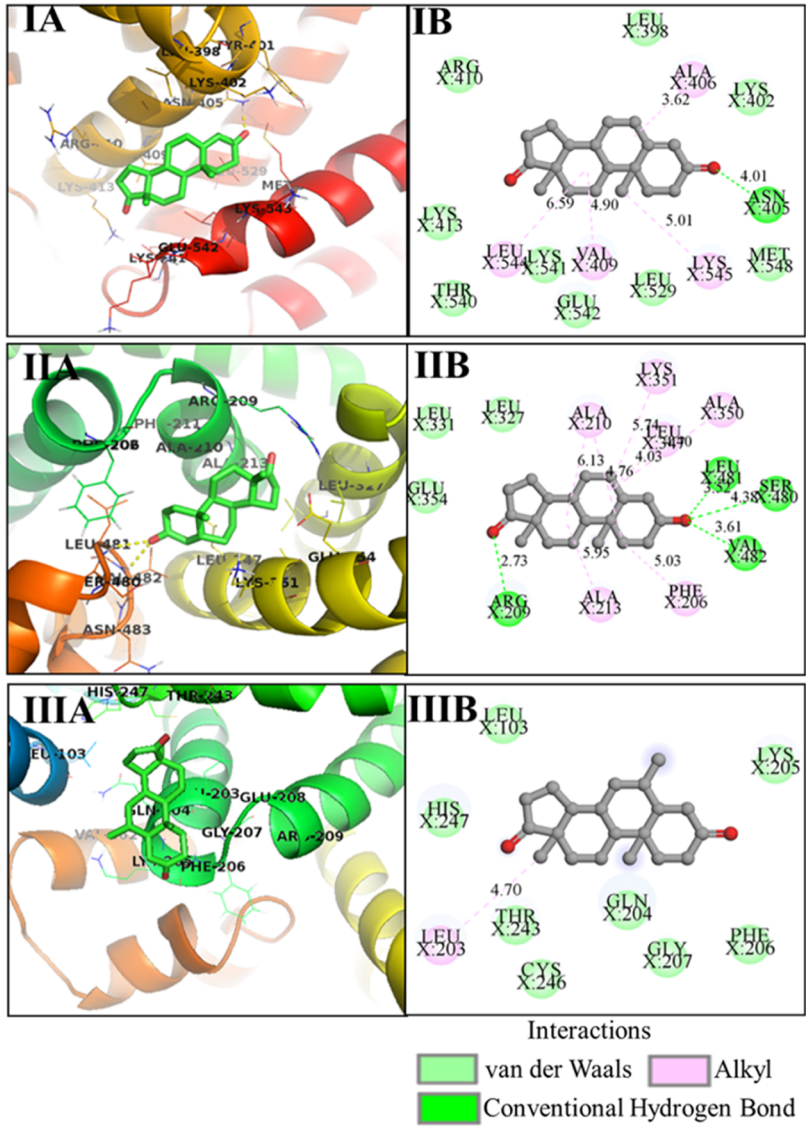

Figure 8. Interactions of (I) 4A, (II) 5A, and (III) 6M to HSA were shown after 3 ns of MDS. The 3D and 2D views of the interactions are shown in panels A and B, respectively. The 3D figure is showing the orientation of the molecule in the binding groove, and the nature of the interactions is shown in 2D visualization.

and IIA region of HSA show less RMSFs in the cases of 5A and 6M binding, respectively, compared to HSA protein alone.

Further, the interactions of 4A, 5A, and 6M to HSA were visualized at every 3, 6, and 10 ns time point from the 100 ns MDS data to get better insights into the complex stability. The snapshots for HSA−4A, HSA−5A, and HSA−6M at 3 ns time intervals are shown in Figure 8. Initially, 4A is interacting to Lys413 by a hydrogen bond (Figure 5), in time course, reoriented toward Asn405 in the binding groove itself, and form a hydrogen bond with Asn405. From 3 ns time point, 4A is interacting with Asn405 by a hydrogen bond, and this is stable up to 10 ns (Figure S3). The molecule is held by van der Waals interactions and hydrophobic interactions given by the binding site residues (Figures 5, 8, and S3). In a similar way, the stabilities of 5A and 6M were shown by plotting the interactions at 3 ns (Figure 8), 6, and 10 ns. Interactions at 6 and 10 ns are shown for 5A and 6M in Figures S4 and S5, respectively.

3. CONCLUSIONS

The present study gives the detailed description about the binding mechanism of androstenedione and its derivatives to HSA and AGP with various biophysical techniques. Fluorescence studies show that the synthesized compounds (4A, 5A, and 6M) can interact with both HSA and AGP, however, with more affinity toward HSA. The association constants and free energies were found to be $5.3 \pm 2 \times 10^4$, $5.3 \pm 1 \times 10^4$, and $9.5 \pm 0.2 \times 10^4$ M^{-1} and −6.59, −6.51, and −6.83 kcal/mol, respectively, with HSA. Among 4A, 5A, and 6M, the methyl derivative (6M) has high affinity toward HSA and AGP. Competitive binding studies by site-specific markers indicate that the compounds 4A and 5A are binding to domain III of HSA, whereas 6M is binding to domain II of HSA. Conformational changes in the protein upon ligand binding were observed by CD spectroscopy, which indicates that there is a partial unfolding of the protein upon binding of 4A, 5A, and 6M. Further, these studies were corroborated by in silico studies wherein hydrogen bonding, hydrophobic interactions, and van der Waals interactions are major driving forces toward

DOI: 10.1021/acsomega.7b00577
ACS Omega 2017, 2, 6514−6524

high affinities to HSA. Furthermore, the rmsd values from MDS data show that the complexes are stabilized after 15 ns. The Rg data calculated using MDS further support the partial unfolding of the protein during ligand binding as observed in CD spectroscopy.

The synthesized molecule 6M is a methyl derivative of 5A and shows approximately 2-fold and 10-fold increased affinity toward HSA and AGP, respectively, because of the presence of additional methyl group wherein hydrophobic interactions slightly dominate over other forces. The present study reiterates the importance of synthetic molecules in the drug discovery that enhance the drug distribution at the target sites without sacrificing the drug activity.

4. MATERIALS AND METHODS

4.1. Preparation of Stock Solutions. Pure fat-free HSA and AGP (purchased from Sigma-Aldrich) were dissolved at a concentration of 1.0 mM in an aqueous solution of 0.1 M phosphate buffer at a physiological pH 7.4. Stock solutions of 5 mM 4A, 5A, and 6M (Scheme 1) were prepared by dissolving appropriate amounts of 4A, 5A, and 6M in dimethyl sulfoxide (DMSO). The compounds 4A, 5A, and 6M were synthesized through organocatalysis, and these compounds were pure as reported earlier.[12] The site-specific markers were prepared as 1 mM stock solution. Final working concentrations were maintained at 0.1 mM for all ligands and site-specific probes. All other chemicals were of analytical grade and purchased from Sigma-Aldrich.

4.2. Measurements of Fluorescence Emission. Fluorescence emission spectra were recorded at 25 °C from a wavelength range of 300−500 nm with an excitation wavelength of 285 nm and a slit width of 8.0 nm for both excitation and emission using a PerkinElmer LS55 fluorescence spectrophotometer. Final concentration of HSA and AGP were fixed at 1×10^6 M^{-1}, and the increasing concentrations of compounds varied from 1 to 9×10^6 M^{-1} were suspended in 0.1 M phosphate buffer with pH 7.4. Three independent experiments were performed, and each time, identical spectra were obtained. The binding constant was calculated by taking the maximum fluorescence emission at 350 nm for HSA and 340 nm for AGP using the Stern−Volmer equation.

4.3. Molecular Displacement Experiment with Site-Specific Markers. For competitive binding studies, the site-specific probes were used. The site markers phenylbutazone and ibuprofen specifically bind to subdomains IIA and IIIA of HSA. The solution having the protein and the site marker in a ratio of 1:1 was titrated with increasing concentrations of 4A, 5A, and 6M from 1:1 to 1:10 to HSA. The fluorescence emission spectra were recorded as mentioned above. The binding constant values were evaluated using the Stern−Volmer equation.

4.4. CD Spectroscopy Measurements. The CD measurements of HSA in the presence and absence of 4A, 5A, and 6M were made in the range of 195−260 nm using a JASCO J-815 CD spectropolarimeter and a quartz cell with a path length of 0.2 cm. For all spectra, the baseline was subtracted using buffer. HSA was made into a solution using 10 mM phosphate buffer at pH 7.4. The HSA-to-ligand concentration was varied in a ratio of 1:1 to 1:5, and the CD spectra were recorded. Three scans were accumulated at a scan speed of 100 nm min^{-1}, and the bandwidth was kept at 2 nm. Finally, the CD spectra data collected were deconvoluted using CDNN 2.1 software to get the percentages of secondary structural elements. The JASCO J-815 CD spectropolarimeter was attached to a Peltier, which facilitated the measurement of secondary structural changes with increasing temperatures from 25 to 85 °C.

4.5. Molecular Docking. To find out the binding site, interacting residues, and the type of interactions involved in the complex formation, in silico docking was performed using AutoDock 4.2.3 program.[46] AutoDock 4.2.3 uses the Lamarckian genetic algorithm (GA).[47] The known crystal structure of HSA was taken from the protein data bank (PDB), and its PDB ID is 1AO6. The protein was edited in AutoDock. Before using it, water molecules and ions were removed. Hydrogen atoms were added to the functional groups and ionized as required at physiological pH. Further, Kollman united atom partial charges were assigned to HSA. The ligand structures (4A, 5A, and 6M) were designed using Discovery Studio 3.5. The two-dimensional (2D) structures of the ligands were drawn, and the geometry was optimized. The energy minimization was performed to relieve the steric effects. Both protein and ligand files were saved as the PDBQT format. PDBQT is the readable format for AutoDock. HSA was held rigid, all torsion bonds of the ligands were considered as free, and there was no consideration regarding the effect of solvent on the interactions. Blind docking was performed to locate the binding site of the ligands. The size of the grid box was set to a maximum with 0.0637 nm grid spacing. The center of the grid was set to 2.95, 3.18, and 2.35 nm. The docking parameters used were as follows: GA population size: 150 and maximum number of energy evolutions: 250 000. During docking, a maximum number of top 30 conformers were considered, and the rms cluster tolerance was set to 0.2 nm. A conformer with the least free energy and whose binding energy was close to the experimentally determined free energy values was considered. The conformer was visualized using PyMOL software.[48]

4.6. Molecular Dynamics Simulations. GROMACS 4.0 package was used for molecular dynamics studies, using GROMOS96 43a1 force field.[49] The protein conformation with lowest binding energy, which is close to the experimentally obtained value, was taken as an initial structure. The protein topology was prepared using pdb2gmx, which can read PDB files and generate coordinate and topology in the GROMACS format. The topology parameters of the ligands were created using PRODRG2.5 server.[50−52] The box type used is dodecahedron, which defines the unit cell. The protein was placed at 1.0 nm from the box edge. The simulation was done in the aqueous system by taking a simple point charge water model. HSA is a negatively charged protein, and the neutralization was done by adding 15 Na^+ ions. Energy minimization was done for the entire system having proteins, ligands, ions, and water molecules to release conflicting contacts. The minimization was performed, which optimizes the geometry and solvent orientation, using the steepest descent method of 1000 steps, followed by another 1000 steps of conjugate gradient energy minimization. Before proceeding to production, MD step equilibration was done. Equilibration of the system brings it to proper temperature and pressure conditions. The equilibration was performed in two phases. In the first phase, NVT, position restrain of the solute was done at 300 K for 100 ps, followed by NPT at 1 bar pressure. Berendsen thermostat and Parrinello-Rahman pressure coupling were used for temperature coupling and pressure coupling, respectively.[52] Then, the system was subjected to 100 ns MD at 300 K temperature and 1 bar pressure. The

DOI: 10.1021/acsomega.7b00577
ACS Omega 2017, 2, 6514−6524

motion equations were integrated using the leap-frog algorithm. The trajectories were recorded at every 10 ps interval.

■ ASSOCIATED CONTENT

Supporting Information

The Supporting Information is available free of charge on the ACS Publications website at DOI: 10.1021/acsomega.7b00577.

Fluorescence emission and absorption spectra of the selected ligands; Stern−Volmer plots for the interaction of HSA to the selected androstenedione derivatives; and interaction of the selected androstenedione derivatives to HSA at 6 and 10 ns from 100 ns MDS (PDF)

■ AUTHOR INFORMATION

Corresponding Author

*E-mail: srgsl@uohyd.ernet.in. Phone: +91-40-23134572. Fax: +91-40-23010120 (R.S.).

ORCID

Rajagopal Subramanyam: 0000-0003-3872-8390

Notes

The authors declare no competing financial interest.

■ ACKNOWLEDGMENTS

This work was supported by UPE-2 University of Hyderabad, Science and Engineering Research Board (SB/EMEQ-064/2014 dated 14-07-2015 and DST-FIST) and UGC-SAP. We thank BIF for Bioinformatics facilities. A.N. acknowledges CSIR for fellowship.

■ REFERENCES

(1) Peters, T., Jr. *All About Albumin: Biochemistry, Genetics, and Medical Application*; Academic Press: San Diego, 1996; pp 76−132.

(2) Fanali, G.; di Masi, A.; Trezza, V.; Marino, M.; Fasano, M.; Ascenzi, P. Human Serum Albumin: From Bench to Bedside. *Mol. Aspects Med.* **2012**, *33*, 209−290.

(3) Pearlman, W. H.; Crépy, O. Steroid-Protein Interaction with Particular Reference to Testosterone Binding by Human Serum. *J. Biol. Chem.* **1967**, *242*, 182−189.

(4) Varshney, A.; Sen, P.; Ahmad, E.; Rehan, M.; Subbarao, N.; Khan, R. H. Ligand Binding Strategies of Human Serum Albumin: How Can the Cargo be Utilized? *Chirality* **2010**, *22*, 77−87.

(5) Westphal, U.; Harding, G. B. Steroid-Protein Interactions XXVII. Progesterone Binding to Polymers of Human Serum Albumin. *Biochim. Biophys. Acta* **1973**, *310*, 518−527.

(6) Kragh-Hansen, U.; Minchiotti, L.; Brennan, S. O.; Sugita, O. Hormone Binding to Natural Mutants of Human Serum Albumin. *Eur. J. Biochem.* **1990**, *193*, 169−174.

(7) Kute, T.; Westphal, U. Steroid-Protein Interactions. XXXIV. Chemical Modification of α1-Acid Glycoprotein for Characterization of the Progesterone Binding Site. *Biochim. Biophys. Acta* **1976**, *420*, 195−213.

(8) De Ceukeleire, M.; Albani, J. R. Interaction Between Carbohydrate Residues of α1-Acid Glycoprotein (Orosomucoid) and Progesterone. A Fluorescence Study. *Carbohydr. Res.* **2002**, *337*, 1405−1410.

(9) Malaviya, A.; Gomes, J. Androstenedione Production by Biotransformation of Phytosterols. *Bioresour. Technol.* **2008**, *99*, 6725−6737.

(10) Bahrke, M. S.; Yesalis, C. E. Abuse of Anabolic Androgenic Steroids and Related Substances in Sport and Exercise. *Curr. Opin. Pharmacol.* **2004**, *4*, 614−620.

(11) Jasuja, R.; Ramaraj, P.; Mac, R. P.; Singh, A. B.; Storer, T. W.; Artaza, J.; Miller, A.; Singh, R.; Taylor, W. E.; Lee, M. L.; Davidson, T.; Sinha-Hikim, I.; Gonzalez-Cadavid, N.; Bhasin, S. Δ-4-Androstene-3,17-Dione Binds Androgen Receptor, Promotes Myogenesis *in Vitro*, and Increases Serum Testosterone Levels, Fat-Free Mass, and Muscle Strength in Hypogonadal Men. *J. Clin. Endocrinol. Metab.* **2005**, *90*, 855−863.

(12) Ramachary, D. B.; Sakthidevi, R.; Srinivasa Reddy, P. Direct Organocatalytic Stereoselective Transfer Hydrogenation of Conjugated Olefins of Steroids. *RSC Adv.* **2013**, *3*, 13497−13506.

(13) Curry, S. Beyond Expansion: Structural Studies on the Transport Roles of Human Serum Albumin. *Vox Sang.* **2002**, *83*, 315−319.

(14) Ghuman, J.; Zunszain, P. A.; Petitpas, I.; Bhattacharya, A. A.; Otagiri, M.; Curry, S. Structural Basis of the Drug-Binding Specificity of Human Serum Albumin. *J. Mol. Biol.* **2005**, *353*, 38−52.

(15) He, X. M.; Carter, D. C. Atomic Structure and Chemistry of Human Serum Albumin. *Nature* **1992**, *358*, 209−215.

(16) Petitpas, I.; Grüne, T.; Bhattacharya, A. A.; Curry, S. Crystal Structures of Human Serum Albumin Complexed with Monounsaturated and Polyunsaturated Fatty Acids. *J. Mol. Biol.* **2001**, *314*, 955−960.

(17) Fasano, M.; Curry, S.; Terreno, E.; Galliano, M.; Fanali, G.; Narciso, P.; Notari, S.; Ascenzi, P. The Extraordinary Ligand Binding Properties of Human Serum Albumin. *IUBMB Life* **2005**, *57*, 787−796.

(18) Roche, M.; Rondeau, P.; Singh, N. R.; Tarnus, E.; Bourdon, E. The Antioxidant Properties of Serum Albumin. *FEBS Lett.* **2008**, *582*, 1783−1787.

(19) Kragh-Hansen, U. Molecular and Practical Aspects of The Enzymatic Properties of Human Serum Albumin and of Albumin−Ligand Complexes. *Biochim. Biophys. Acta* **2013**, *1830*, 5535−5544.

(20) Bhattacharya, A. A.; Grüne, T.; Curry, S. Crystallographic Analysis Reveals Common Modes of Binding of Medium and Long-chain Fatty Acids to Human Serum Albumin. *J. Mol. Biol.* **2000**, *303*, 721−732.

(21) Minomo, A.; Ishima, Y.; Chuang, V. T. G.; Suwa, Y.; Kragh-Hansen, U.; Narisoko, T.; Morioka, H.; Maruyama, T.; Otagiri, M. Albumin Domain II Mutant with High Bilirubin Binding Affinity has A Great Potential as Serum Bilirubin Excretion Enhancer for Hyperbilirubinemia Treatment. *Biochim. Biophys. Acta* **2013**, *1830*, 2917−2923.

(22) Petitpas, I.; Petersen, C. E.; Ha, C.-E.; Bhattacharya, A. A.; Zunszain, P. A.; Ghuman, J.; Bhagavan, N. V.; Curry, S. Structural Basis of Albumin-Thyroxine Interactions and Familial Dysalbuminemic Hyperthyroxinemia. *Proc. Natl. Acad. Sci. U.S.A.* **2003**, *100*, 6440−6445.

(23) Bal, W.; Sokołowska, M.; Kurowska, E.; Faller, P. Binding of Transition Metal Ions to Albumin: Sites, Affinities and Rates. *Biochim. Biophys. Acta* **2013**, *1830*, 5444−5455.

(24) Naveenraj, S.; Anandan, S. Binding of Serum Albumins with Bioactive Substances—Nanoparticles to Drugs. *J. Photochem. Photobiol., C* **2013**, *14*, 53−71.

(25) Yamasaki, K.; Chuang, V. T. G.; Maruyama, T.; Otagiri, M. Albumin−Drug Interaction and Its Clinical Implication. *Biochim. Biophys. Acta* **2013**, *1830*, 5435−5443.

(26) Fournier, T.; Medjoubi-N, N.; Porquet, D. Alpha-1-acid glycoprotein. *Biochim. Biophys. Acta* **2000**, *1482*, 157−171.

(27) Kim, K. A.; Lee, E. Y.; Kang, J. H.; Lee, H. G.; Kim, J. W.; Kwon, D. H.; Jang, Y. J.; Yeom, Y. I.; Chung, T. W.; Kim, Y. D.; Yoon, D. Y.; Song, E. Y. Diagnostic Accuracy of Serum Asialo-α1-Acid Glycoprotein Concentration for the Differential Diagnosis of Liver Cirrhosis and Hepatocellular Carcinoma. *Clin. Chim. Acta* **2006**, *369*, 46−51.

(28) Schönfeld, D. L.; Ravelli, R. B. G.; Mueller, U.; Skerra, A. The 1.8-Å Crystal Structure of α1-Acid Glycoprotein (Orosomucoid) Solved by UV RIP Reveals the Broad Drug-Binding Activity of This Human Plasma Lipocalin. *J. Mol. Biol.* **2008**, *384*, 393−405.

(29) Lupidi, G.; Camaioni, E.; Khalifé, H.; Avenali, L.; Damiani, E.; Tanfani, F.; Scirè, A. Characterization of Thymoquinone Binding to Human α1-Acid Glycoprotein. *J. Pharm. Sci.* **2012**, *101*, 2564−2573.

(30) Müller, W. E.; Stillbauer, A. E. Characterization of a Common Binding Site for Basic Drugs on Human α2-Acid Glycoprotein

DOI: 10.1021/acsomega.7b00577
ACS Omega 2017, 2, 6514−6524

(Orosomucoid). *Naunyn-Schmiedeberg's Arch. Pharmacol.* **1983**, *322*, 170−173.
(31) Kallubai, M.; Rachamallu, A.; Yeggoni, D. P.; Subramanyam, R. Comparative Binding Mechanism of Lupeol Compounds with Plasma Proteins and Its Pharmacological Importance. *Mol. Biosyst.* **2015**, *11*, 1172−1183.
(32) Yeggoni, D. P.; Rachamallu, A.; Kallubai, M.; Subramanyam, R. Cytotoxicity and Comparative Binding Mechanism of Piperine with Human Serum Albumin and α-1-Acid Glycoprotein. *J. Biomol. Struct. Dyn.* **2014**, *33*, 1336−1351.
(33) Lakowicz, J. R. *Principles of Fluorescence Spectroscopy*, 3rd ed.; Springer: New York, 2009; pp 277−318.
(34) Yeggoni, D. P.; Gokara, M.; Manidhar, D. M.; Rachamallu, A.; Nakka, S.; Reddy, C. S.; Subramanyam, R. Binding and Molecular Dynamics Studies of 7-Hydroxycoumarin Derivatives with Human Serum Albumin and Its Pharmacological Importance. *Mol. Pharm.* **2014**, *11*, 1117−1131.
(35) Subramanyam, R.; Gollapudi, A.; Bonigala, P.; Chinnaboina, M.; Amooru, D. G. Betulinic acid Binding to Human Serum Albumin: A Study of Protein Conformation and Binding Affinity. *J. Photochem. Photobiol., B* **2009**, *94*, 8−12.
(36) Yeggoni, D. P.; Kuehne, C.; Rachamallu, A.; Subramanyam, R. Elucidating the binding interaction of andrographolide with the plasma proteins: biophysical and computational approach. *RSC Adv.* **2017**, *7*, 5002−5012.
(37) Sharma, A. S.; Anandakumar, S.; Ilanchelian, M. A Combined Spectroscopic and Molecular Docking Study on Site Selective Binding Interaction of Toluidine Blue O with Human and Bovine Serum Albumins. *J. Lumin.* **2014**, *151*, 206−218.
(38) Tabassum, S.; Al-Asbahy, W. M.; Afzal, M.; Arjmand, F. Synthesis, Characterization and Interaction Studies of Copper Based Drug With Human Serum Albumin (HSA): Spectroscopic and Molecular Docking Investigations. *J. Photochem. Photobiol., B* **2012**, *114*, 132−139.
(39) Sudlow, G.; Birkett, D. J.; Wade, D. N. The Characterization of Two Specific Drug Binding Sites on Human Serum Albumin. *Mol. Pharmacol.* **1975**, *11*, 824−832.
(40) Anand, U.; Mukherjee, S. Binding, Unfolding and Refolding Dynamics of Serum Albumins. *Biochim. Biophys. Acta, Gen. Subj.* **2013**, *1830*, 5394−5404.
(41) Gowda, J. I.; Nandibewoor, S. T. Binding and Conformational Changes of Human Serum Albumin upon Interaction with 4-Aminoantipyrine Studied by Spectroscopic Methods and Cyclic Voltammetry. *Spectrochim. Acta, Part A* **2014**, *124*, 397−403.
(42) Pan, F.; Xu, T.; Yang, L.; Jiang, X.; Zhang, L. Probing the Binding of An Endocrine Disrupting Compound-Bisphenol F to Human Serum Albumin: Insights Into The Interactions of Harmful Chemicals With Functional Biomacromolecules. *Spectrochim. Acta, Part A* **2014**, *132*, 795−802.
(43) Gorelik, B.; Goldblum, A. High Quality Binding Modes in Docking Ligands to Proteins. *Proteins: Struct., Funct., Bioinf.* **2008**, *71*, 1373−1386.
(44) Curry, S. Lessons From the Crystallographic Analysis of Small Molecule Binding to Human Serum Albumin. *Drug Metab. Pharmacokinet.* **2009**, *24*, 342−357.
(45) Malleda, C.; Ahalawat, N.; Gokara, M.; Subramanyam, R. Molecular Dynamics Simulation Studies of Betulinic Acid with Human Serum Albumin. *J. Mol. Model.* **2012**, *18*, 2589−2597.
(46) Morris, G. M.; Huey, R.; Lindstrom, W.; Sanner, M. F.; Belew, R. K.; Goodsell, D. S.; Olson, A. J. AutoDock4 and AutoDockTools4: Automated Docking with Selective Receptor Flexibility. *J. Comput. Chem.* **2010**, *30*, 2785−2791.
(47) Morris, G. M.; Goodsell, D. S.; Halliday, R. S.; Huey, R.; Hart, W. E.; Belew, R. K.; Olson, A. J. Automated Docking Using a Lamarckian Genetic Algorithm and an Empirical Binding Free Energy Function. *J. Comput. Chem.* **1998**, *19*, 1639−1662.
(48) *PyMOL: The PyMOL Molecular Graphics System*, version 1.8; Schrödinger, LLC, 2015.
(49) Berendsen, H. J. C.; van der Spoel, D.; van Drunen, R. GROMACS: A Message-Passing Parallel Molecular Dynamics Implementation. *Comput. Phys. Commun.* **1995**, *91*, 43−56.
(50) Schüttelkopf, A. W.; van Aalten, D. M. F. PRODRG: A Tool for High-Throughput Crystallography of Protein−Ligand Complexes. *Acta Crystallogr., Sect. D: Biol. Crystallogr.* **2004**, *60*, 1355−1363.
(51) Spoel, D. V.; Lindahl, E.; Hess, B.; GROMACS Development Team. *GROMACS User Manual*, version 4.6.7, 2014.
(52) Sudhamalla, B.; Gokara, M.; Ahalawat, N.; Amooru, D. G.; Subramanyam, R. Molecular Dynamics Simulation and Binding Studies of β-Sitosterol With Human Serum Albumin and Its Biological Relevance. *J. Phys. Chem. B* **2010**, *114*, 9054−9062.

DOI: 10.1021/acsomega.7b00577
ACS Omega 2017, 2, 6514−6524

Mechanistic binding of bioactive compounds with recombinant truncated domains and native mutants of human serum albumin

by Aparna Nerusu

Mechanistic binding of bioactive compounds with recombinant truncated domains and native mutants of human serum albumin

ORIGINALITY REPORT

31%	6%	31%	5%
SIMILARITY INDEX	INTERNET SOURCES	PUBLICATIONS	STUDENT PAPERS

PRIMARY SOURCES

1	Aparna Nerusu, P. Srinivasa Reddy, Dhevalapally B. Ramachary, Rajagopal Subramanyam. "Unraveling the Stability of Plasma Proteins upon Interaction of Synthesized Androstenedione and Its Derivatives—A Biophysical and Computational Approach", ACS Omega, 2017 Publication	23%
2	Gabriella Fanali, Alessandra di Masi, Viviana Trezza, Maria Marino, Mauro Fasano, Paolo Ascenzi. "Human serum albumin: From bench to bedside", Molecular Aspects of Medicine, 2012 Publication	1%
3	Mariotti, Paolo <1980>(Scarlato, Vincenzo). "Characterization of the structure and iron uptake mechanisms of the Staphylococcus aureus ferric hydroxamate-binding lipoprotein FhuD2", Alma Mater Studiorum - Università di	<1%

Bologna, 2012.
Publication

4	Keishi Yamasaki, Victor Tuan Giam Chuang, Toru Maruyama, Masaki Otagiri. "Albumin–drug interaction and its clinical implication", Biochimica et Biophysica Acta (BBA) - General Subjects, 2013 Publication	<1%
5	Mohammad Rehan Ajmal, Fahad Almutairi, Nida Zaidi, Parvez Alam et al. "Biophysical insights into the interaction of clofazimine with human alpha 1-acid glycoprotein: A multitechnique approach", Journal of Biomolecular Structure and Dynamics, 2018 Publication	<1%
6	link.springer.com Internet Source	<1%
7	Yeggoni, Daniel Pushparaju, Aparna Rachamallu, Monika Kallubai, and Rajagopal Subramanyam. "Cytotoxicity and comparative binding mechanism of piperine with human serum albumin and α-1-acid glycoprotein", Journal of Biomolecular Structure and Dynamics, 2014. Publication	<1%
8	"Albumin in Medicine", Springer Nature, 2016 Publication	<1%

9	Ruth Huey. "A semiempirical free energy force field with charge-based desolvation", Journal of Computational Chemistry, 04/30/2007 Publication	<1%
10	tel.archives-ouvertes.fr Internet Source	<1%
11	pubs.acs.org Internet Source	<1%
12	www.chemlabinkaist.net Internet Source	<1%
13	Gokara, Mahesh, Vidadala V. Narayana, Vineet Sadarangani, Shatabdi Roy Chowdhury, Sreelaxmi Varkala, Dhevalapally B. Ramachary, and Rajagopal Subramanyam. "Unravelling the Binding Mechanism and Protein Stability of Human Serum Albumin while Interacting with Nefopam Analogues: A Biophysical and Insilco approach", Journal of Biomolecular Structure and Dynamics, 2016. Publication	<1%
14	Fujiwara, Shin-ichi, and Takashi Amisaki. "Fatty acid binding to serum albumin: Molecular simulation approaches", Biochimica et Biophysica Acta (BBA) - General Subjects, 2013. Publication	<1%

15	Nicoletta Giamblanco, Nunzio Tuccitto, Gabriella Zappalà, Gianfranco Sfuncia, Antonino Licciardello, Giovanni Marletta. "Chelating Surfaces for Native State Proteins Patterning: The Human Serum Albumin Case", ACS Applied Materials & Interfaces, 2015 Publication	<1%
16	Ulrich Kragh-Hansen, Lorenzo Minchiotti, Monica Galliano, Theodore Peters. "Human serum albumin isoforms: Genetic and molecular aspects and functional consequences", Biochimica et Biophysica Acta (BBA) - General Subjects, 2013 Publication	<1%
17	K. Kikuchi. "RNA Aptamers Targeted to Domain II of Hepatitis C Virus IRES That Bind to Its Apical Loop Region", Journal of Biochemistry, 03/01/2003 Publication	<1%
18	Submitted to SASTRA University Student Paper	<1%
19	Submitted to Universiti Putra Malaysia Student Paper	<1%
20	febs.onlinelibrary.wiley.com Internet Source	<1%
21	www.jbc.org	

	Internet Source	<1%
22	amb-express.springeropen.com Internet Source	<1%
23	Arumugam Selva Sharma, Shanmugam Anandakumar, Malaichamy Ilanchelian. "A combined spectroscopic and molecular docking study on site selective binding interaction of Toluidine blue O with Human and Bovine serum albumins", Journal of Luminescence, 2014 Publication	<1%
24	Espiritu, Rafael Atillo, Nobuaki Matsumori, Michio Murata, Shinichi Nishimura, Hideaki Kakeya, Shigeki Matsunaga, and Minoru Yoshida. "Interaction between the Marine Sponge Cyclic Peptide Theonellamide A and Sterols in Lipid Bilayers as Viewed by Surface Plasmon Resonance and Solid State ^{2}H NMR", Biochemistry, 2013. Publication	<1%
25	Submitted to Indian Institute of Science, Bangalore Student Paper	<1%
26	Z. Jurasekova. "Use of Raman spectroscopy for the identification of radical-mediated	<1%

damages in human serum albumin", Analytical and Bioanalytical Chemistry, 04/16/2011
Publication

---

27 H. G. Mahesha. "A spectroscopic study of the interaction of isoflavones with human serum albumin", FEBS Journal, 2/2006 <1%
Publication

---

28 Peter Krisper. "Clearing of toxic substances: are there differences between the available liver support devices? : Toxin clearance by liver support systems", Liver International, 09/2011 <1%
Publication

---

29 Ayaz Mohd. "Interaction of Clofazimine with Divalent Metal Ions: A Fluorescence Quenching Study", Journal of Dispersion Science and Technology, 2011 <1%
Publication

---

30 Submitted to Imperial College of Science, Technology and Medicine <1%
Student Paper

---

31 ir.canterbury.ac.nz <1%
Internet Source

---

32 P. Chanphai, H.A. Tajmir-Riahi. "Tea polyphenols bind serum albumins:A potential application for polyphenol delivery", Food Hydrocolloids, 2018 <1%
Publication

33	Daniel Pushparaju Yeggoni, Mahesh Gokara, Darla Mark Manidhar, Aparna Rachamallu et al. "Binding and Molecular Dynamics Studies of 7-Hydroxycoumarin Derivatives with Human Serum Albumin and Its Pharmacological Importance", Molecular Pharmaceutics, 2014 Publication	<1%
34	folding.bmc.uu.se Internet Source	<1%
35	www.dovepress.com Internet Source	<1%
36	Ding, F.. "Determining the binding affinity and binding site of bensulfuron-methyl to human serum albumin by quenching of the intrinsic tryptophan fluorescence", Journal of Luminescence, 201011 Publication	<1%
37	www.uic.edu Internet Source	<1%
38	Daniel Pushparaju Yeggoni, Aparna Rachamallu, Rajagopal Subramanyam. "Protein stability, conformational change and binding mechanism of human serum albumin upon binding of embelin and its role in disease control", Journal of Photochemistry and Photobiology B: Biology, 2016 Publication	<1%

39	Li, Y.. "Expression of common carp growth hormone in the yeast Pichia pastoris and growth stimulation of juvenile tilapia (Oreochromis niloticus)", Aquaculture, 20030210 Publication	<1%
40	krishikosh.egranth.ac.in Internet Source	<1%
41	Yang, F.. "Effect of human serum albumin on drug metabolism: Structural evidence of esterase activity of human serum albumin", Journal of Structural Biology, 200702 Publication	<1%
42	Submitted to Indian Institute of Technology, Madras Student Paper	<1%
43	Neelan J. Marianayagam, Sophie E. Jackson. "The folding pathway of ubiquitin from all-atom molecular dynamics simulations", Biophysical Chemistry, 2004 Publication	<1%
44	Abdulrazack Parveen, Venkatesan Sughanya, Samuthira Nagarajan. "Quenching of fluorescence in C60 fulleropyrrolidines by chloroform", Spectrochimica Acta Part A: Molecular and Biomolecular Spectroscopy,	<1%

2016
Publication

45	Subha Narayan Das, Martin Wagenknecht, Pavan Kumar Nareddy, Bhoopal Bhuvanachandra et al. " Amino Groups of Chitosan Are Crucial for Binding to a Family 32 Carbohydrate Binding Module of a Chitosanase from ", Journal of Biological Chemistry, 2016 Publication	<1%
46	Gokara, Mahesh, Tirupathi Malavath, Suresh Kumar Kalangi, Pallu Reddana, and Rajagopal Subramanyam. "Unraveling the binding mechanism of asiatic acid with human serum albumin and its biological implications", Journal of Biomolecular Structure and Dynamics, 2014. Publication	<1%
47	Sophie Liabeuf, Tilman B. Drüeke, Ziad A. Massy. "Protein-Bound Uremic Toxins: New Insight from Clinical Studies", Toxins, 2011 Publication	<1%
48	www.omicsonline.org Internet Source	<1%
49	lastperson.suncircle.org Internet Source	<1%
50	Submitted to Cardiff University Student Paper	<1%

51	Ling Ye. "Spectroscopic Studies on the Interaction of Efonidipine with Bovine Serum Albumin", 2008 2nd International Conference on Bioinformatics and Biomedical Engineering, 05/2008 Publication	<1%
52	cduv.net Internet Source	<1%
53	Submitted to University of Keele Student Paper	<1%
54	Submitted to Universiti Sains Malaysia Student Paper	<1%
55	Submitted to University of Queensland Student Paper	<1%
56	Michael Murphy. "Using Biacore to Measure the Binding Kinetics of an Antibody-Antigen Interaction", Current Protocols in Protein Science, 09/2006 Publication	<1%
57	Submitted to King's College Student Paper	<1%
58	Yeggoni, Daniel Pushparaju, and Rajagopal Subramanyam. "Binding studies of l-3,4-dihydroxyphenylalanine with human serum albumin", Molecular BioSystems, 2014. Publication	<1%

Exclude quotes	On	Exclude matches	< 14 words
Exclude bibliography	On		